



RESEARCH

2008-35

Design Tool for Controlling Runoff and Sediment from Highway Construction



LRRB
LOCAL
ROAD RESEARCH
BOARD

Take the



steps...

Research... Knowledge... Innovative Solutions!

Transportation Research

Technical Report Documentation Page

1. Report No. MN/RC 2008-35	2.	3. Recipients Accession No.	
4. Title and Subtitle Design Tool for Controlling Runoff and Sediment from Highway Construction		5. Report Date August 2008	
		6.	
7. Author(s) Bruce N. Wilson, Ph.D., Aleksey Sheshukov, Ph.D., Aida Mendez, Ph.D.		8. Performing Organization Report No.	
9. Performing Organization Name and Address Department of Bioproducts and Biosystems Engineering University of Minnesota 1390 Eckles Avenue St. Paul, Minnesota 55108		10. Project/Task/Work Unit No.	
		11. Contract (C) or Grant (G) No. (c) 81655 (wo) 161	
12. Sponsoring Organization Name and Address Minnesota Department of Transportation 395 John Ireland Boulevard, Mail Stop 330 St. Paul, Minnesota 55155		13. Type of Report and Period Covered Final Report	
		14. Sponsoring Agency Code	
15. Supplementary Notes http://www.lrrb.org/PDF/200835.pdf			
16. Abstract (Limit: 200 words) <p>Regulations require that stormwater pollution prevention plans be developed for construction activities that disturb an area that is equal to or greater than one acre. Different strategies, including a combination of practices, can be used to develop these plans. The WATER model was a tool developed from a previous project to assess the effectiveness of different on-site sediment control practices. This model is expanded in this study to consider off-site practices, to include processes at the watershed scale, and to allow spatial data sets to be integrated into the simulation framework. Routines to simulate the impact of off-site practices of rock check dams, vegetative filters, and detention ponds are added to the WATER model. The detention pond model has been modified to allow rock and gravel infiltration filters to be included as an off-site practice. Two different algorithms are used: (1) the Protocol Method based purely on empirical data and (2) the Process-Based Method using process-based relationships developed for porous media flow.</p>			
17. Document Analysis/Descriptors Erosion Control, Best Management Practices, Risk Assessment, Simulation Model		18. Availability Statement No restrictions. Document available from: National Technical Information Services, Springfield, Virginia 22161	
19. Security Class (this report) Unclassified	20. Security Class (this page) Unclassified	21. No. of Pages 109	22. Price

Design Tool for Controlling Runoff and Sediment from Highway Construction

Final Report

Prepared by:

Bruce N. Wilson, Ph.D.
Aleksy Sheshukov, Ph.D.
Aida Mendez, Ph.D.

Department of Bioproducts and Biosystems Engineering
University of Minnesota

August 2008

Published by:

Minnesota Department of Transportation
Research Services Section
395 John Ireland Boulevard, Mail Stop 330
St. Paul, Minnesota 55118

This report represents the results of research conducted by the authors and does not necessarily represent the views or policies of the Minnesota Department of Transportation and/or the Center for Transportation Studies. This report does not contain a standard or specified technique.

The authors and the Minnesota Department of Transportation and Center for Transportation Studies do not endorse products or manufacturers. Trade or manufacturers' names appear herein solely because they are considered essential to this report.

Acknowledgements

The authors appreciate the support of the Office of Environmental Services of the Minnesota Department of Transportation for this research. We particularly appreciate the assistance and support provided by Mr. Brett Troyer, Mr. Leo Holm, and Mr. Dwayne Stenlund in the development of the WATER model. The support of a companion project funded by the Minnesota Local Road Research Board (LRRB) contributed to the success of the project. The authors sincerely appreciate LRRB's support as well. The Minnesota Agricultural Experiment Station, Regional Projects S-1004, also provided support for the project.

The authors would also like to acknowledge several people whose work was instrumental to the completion of this study.

- Leo Holm for his support and vision in developing improved risk assessment tools for sediment control from construction sites.
- Brett Troyer and Dwayne Stenlund of Mn/DOT for their input of important features to include in the model and their willingness to share the needs of the construction industry with the authors.
- Technical advisory team members of Larry Berkland and Keith Cherryholmes for their input.
- Dan Warzala of Mn/DOT for his assistance in administrating the project.
- Nick Gervino of the Minnesota Pollution Control Agency for his support and advice in the development of important components used in the WATER model.

Table of Contents

Chapter One Introduction	1
Background Information	1
Objectives of the Study	1
Chapter Two Operational Structure and Interface Routines	3
Introduction	3
Folder Structure	3
File and Data Structure	4
Overview	4
Scalar Parameters	6
Tabular Parameters	6
Group Parameters	7
Output Data	8
Hydrologic Unit	9
Reach	10
Routed Reach	11
Combined Unit	11
Use of Wizards	12
Introduction	12
New Project	12
Opening Saved Project	13
Menu and Toolbar	13
New Hydrologic Unit	14
New Reach	16
New Routed Reach	17
New Combined Unit	18
Properties Dialog Windows	19
Input Parameters	19
Simulation Options	20
Output Results	20
Overview	20
Debug/Summary Files	21
Graphical Output	22
Simulate Multiple Land Uses	25
GIS Viewer in WATER	26
Overview	26
MapWindow Project and MapWinGIS Control	27
Objects in MapWinGIS	27
GIS Control	28
GIS Toolbar	30
Chapter Three Algorithms for Off-Site Practices and Channel Routing	31
Introduction	31
Off-Site Sediment Control Practices	31
Check Dams	31

Vegetative Filters and Buffers	32
Detention Ponds	34
Channel Routing of Flows and Sediment	36
Volumetric Flow Rates	36
<i>St. Venant Equations</i>	36
<i>Muskingum Storage Model</i>	39
Sediment	41
<i>Delivery Ratio</i>	41
<i>Sediment Transport Capacity</i>	41
Chapter Four Algorithms for Rock and Gravel Infiltration Filters	43
Introduction	43
General Considerations for Porous Media Flow	44
Hydraulic Flow	44
<i>Darcy Flow</i>	44
<i>Inertia Form</i>	45
<i>Permeability from Observed Data</i>	46
Sediment Removal	49
<i>Definitions</i>	49
<i>Sediment Removal Using Relative Permeability</i>	49
<i>Process-based Dimensionless Parameters</i>	51
Analysis of Observed Data	52
Description of Data Sets	52
<i>Minnesota Department of Agriculture's Study</i>	52
<i>Oveson's Master of Science (MS) Project</i>	53
<i>Summary of Tests</i>	54
Analysis of Permeability Data	55
<i>Clean Permeability</i>	55
<i>Observed Trends in Relative Permeability</i>	57
<i>Analysis of Relative Permeability</i>	57
Analysis of Removal Efficiencies	64
Evaluation of Data for 0.3 κc	67
Protocol Method	71
Description	71
Algorithm	71
Development of Process-Based Model	73
Pore-Scale Approach	73
<i>General Concepts</i>	73
<i>Specific Discharge using Pore Velocity And Area</i>	75
Fractal Representation of Porous Media	76
Background	76
<i>Areal Porosity and Moisture Content</i>	78
<i>Fractal Representation with Sediment Deposition</i>	80
Fractal Model of Relative Permeability	82
<i>Theoretical Representation</i>	82
<i>Estimating Fractal Model Parameters from Observed Data</i>	84

Analyses of Fractal Model Parameters	86
<i>Direct Estimate of Deposition</i>	86
<i>Predicted Estimate of Deposition</i>	86
Process-Based Method	89
Description	89
Algorithm	92
Chapter Five Summary and Conclusions	94
References	96

List of Tables

Table 4.1 Summary of Characteristics of Data Sets.	54
Table 4.2 Summary of Characteristics of Data Sets at $\kappa_r = 0.3$.	71
Table 4.3 Box-Counting Relationships for Defining Fractal Numbers.	78
Table 4.4 Optimal Parameter Values for the Fractal Model.	87

List of Figures

Figure 2.1 Folder tree structure.	4
Figure 2.2 Example of the input data file with a list of scalar parameters.	5
Figure 2.3 Example of the parameter line in an input data file.	6
Figure 2.4 Example of the input data file with a list of array parameters.	6
Figure 2.5 Example of the input data file with a list of grouped parameters.	8
Figure 2.6 Folder structure of the custom project with multiple watersheds and reaches.	9
Figure 2.7 Folder structure of the hydrologic unit created in a watershed-type project.	9
Figure 2.8 Example of an output data file.	10
Figure 2.9 Folder structure of the reach created in a watershed-type project.	10
Figure 2.10 Folder structure of the routed reach created in a watershed-type project.	11
Figure 2.11 Folder structure of the combined hydrologic unit in a watershed-type project.	11
Figure 2.12 New project wizard window.	12
Figure 2.13 Open project main window.	13
Figure 2.14 Toolbar with the buttons for operations with watershed units.	13
Figure 2.15 Toolbar and menu group for simulation procedures.	14
Figure 2.16 New hydrologic unit dialog window.	15
Figure 2.17 New hydrologic unit window.	15
Figure 2.18 New reach window.	16
Figure 2.19 Main window for routing flow through a reach.	17
Figure 2.20 Window for routing with additional computational parameters.	18
Figure 2.21 Window for combining the contribution from the watershed with reach flow.	19
Figure 2.22 Dialog window for viewing input data values.	20
Figure 2.23 Dialog window for viewing/changing simulation options.	21
Figure 2.24 Main window displaying output summary and debug files.	22
Figure 2.25 Plotting options dialog window.	23
Figure 2.26 Main graphical output window.	24
Figure 2.27 Plotting options control window.	25
Figure 2.28 Illustrative schematic of a watershed with multiple land uses.	26
Figure 2.29 GIS main pane window.	29
Figure 2.30 GIS toolbar.	30
Figure 3.1 Schematic of a vegetative filter.	32
Figure 3.2 Cross-sectional view of a hypothetical pond.	35
Figure 3.3 Cross-section of flow for development of the St. Venant equations.	37
Figure 3.4 Control volume for the Muskingum method.	39
Figure 3.5 Idealized storage of the Muskingum method.	40
Figure 4.1 Evaluation of representation of specific discharge.	46
Figure 4.2 Trends in power function coefficients for predicting specific discharge.	47
Figure 4.3 Particle size distributions for the rock media.	54
Figure 4.4 Particle size distributions for the influent sediment.	55
Figure 4.5 Prediction of clean media permeability using median diameter.	56
Figure 4.6 Prediction of clean media permeability using median diameter and the ratio of diameters of 75% and 25% values.	56
Figure 4.7 Change in permeability with inflow mass for camas 7 rock media.	58
Figure 4.8 Change in permeability with inflow mass for camas 6 rock media.	58

Figure 4.9 Change in permeability with inflow mass for ums 1 rock media.	59
Figure 4.10 Change in permeability with inflow mass for ums 2 rock media.	60
Figure 4.11 Change in permeability with inflow mass for ums 3 rock media.	60
Figure 4.12 Exponential models of relative permeability for camas 7.	61
Figure 4.13 Exponential models of relative permeability for camas 67.	61
Figure 4.14 Exponential models of relative permeability for camas 6.	62
Figure 4.15 Exponential models of relative permeability for ums 1.	62
Figure 4.16 Exponential models of relative permeability for ums 2.	63
Figure 4.17 Exponential models of relative permeability for ums 3.	63
Figure 4.18 Observed influent and effluent concentrations for camas 7.	65
Figure 4.19 Observed influent and effluent concentrations for ums 2.	65
Figure 4.20 Removal efficiency as a function of relative permeability.	66
Figure 4.21 Cumulative trap efficiency as a function of weighted relative permeability.	66
Figure 4.22 Predicted and observed removal efficiencies using power model of process-based parameters.	68
Figure 4.23 Predicted and observed removal efficiencies using additive model of process-based parameters.	68
Figure 4.24 Predicted and observed cumulative inflow mass at $0.3\kappa_c$.	69
Figure 4.25 Predicted and observed $t_{e0.30}$ using sediment and media sizes.	70
Figure 4.26 Predicted and observed $t_{e0.30}$ using particle sizes and influent concentration.	70
Figure 4.27 Concepts for darcian scale and pore scale representation of flow.	74
Figure 4.28 Hypothetical representation of the pores in rock filters.	74
Figure 4.29 Serpinski carpet to illustrate fractal concepts for porous media.	77
Figure 4.30 Predicted relative permeability using the best fit fractal model.	88
Figure 4.31 Predicted relative permeability using field parameters and deposition for the camas 7 rock media.	90
Figure 4.32 Predicted relative permeability using field parameters and deposition for the UMS 2 rock media.	90
Figure 4.33 Selected tests of predicted and observed relative permeability for the MDOA silt.	91
Figure 4.34 Selected tests of predicted and observed relative permeability for the silt a.	91

Executive Summary

Regulations require that stormwater pollution prevention plans be developed for construction activities that disturb an area that is equal to or greater than one acre. Different strategies, including a combination of practices, can be used to develop these plans. Simulation models are valuable tools that can be used to assess the effectiveness of different sediment control practices. A previous project funded by the Minnesota Local Road Research Board and Minnesota Department of Transportation supported the development of a risk simulation tool called the WATER (Watershed Assessment Tool for Environmental Risk) model. This model was developed to predict runoff and erosion for a single construction site. The WATER model is expanded in this study to consider off-site practices, to include processes at the watershed scale, and to allow spatial data sets to be integrated into the simulation framework.

The WATER model has been expanded to consider five different types of modeling projects. Projects of interest in this study are: risk assessment for a single construction site, multiple land uses within a watershed, and stand-alone modules for off-site processes. The model can retrieve and edit input data, proceed with continuous simulations, view output results graphically, and work with layers for Geographical Information Systems. The WATER model has been expanded to allow flow and sediment from different areas within a watershed to be routed through stream networks and to be combined to determine the overall response of watersheds.

Routines have been added to the WATER model to simulate the impact of off-site practices of rock check dams, vegetative filters, and detention ponds. Rock check dams are modeled using a single-step backwater curve with trap efficiency predicted by an overflow-rate-type relationship. The sediment removal of vegetative filters and buffers is modeled by dividing the flow processes into a zone at the inlet, where deposition is dominated by a change in transport capacity, and a non-inlet zone, where deposition is dominated by the settling of suspended sediment. The response of detention ponds is based on dividing the pond into a series of chambers of equal volume. A mass balance in the vertical direction is evaluated for each of the chambers.

The detention pond model has also been modified to allow rock and gravel infiltration filters to be included as off-site practices. Two different algorithms are used. One of the algorithms, referred to as the Protocol Method, is a purely empirical method based on the evaluation of experimental data collected in a laboratory setting. The other algorithm, referred to as the Process-Based Method, is based on process-based relationships developed for porous media flow.

Chapter One

Introduction

Background Information

Stormwater runoff from construction sites can degrade the quality of waters in streams and lakes. The Clean Water Act was amended in 1987 to implement a comprehensive national program to reduce the impact of stormwater runoff. Stormwater regulations became a part of the National Pollutant Discharge Elimination System (NPDES) permit program. The permitting authority for NPDES in Minnesota is the Pollution Control Agency (MPCA). Since 2003, the MPCA has required that stormwater pollution prevention plans (SWPPPs) be developed for construction activities that disturb an area that is equal to or greater than one acre.

Different strategies, including a combination of practices, can be used to develop SWPPPs. For example, the sediment control plan for the construction of Highway 23 near Willmar, MN, included 1000 bales of straw for mulch protection, 44 detention ponds, numerous silt fences and several rock check dams (D. Stendlund, Mn/DOT, 2006). Simulation models are valuable tools that can be used to assess the effectiveness of different SWPPPs, especially those plans that include a combination of different practices. Simulation models also provide a useful vehicle for allowing recent experimental data to be easily used by practitioners in their designs.

To improve the usefulness of experimental data and the design of erosion/sediment control practices, Minnesota Local Road Research Board (LRRB) and Minnesota Department of Transportation (Mn/DOT) supported the development of a risk simulation tool called WATER (Watershed Assessment Tool for Environmental Risk) (Wilson et al, 2006). This model simulates the impact of highly variable weather conditions on the runoff and erosion for a single construction site. This work was the first step of a larger modeling project. Widely used off-site practices, such as detention ponds, are not included in the original version of the WATER model and need to be added to develop appropriate SWPPPs. Additional expansion is needed to integrate processes at a watershed scale for assessing the downstream impacts of construction activities. Improved interface and input routines are also needed to utilize readily available spatial data bases.

Objectives of the Study

The overall goal of the proposed effort is to develop a tool for the design of effective sediment control strategies for construction sites. The specific research objectives are:

- (1) To develop and incorporate off-site sediment control practices in the WATER simulation model,
- (2) To expand the WATER model to include processes at a watershed scale by linking together the responses of different land uses, and
- (3) To develop user-friendly interface routines that allow spatial data sets to be integrated

into the WATER model.

A description of the operation format and interface routines is given first in Chapter 2. This includes the organization of data and executable files, approach used to simulate multiple land uses within a watershed, and routines for spatial analysis within a geographical information system (GIS). Algorithms for simulating the routing of flows and sediment through channels and off-site treatment methods of rock check dams, vegetative filters, and detention ponds are described in Chapter 3. These algorithms are based on work done as part of other studies. Algorithms to simulate rock and gravel filters have been developed as part of this project. Since these algorithms are based on unpublished materials, they are described in greater detail in Chapter 4. An overall summary and conclusions are given in the final chapter.

Chapter Two

Operational Structure and Interface Routines

Introduction

Operational structure and interface routines are important to allow the users to successfully use models for their applications. The WATER model is a continuous simulation modeling tool that provides a user with capabilities to create five different types of modeling projects, such as, a construction site risk assessment, a modeling multiple watersheds, working with stand-alone modules, calculating a feedlot runoff, and application of statistical tools for environment problems. The model can retrieve and edit input data, proceed with continuous simulations, view output results graphically, and work with GIS layers. Each modeling project deals with retrieving input parameters and storing output results. Both of these types of data is formatted in a simple ASCII text format and organized on a disk in a certain folder structure. The chapter first discusses the folder structure and graphical user interface. This includes a brief description of input format for multiple land uses within the watershed. A more detailed description of the computational logic for this option is given in a separate section. The final section discusses the Geographic Information System features utilized in the WATER model.

Folder Structure

A user has an option to load default input parameters from the pre-defined folder or prepare the data himself/herself in the same format and load it individually into the project. Let's discuss the default folder structure in greater details. WATER uses a set of default input parameters stored in one folder called "InstallDir\Data" with many subfolders. Right now that directory is created under a main project folder in a disk, but upon the completion of the computer product the data will be transferred to a main program files folder where the executable file will be also located.

The data is organized in a form that every set of parameters (scalars, vectors, and tables) is placed in a subfolder named after its component name. For example, all input data for the weather module is stored in the folder named "Weather", for the erosion module the data is placed in a "Erosion" folder, etc. Each file in these folders is a simple ASCII file with the parameters characteristics saved in a space-separated format. Since the input parameters can have different numeric format we use additional flags in a file to identify the type of the parameter: integer, float, or string. Names of the parameters and the corresponding units are also stored in the same file, and retrieved along with the parameter value.

The output results are stored in a folder specified by the user when the modeling project has been created. The files have two different formats. The first format is similar to the format of input data files and represents a simple space-separated ASCII text. Details of the content of the files are discussed in greater details in the section below. The other format is a binary file, and it stores the project-related information, similar to a way the Microsoft Word stores the

files in DOC format. Every project and every hydrologic unit in the project have that type of file in its folder. Name of the file is specified while the project is created, but the file extension depends on the project type, for example, “.wtr” for a watershed project and “.wta” for a stand-alone project.

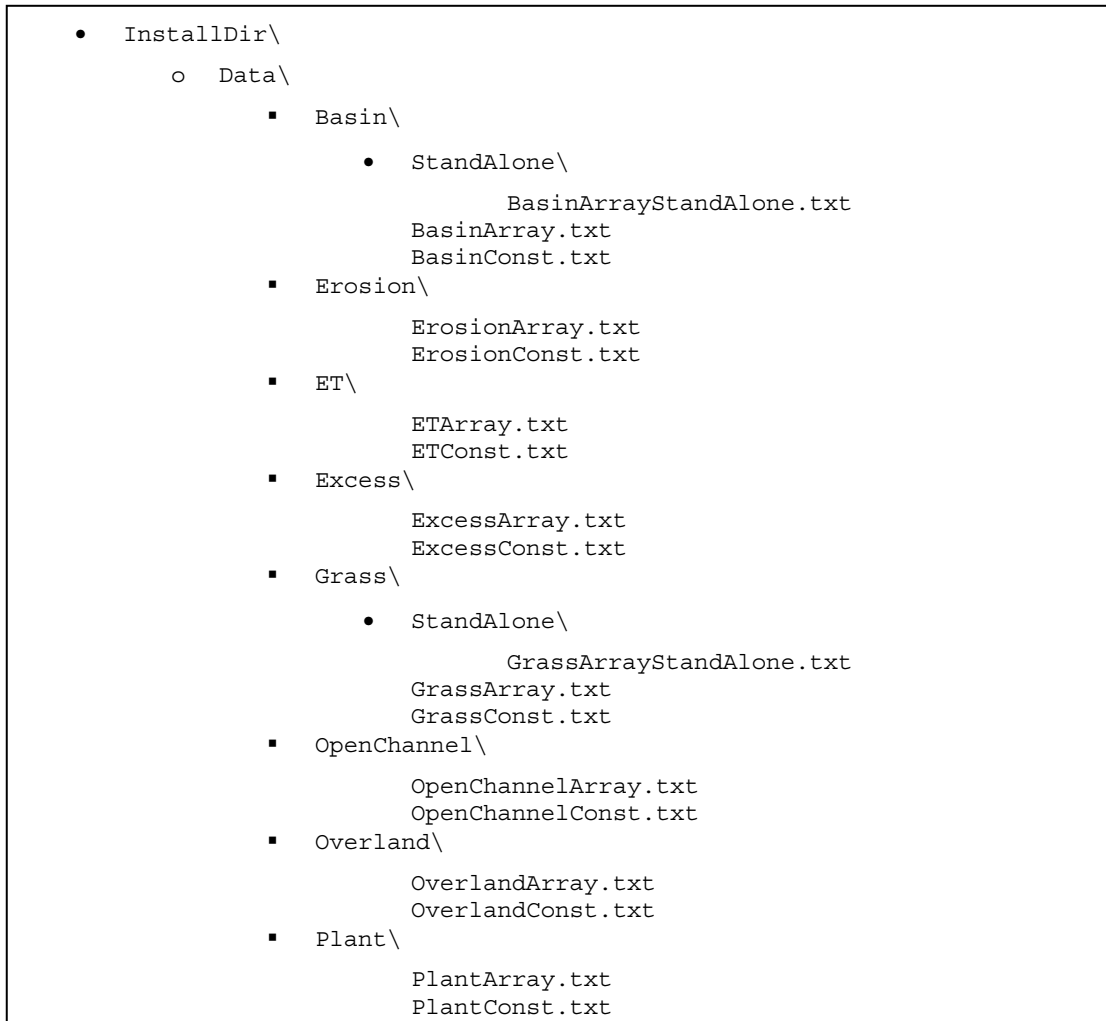


Figure 2.1. Folder Tree Structure.

File and Data Structure

Overview

The default input data is stored in a folder called “InstallDir\Data\”. The data is divided into either two or three files for each component and stored in subfolders entitled by the component names.

- The first file stores the input information about scalar parameters, such as the name, units, value, and type, and has a ‘Const’ word in its filename along with the component name, i.e. “ErosionConst.txt” for the erosion module.
- The second file stores the tabular data such as matrices or a list of values of the parameters for different classes, i.e. values of parameters for different soil types stored in a “SoilBalanceArray.txt” file. Additional information about the table (type of the value, its width, number of decimals, etc) precedes the actual table of data.
- The third file deals with the data that can be grouped by any grouping principle, and it is named with the word “Group” in its name. This type of data is designed to be used for defining the same set of parameters for different groups, see plant characteristics defined similarly for every plant group in the “PlantGroup.txt” file.

Figure 2.1 presents a tree structure of the folder that holds information about the default input parameters.

```

Main Menu label: * no units* 3 -9999 1.000000 Basin* 10 2 0
Dialog/Output title: * no units* 3 -9999 1.000000 General Parameters* 10 2 0
Cum. deposition all events (0-no, 1-yes): * no units* 2 1 1.000 1.0* 4 0 4
Input diffusion coefficients (0-no, 1-yes): * no units* 2 0 0.000 0.0* 4 0 4
Input surface subareas (0-no, 1-yes): * no units* 2 0 0.000 0.0* 4 0 4
Bed specific gravity: * (kg/kg)*2 10 1.400000 1.40* 7 2 4
Number of particle size classes: * no units*1 5 5.00 4* 4 0 4
Discharge levels: * no units*1 5 5.0 5* 4 0 4
Number of velocity segments: * no units*1 15 15.0 15* 4 0 4
Bed roughness parameter: * mm*2 10 0.050000 0.0500* 8 4 4
Log-velocity constant: * m s-1/m s-1*2 10 8.500000 8.50* 7 2 4
Wilson's erosion parameter bo:* g s-1/(N/m2)1/2*2 10 37.4029 37.4029* 7 3 4
Wilson's erosion parameter b1: * N/m2*2 10 8.00 8.0* 7 2 4
Adjustment in bo for old sediment: * no units*2 10 0.0 0.0* 7 3 4
Height of approximately uniform velocity: * m*2 10 0.000000 0.00* 7 2 4
Initial bottom velocity ratio: * m s-1/m s-1*2 10 2.000000 2.00* 7 2 4
Initial time for h1: * hr*2 10 1.000000 1.00* 7 2 4
Time for h2=h1: * hr*2 10 2.000000 2.00* 7 2 4
Halt routing inflow volume: * percent*2 1 98.00000 98.0* 6 1 4
Number of cstrs: * no units*1 2 2.00 2* 4 0 4
Number of nodes: * no units*1 18 18.00 18* 4 0 4
Numerical time step: * hr*2 10 0.002778 0.002778* 10 6 4
Number of stage points: * no units*1 9 9.00 14* 8 0 4
Principal spillway elevation: * m* 2 8 304.800 8* 8 4 4
Initial water level: * m*2 8 304.800 8* 8 4 4
Dead space: * percent*2 10 25.00000 6.4* 7 1 4
Standard inlet velocity: * m/s*2 1 0.1900 1.00* 7 4 4
Corresponding standard inlet flow rate: * m3/s*2 10 1.410000 0.500* 7 3 4
Evapotranspiration-Seepage Loss: * mm/d*2 10 10.00 0.500* 7 3 4
User Input Elevation-Flow Values (0-no, 1-yes):* no units* 2 0 0.0 1.0* 4 0 4
Number of principal spillways: * no units*1 0 0.00 2* 4 0 4
Number of emergency spillways: * no units*1 1 1.00 2* 4 0 4
Number of rock spillways (max=1): * no units*1 1 1.00 2* 4 0 4
Maximum simulation time: * hr*2 1 100.00 1.00* 8 2 4
Not defined: * no units* 2 -9999 -9999.900000 -9999.9* 10 2 4

```

Figure 2.2. Example of the Input Data File with a List of Scalar Parameters.

Scalar Parameters

Now let's take a closer look at the file with scalar parameters shown in Figure 2.2. The first two lines contain general information about the component. The remaining lines define the input scalar parameters. We use the line in Figure 2.3 to explain the format. There are nine fields with the following definitions:

1. Name (all characters up to the star sign) - Standard inlet velocity
2. Units (all characters up to the star sign) - m/s
3. Scalar type (0 – integer, 1 – float, 2 - string) - 2
4. Integer value (if scalar type is 1) - 1 (not used)
5. Float value (if scalar type is 2) - 0.19
6. String value (if scalar type is 3 – all characters up to the star sign) - 1.000 (not used)
7. Total number of digits in a float value - 7
8. Number of decimals in a float value - 4
9. Not used in a current version - 4

```
Standard inlet velocity: * m/s*2 1 0.1900 1.00* 7 4 4
```

Figure 2.3. Example of the Parameter Line in an Input Data File.

Tabular Parameters

Tabular parameters are stored in a file with a name formatted as “###Array.txt” where “###” represents the module name. An example of this file is shown in Figure 2.4.

```
Input Basin Parameters:  Number of sets of arrays in file
10
Stage (m) - area (ha) - flow rate (m3/s) and distance to inlet contour line (m)
4 9
1 1 1 1
2 2 2 2
6 6 6 6
3 3 3 3
Stage* Area* Discharge* Distance*
m* ha* m3/s* m*
304.800 0.4047 0.0000 0.00
306.324 2.0235 0.0000 142.25
307.848 4.0530 0.0000 201.17
308.000 4.2365 0.1897 205.15
308.458 9.3443 0.6059 307.29
309.372 9.4522 0.8324 305.53
310.896 43.159 0.9683 657.84
311.201 45.300 3.1823 672.84
311.506 55.159 8.8364 743.33
```

Figure 2.4. Example of the Input Data File with a List of Array Parameters.

The first line of the file shown in Figure 2.4 contains general information about the file and the component. It is skipped when the data is read by the program. The second line provides with the number of arrays in the file. All the lines starting with the third line show an example of a data structure of a one array. The other nine arrays are prepared in the same way. They all have the general format as given below:

1. General information about an array – (Stage (m) - area (ha) - ...)
2. Number of columns (4) and rows (9)
3. The following 4 lines provide the following formatting information for each value in each column: label(not always used), type (0-integer, 1-float), width of a float value, number of decimals
4. Names of the variables in the columns, separated by the star sign
5. Units of the variables, separated by the star sign
6. The final 9 lines contain the actual (4x9) matrix values

Group Parameters

Group parameters are stored in a file with a name formatted as “###Group.txt” where “###” represents the computational module. Currently, the group parameters are used only in the Plant Growth module. The file format is very similar to the tabular data file format, and it consists of a set of tables with the first two columns in each of them representing the same set of parameters and their units. During the data scanning (reading), an internal function only reads the information for the first table and passes it to all other tables presented in the file. Normally the first table represents standard values for the aforementioned parameters with the subsequent tables providing the actual values for the list of groups.

The first line of the file shown in Figure 2.5 contains some general information. It is skipped when the data is read by the program. The second line gives the number of tables in the file to be retrieved. All the lines starting with the third line show an example of a data structure of a one table. The other nine arrays are prepared in the same way as the first table. Details of the format are given below:

1. General information about an array – (Stressor parameters for standard plant)
2. Number of columns (8) and rows (6). Each row is a parameter which value is retrieved.
3. The following 4 lines provide the following formatting information for each value in each column: label(not always used), type (0-integer, 1-float, 2-string), width of a float value, number of decimals
4. Names of the variables in the columns, separated by the star sign
5. This line is skipped.

The final six lines contain information about the name of the parameter, its units, and its value for a different property.

```

Input Parameters as Arrays for Plant Growth Class: Number of sets of arrays in
file
10
Stressor Parameters for Standard Plant
8 6
1 1 1 1 1 1 1 1
3 3 2 2 2 2 2 1
25 10 10 10 10 10 10 10
0 0 4 4 4 4 4 0
Stressor* Units* Optimal Value* Minimum Value* Optimal Response* Minimum
Response* Rate Coefficient* Curve Type*
----* ----* ----* ----* ----* ----* ----* ----*
Seeds*          plants/m^2*  -999.9 -999.9 -999.9 -999.9 -999.9 -999
Water Content*  m^3/m^3*  -999.9 -999.9 -999.9 -999.9 -999.9 -999
Nitrogen*       ppm*      -999.9 -999.9 -999.9 -999.9 -999.9 -999
Phosphorus*     ppm*      -999.9 -999.9 -999.9 -999.9 -999.9 -999
Temperature*    C*        -999.9 -999.9 -999.9 -999.9 -999.9 -999
Leaf Area*      m^2/m^2*  -999.9 -999.9 -999.9 -999.9 -999.9 -999
Stressor Parameters for Plant Group 1: Number variables, Number values - Per
variable type, width, decimal
8 6
1 1 1 1 1 1 1 1
3 3 2 2 2 2 2 1
25 10 10 10 10 10 10 10
0 0 4 4 4 4 4 0
Stressor* Units* Optimal Value* Minimum Value* Optimal Response* Minimum
Response* Rate Coefficient* Curve Type*
----* ----* ----* ----* ----* ----* ----* ----*
Seeds*          plants/m^2*  50.00 5.01.00.00.51
Water Content*  m^3/m^3*  0.30 0.10 1.00.00.51
Nitrogen*       ppm*      50.00 0.01.00.00.51
Phosphorus*     ppm*      15.0 0.01.00.00.51
Temperature*    C*        15.00 -1.0 1.00.01.00
Leaf Area*      m^2/m^2*  3.00 0.50 1.00.00.51

```

Figure 2.5. Example of the Input Data File with a List of Grouped Parameters.

Output Data

Output results are stored in a folder specified by the user when the modeling project has been created. Taking a watershed project as an example (see Figure 2.6), we see a project folder entitled “Watershed01” and a list of subfolders representing hydrologic units created in that modeling project. Each subfolder has a different number of the output files, and it depends on the type of the unit and the computational stage of the project. All subfolders are discussed below. The last file in the main project folder is a binary file that holds the information about the unit, and it is reused by the computer model every time the user opens/saves/closes the project.

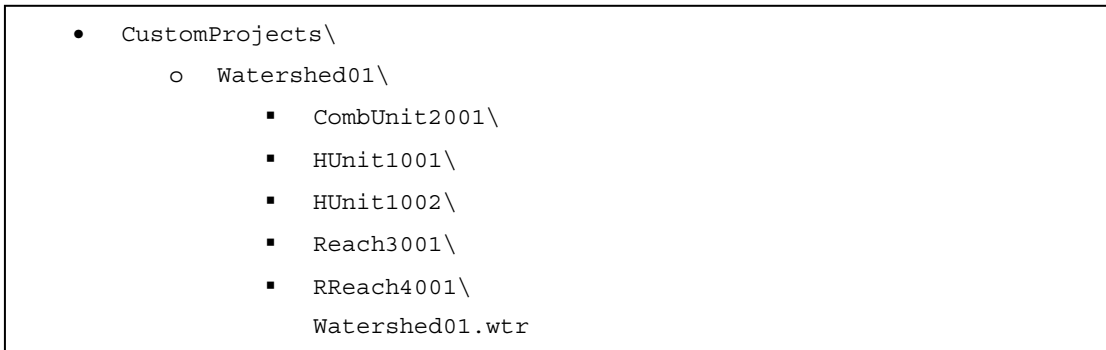


Figure 2.6. Folder Structure of the Custom Project with Multiple Watersheds and Reaches.

Hydrologic Unit

Folder content for a hydrologic unit is very similar to that of the default input data. It also contains several subfolders with the names of the computational modules that are used in the hydrologic unit. An example of the file tree structure is presented in Figure 2.7. The following modules are loaded into the project with corresponding computational results:

- Erosion
- Evapotranspiration
- Excess
- Overland flow
- Plant growth
- Channel routing
- Weather

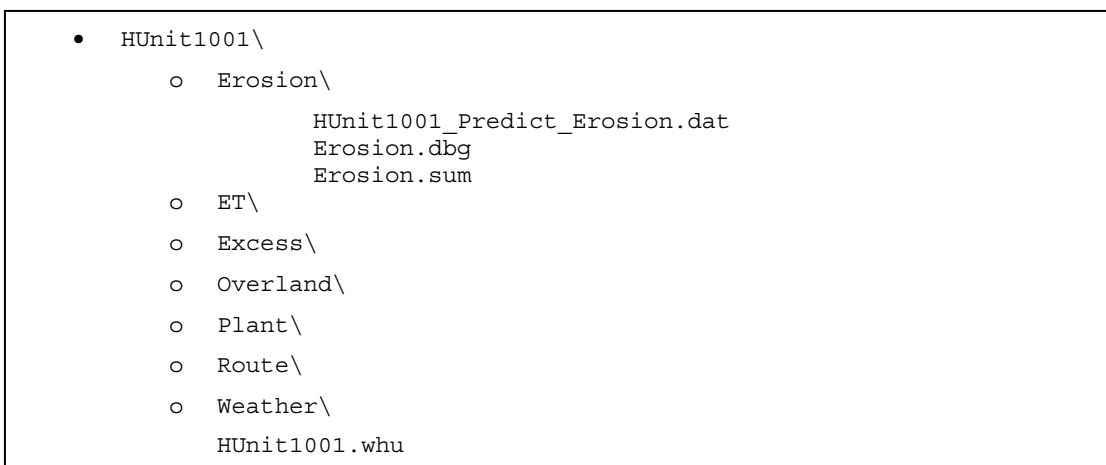


Figure 2.7. Folder Structure of the Hydrologic Unit Created in a Watershed-Type Project.

The file “HUnit1001.whu” is similar to the binary file created for the project, and it contains the internal information about the hydrologic unit. In each subfolder, the three files are created for the above example of Figure 2.7:

- HUnit1001_Predict_Erosion.dat
- Erosion.dbg
- Erosion.sum

The file with “dbg” extension contains the debug and more detailed information, the file with “sum” extension is a summary output file, and the “dat” file is a main output file with the results organized in a column format. An example of the output file is shown in Figure 2.8 where:

- First line contains general information about the computational run
- Second line lists output variables starting with the date parameters:
 - year
 - month
 - day
 - calendar day
 - hour
 - other output variables starting with the 6th column
- Each row after the second line presents the corresponding values in a space-separated format
- Hour value is divided into 15 minute increments, so 1.25 means 1 hour and 15 minute, while the value 99.9 indicates that the output values are for hourly calculations
- Value of -999.900 for any output variable indicates that the value is not computed

WATER Predicted Erosion Variables. File created: 4-29-2008; 14 hr, 21 min						
Year	Month	Day	Cal-Day	Hour	Load	Dep
1	1	1	99.9	-999.900	-999.900	
1	1	1	99.9	-999.900	-999.900	
1	1	1	0.25	0.1	-999.900	
1	1	1	0.50	-999.900	0.034	

Figure 2.8. Example of an Output Data File.

Reach

Folder content for a reach is very simple and does not contain any computational results. The only file is placed there is a binary file with the main information about the reach including reach input characteristics (see Figure 2.9).

- Reach3001\
 - Reach3001.wre

Figure 2.9. Folder Structure of the Reach Created in a Watershed-Type Project.

Routed Reach

Folder content for a routed reach has two subfolders, OpenChannel and Route, as shown in Figure 2.10. The OpenChannel folder has a format similar to any other output folder of a computational module. It has a debug, a summary, and a main output files. The Route folder contains three files:

- Inflow.dat – hourly values of the inflow rate in m³/sec
- Outflow.dat - hourly values of the outflow rate in m³/sec
- RReach4001_Predict_Route.dat – summarized output results formatted in the way of other main results files for the other computational modules

File with the extension “wro” is a binary file with the information on the routed reach.

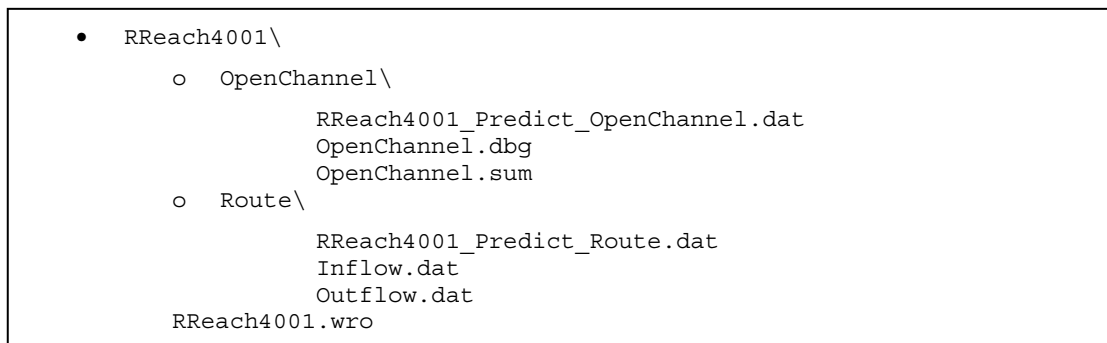


Figure 2.10. Folder Structure of the Routed Reach Created in a Watershed-Type Project.

Combined Unit

Folder content of the combined unit is shown in Figure 2.11. It is similar to the routed reach folder, but it does not have an open channel folder. Since the computational algorithm does not route the flow through the reach, but rather adds the runoff from the hydrologic unit to the reach flow, there is no need to store channel characteristics. File with the extension “wrc” is a binary file with the information on the unit.

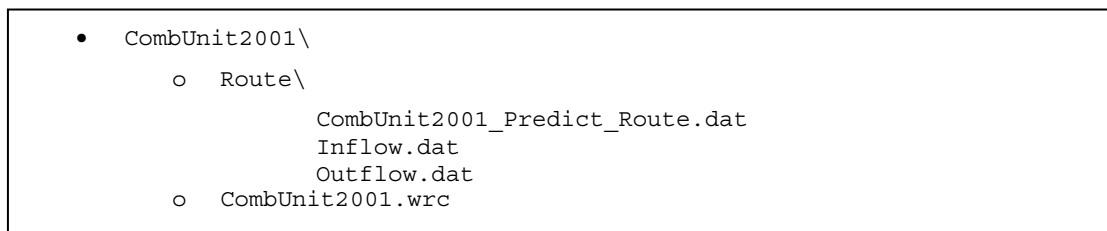


Figure 2.11. Folder Structure of the Combined Hydrologic Unit in a Watershed-Type Project.

Use of Wizards

Introduction

The first step in working with WATER is to create a project by clicking on the ‘New project’ menu item or toolbar button. This invokes the new project wizard dialog and consequently creates a project. The main content of the project is stored in a directory specified by the user during the wizard steps. Once the project created, it can be saved or closed, and then re-opened by clicking on the ‘Open project’ menu item or toolbar button.

Other wizards used in WATER are for creating hydrologic units, reaches, and routing and combining the runoffs from hydrologic units with the stream flows.

New Project

Figure 2.12 shows an example of a new project wizard dialog. The list control presents several project types that the user must select from. Two buttons in a top-left corner of the control allows toggling between list and icon view of the control. In the name and location boxes, the user specifies the name of the project and the directory where its output content is stored. Clicking on Finish button closes the window and creates the project. It then opens a main window discussed in details later.

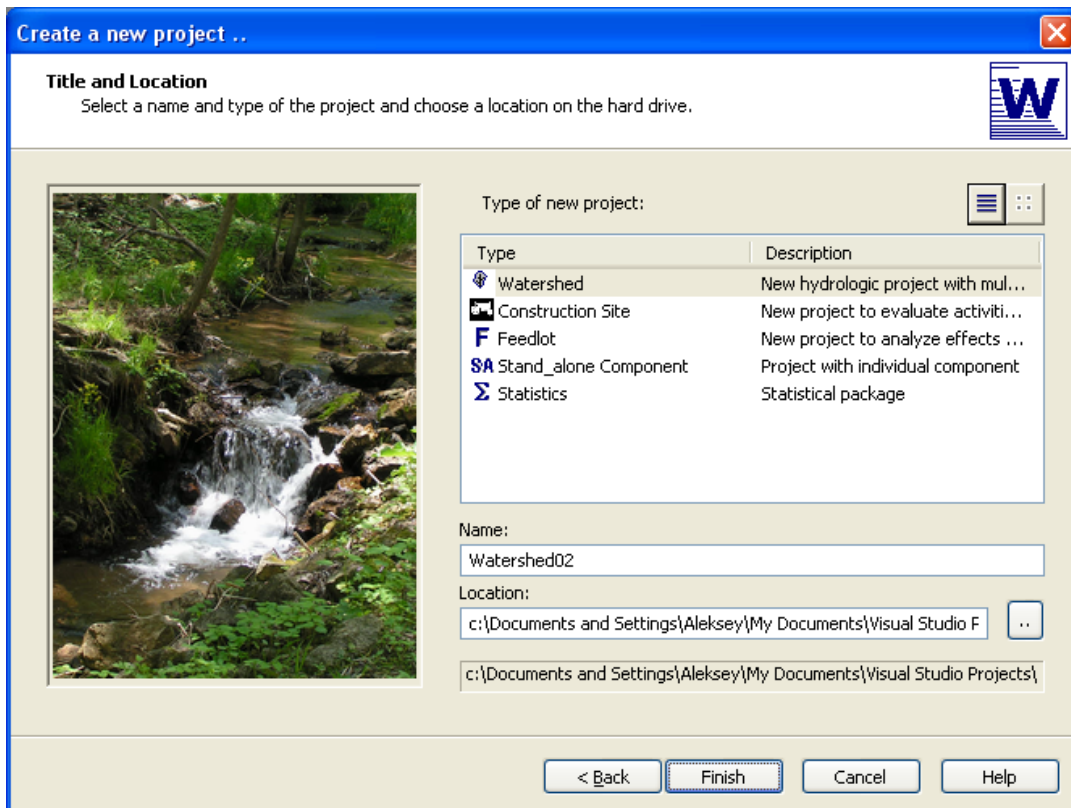


Figure 2.12. New Project Wizard Window Showing Five Types of Projects.

Opening Saved Project

The open project wizard dialog is shown in Figure 2.13. The list-control dialog lists the recently created projects. The user must select one of them and click the Finish button to load it. The button Browse helps the user to navigate to a custom project if it's not present in the list.

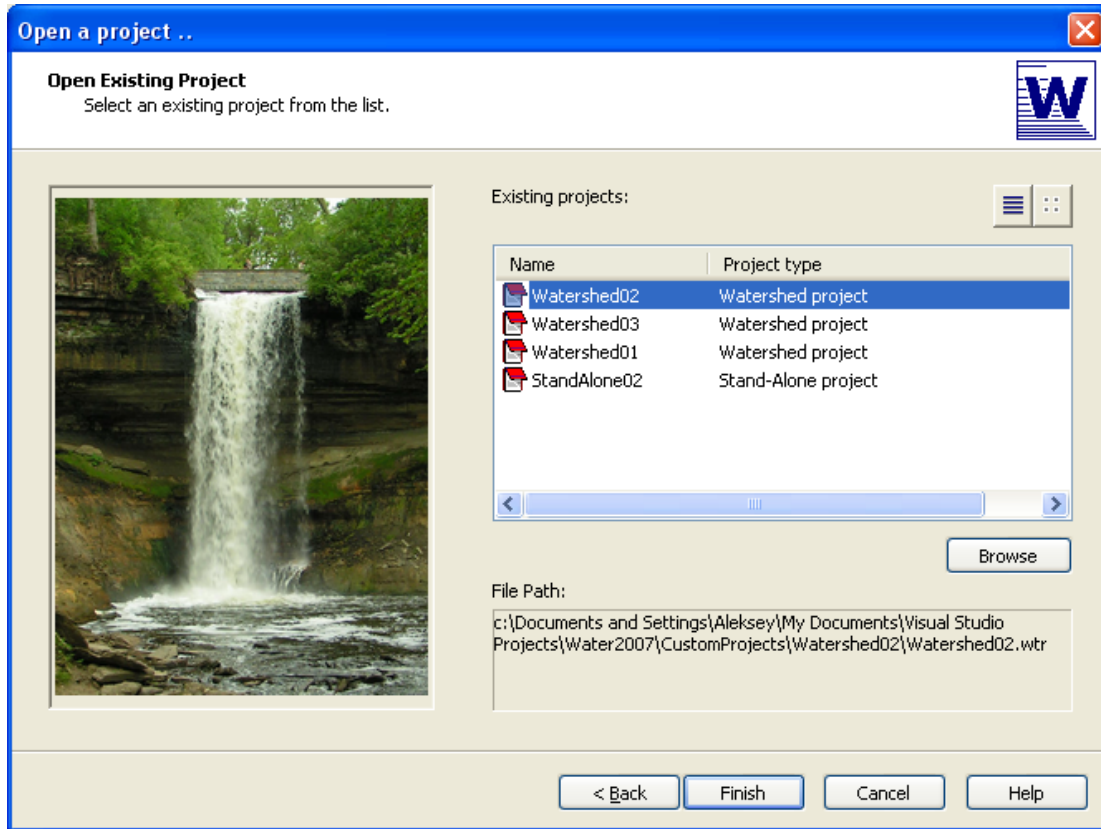


Figure 2.13 An 'Open Project' Main Window. Available Past Projects Are Shown.

Menu and Toolbar

New hydrologic units, reaches, etc, and main watershed related implementation operations can be invoked by clicking on a menu item in Figure 2.15 or a corresponding button in a toolbar shown in Figure 2.14.



Figure 2.14 Toolbar with the Buttons for Operations with Watershed Units.

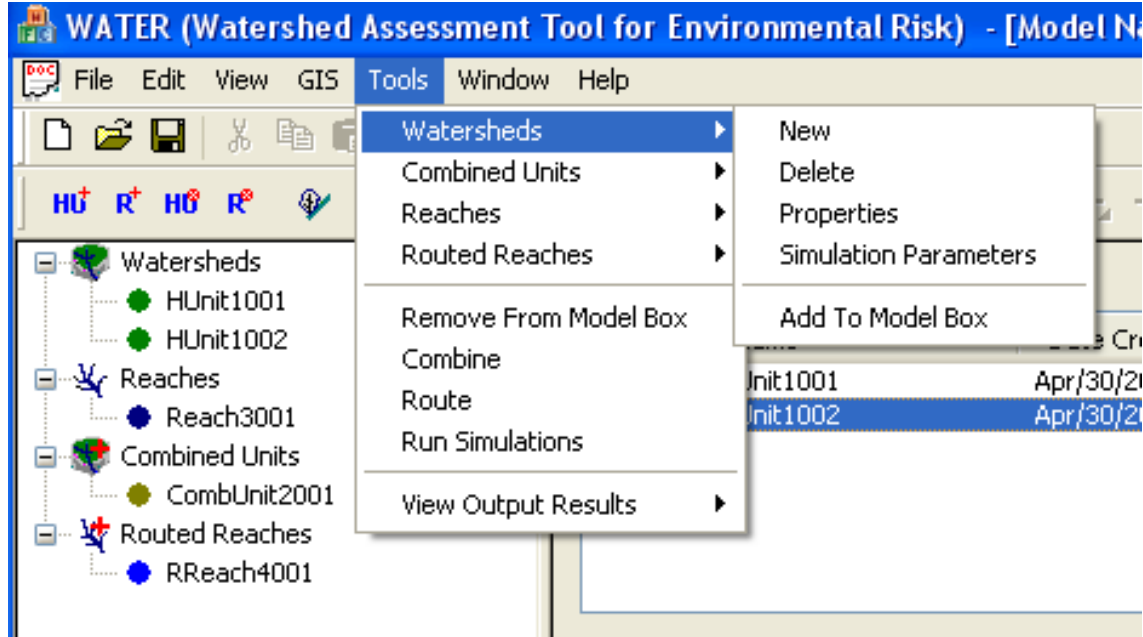


Figure 2.15 Toolbar and Menu Group for Simulation Procedures.

New Hydrologic Unit

New hydrologic unit can be created by clicking on a ‘New watershed’ menu item or a corresponding button in a toolbar shown in Figure 2.14 and Figure 2.15. It invokes a ‘New hydrologic unit’ wizard window as shown in Figure 2.16.

The main window gives a user an option to select a name of the hydrologic unit, its output folder, and geographical information. A user can search for a weather station by either selecting a country and a state from the list, or by coordinates. The station then must be selected from the list. Weather characteristics for this site can be observed by clicking on the ‘Details’ button.

The user proceeds to the next screen by clicking on the ‘Next button’. They then have the option to select the number of years to be simulated and a type of the hydrologic unit. Clicking on a ‘Finish’ button returns the user to the main window. The folder with the specified name is automatically created and the default input data are retrieved and entered into the WATER model.

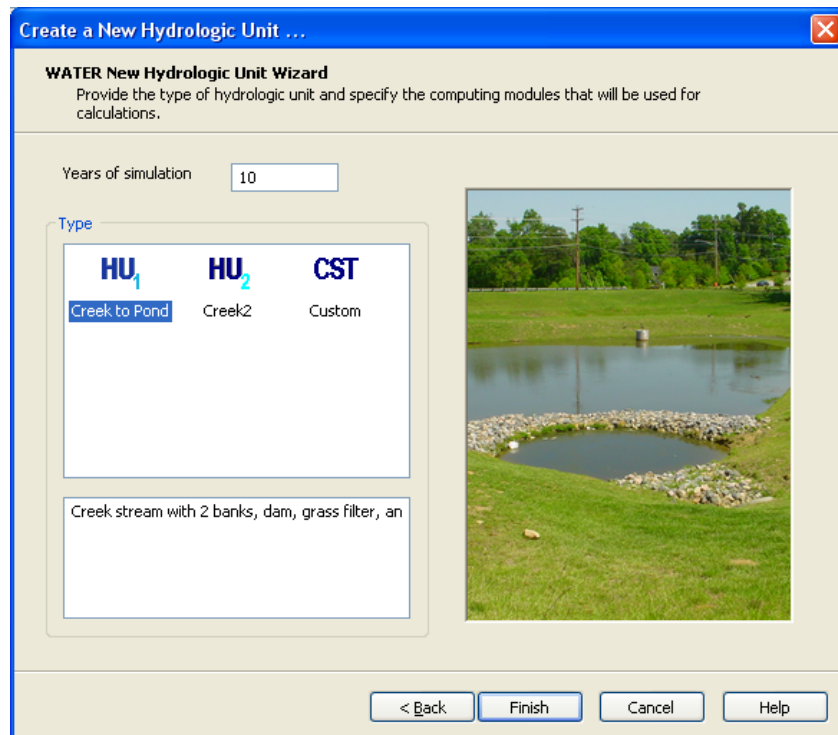
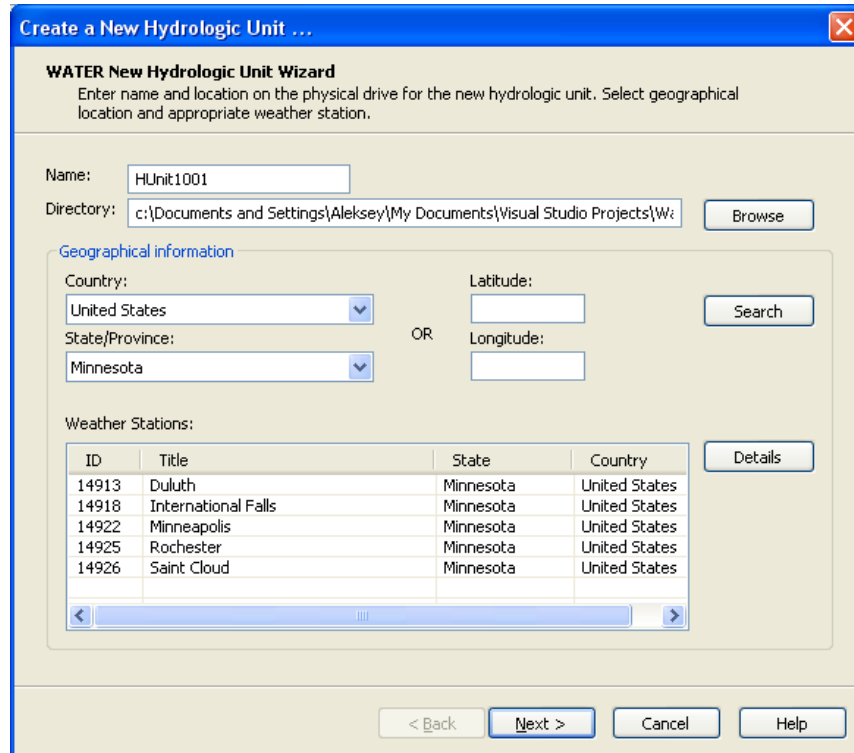


Figure 2.17. A New Hydrologic Unit Window. More Unit Properties.

information as a binary file.

The screenshot shows a Windows-style dialog box titled "Route Flow Through Reach". The dialog contains the following elements:

- Title Bar:** "Route Flow Through Reach" with a close button (X).
- Section Header:** "Routing water flow through reach" with a subtitle: "Select name of the routed reach and specify a location for the output files."
- Main Information Section:**
 - Name:** Text box containing "RReach4001".
 - Folder:** Text box containing "c:\Documents and Settings\Aleksy\My Documents\Visual Studio Projects\Wal" and a "Browse" button.
- Used Hydrologic Units Section:**
 - Reach:** Text box containing "Reach3001" and a "Details" button.
 - Watershed:** Text box containing "HUnit1001" and a "Details" button.
- Navigation Buttons:** "< Back", "Next >", "Cancel", and "Help".

Figure 2.19 Main Window for Routing Flow Through a Reach.

New Routed Reach

A flow from the watershed/hydrologic unit can be routed through the reach by clicking on a “New routed reach” menu item or a toolbar button. It would invoke the ‘New routed reach’ wizard window shown in Figure 2.18. Main wizard window presents the following parameters to be edited:

- Name of the routed reach
- Folder
- Name of the watershed used in routing the flow
- Name of the reach used in routing the flow
- Upstream and downstream conditions. WATER retrieves the data information from the reach and lets a user to modify them if necessary. Inflow distributions can also be viewed by clicking on the ‘View distributions’ button
- Initial conditions. Need to be modified or loaded from an external file.
- Numerical method parameters
 - Number of grid points
 - Mannings coefficient

- Numerical method. Recommended method is a Muskingum routing scheme.
- Output printing interval in terms of internal 15 min time-steps

Clicking on the ‘Next’ button would open a next window shown in Figure 2.20. The parameters that can be edited are below:

Figure 2.20. Window for Routing with Additional Computational Parameters.

New Combined Unit

A flow from a subwatershed can be combined with the routed flow from the main subwatershed by clicking on a “New combined unit” menu item or a toolbar button. This action invokes the ‘New combined unit’ wizard window shown in Figure 2.21. Main wizard window presents the following parameters to be edited:

- Name of the combined
- Folder
- Name of the subwatershed used in routing the flow
- Name of the reach used in routing the flow

Clicking on the 'Finish' button would create the unit and the folder on a disk. Input information would be loaded from the subwatershed runoff flow and stored in a 'Route' subfolder.

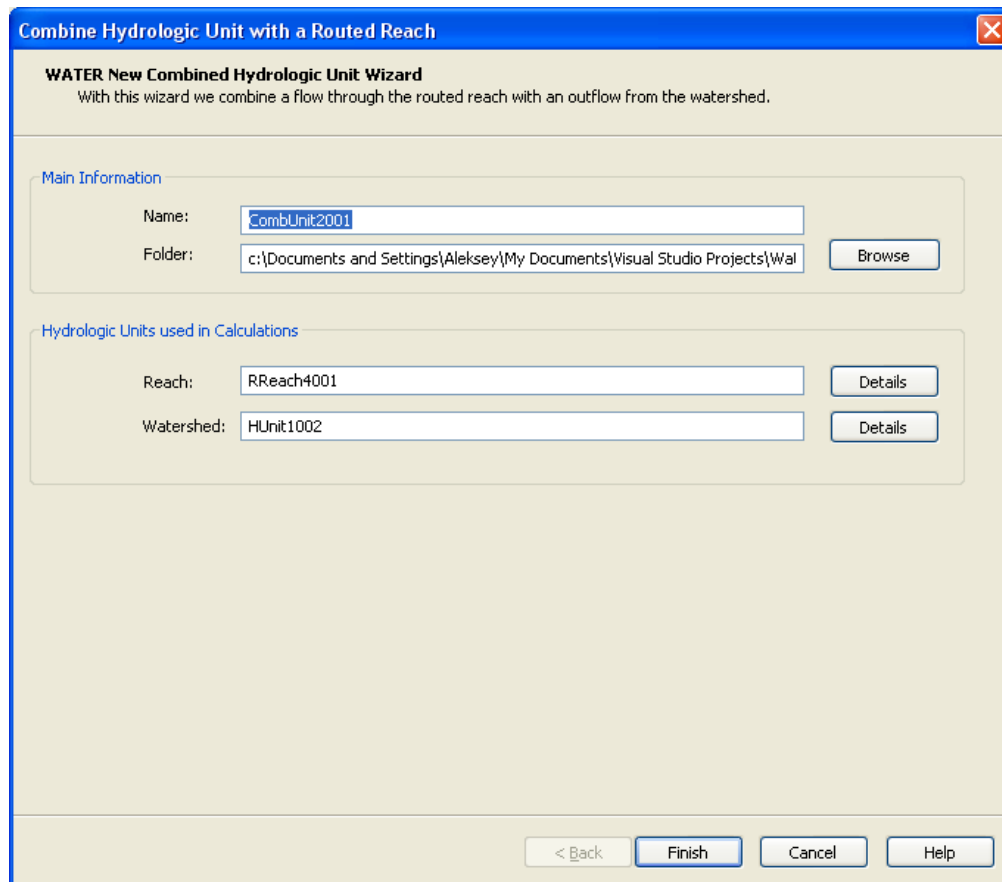


Figure 2.21. Window for Combining the Contribution from the Watershed with Reach Flow.

Properties Dialog Windows

In the previous section we discussed the steps that are necessary to create new projects and hydrologic units. Once the units are created the data content can be viewed and edited by calling the properties dialog windows. All input data is divided into a set of physical properties and a set of simulation options. Dialog windows dealing with both types of the data are discussed below.

Input Parameters

Input parameters are divided into the computational module groups. To accommodate a large set of input parameters and table values, a generic dialog window is used to show values based on the selected computational module. An example of this type of window is shown in Figure 2.22. By clicking on the module in the list control at the left side of the dialog, the input parameters and their values are reloaded. In Figure 2.22, the Excess module is selected,

and the first table from the list of tabular parameters is presented. Switching tabs brings either scalar, or tabular, or group data to show.

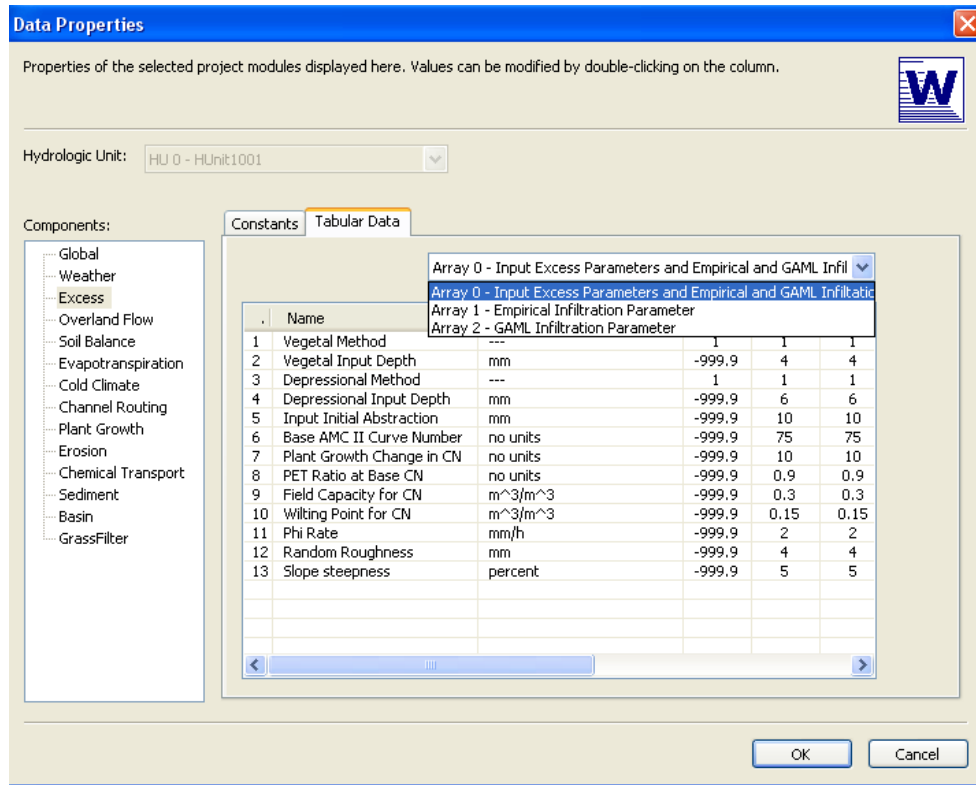


Figure 2.22. Dialog Window for Viewing Input Data Values.

Simulation Options

Simulation parameters are extracted from the general list of parameters and divided into a module groups in the same way used for the physical parameters. In Figure 2.23, three simulation options are shown for the selected overland flow module. Switching computational modules changes the list of parameters in the control box.

Output Results

Overview

Results of simulations are dumped in several ASCII text output files. List of the files depends on the computational module and the type of the hydrologic unit. However, three main files are created in almost every module subfolder. They are:

- debug file with extension 'dbg',
- summary file with extension 'sum'
- main output file with extension 'dat'

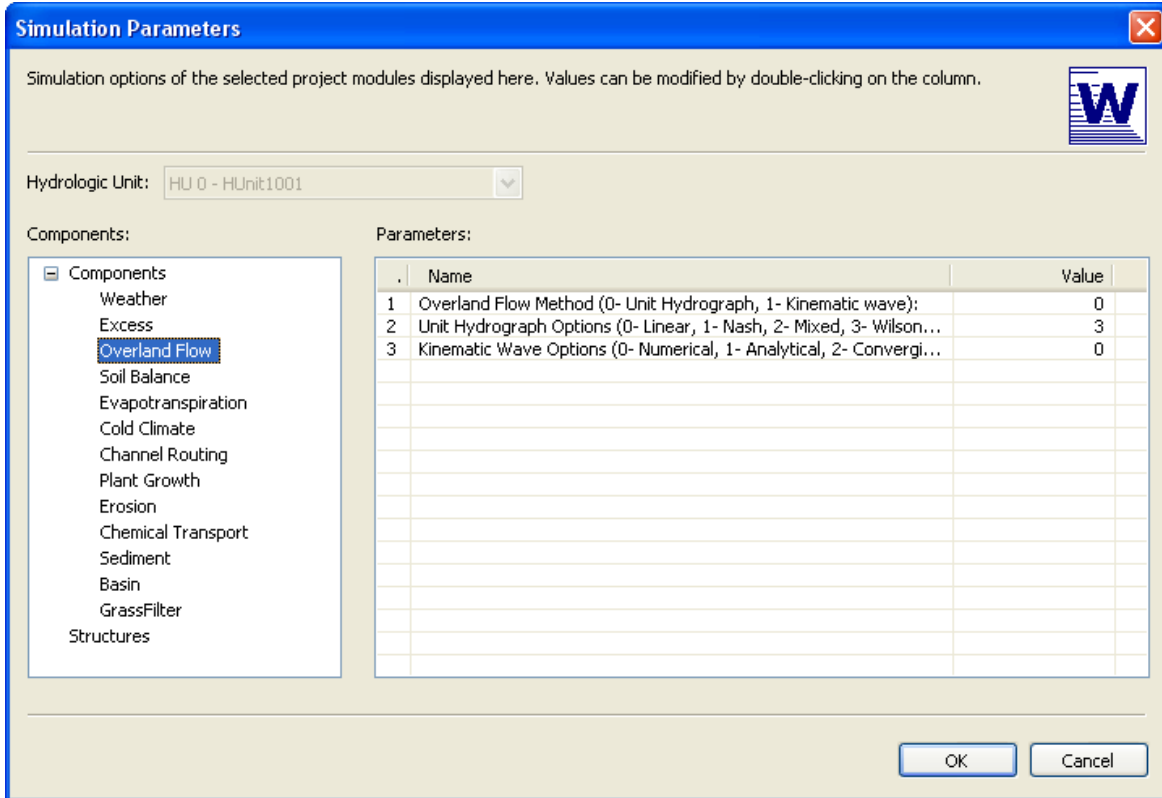


Figure 2.23. A Dialog Window for Viewing/Changing Simulation Options.

To view output files, the following windows were created: (1) window with an embedded text viewer to view debug and summary files, and (2) graphical window with the capability of plotting numerous functions from a long list of output variables stored in main output files.

Debug/Summary Files

Figure 2.24 shows the text viewer window. It consists of two panes: the left pane provides a navigational tree structure with a list of computational modules used in the hydrologic unit, and the right pane controls the viewer itself. Clicking on the modules in the tree switches the content of the viewer according to the applied selection.

Font family, font size, and font color can be changed by clicking on the button in a formatting toolbar.

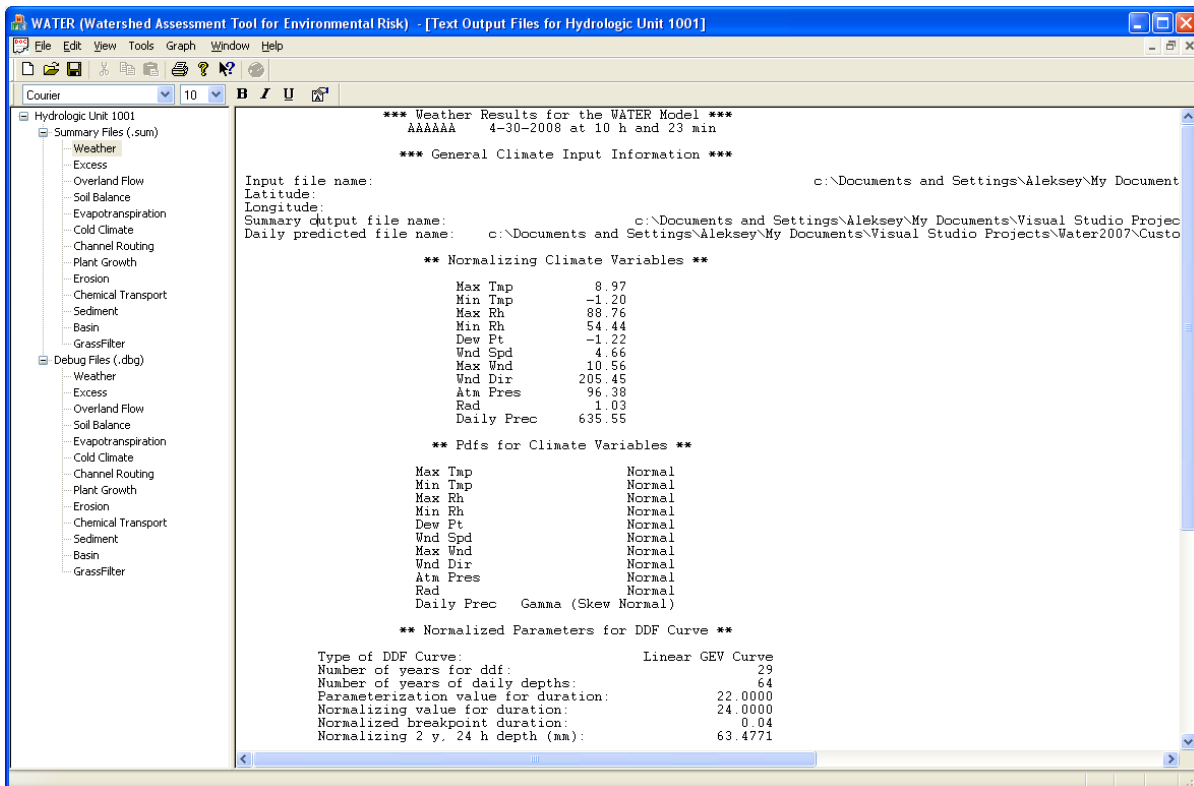


Figure 2.24. Main Window Displaying Output Summary and Debug Files.

Graphical Output

Each computational module produces many sets of output data files stored in a 15 minutes format, as previously discussed. Each column in the main output file stores the results of the column variable with time. Plotting all of these variables is unlikely for most application and therefore users are given the option of selecting variables of greatest interest to them. The dialog window used to select the available graphical output options is shown in Figure 2.25.

In the graphical output window, users first pick a variable from the list of variables for each computational module. They then select a statistical option for that variable and a temporal scale for viewing trends in the statistics. The next step is to add the selected variable to a list of plotting curves in the control box located at the bottom of the window. By clicking on the 'Add as New Curve' button, the user selection is added to the list in the plotting control box. This option is suitable if a user does not want to plot variables, or their statistics, against each other. For the example in Figure 2.25, three curves are selected for plotting. They are maximum temperature, minimum temperatures, and a dew point temperature with respect to calendar day.

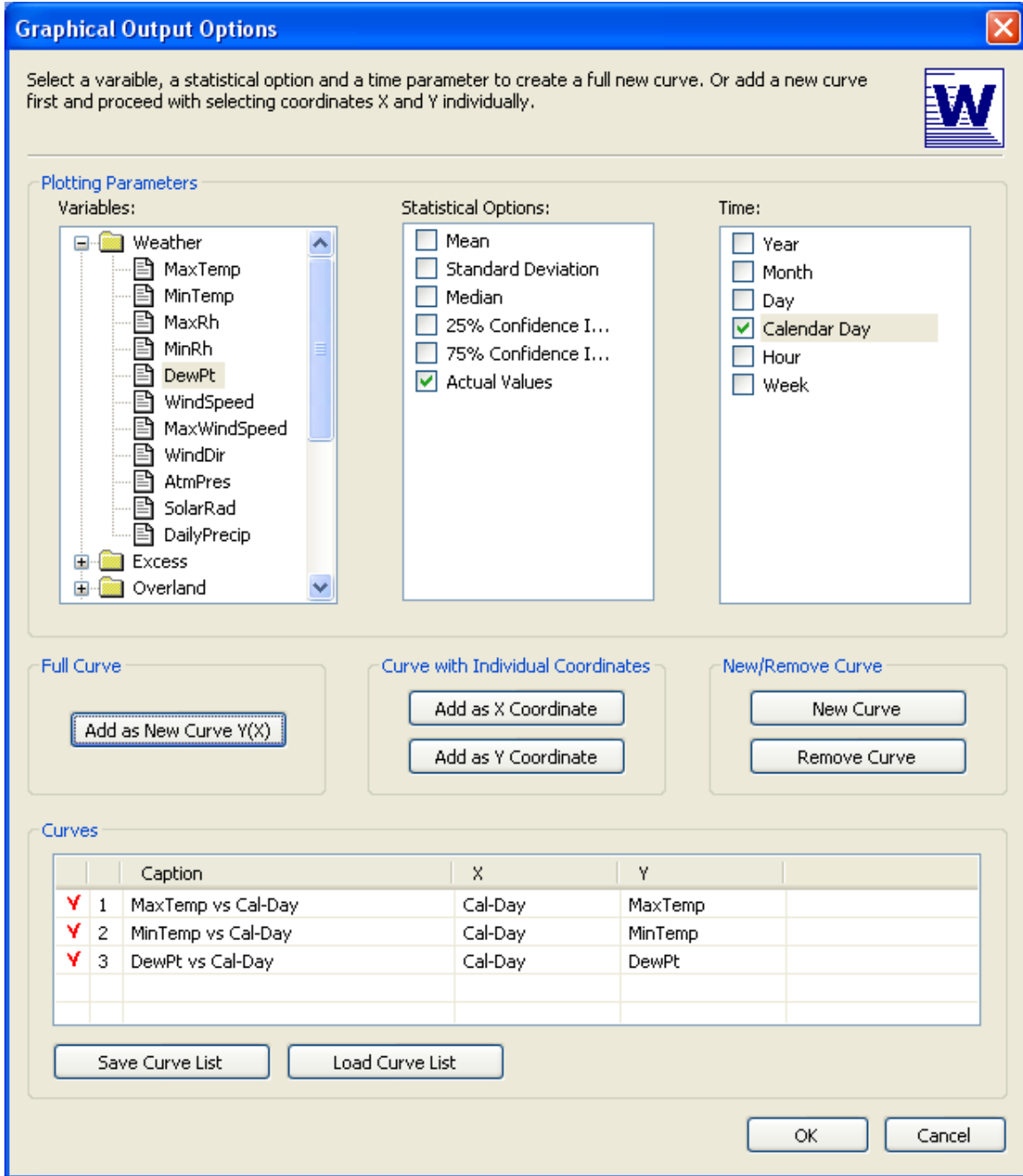


Figure 2.25. Plotting Options Dialog Window.

Another way of adding curves for plotting is to select a variable, along with its statistical option, and add it as a X or Y coordinate of a newly created curve. The second coordinate for that curve also needs to be selected and added for proper plotting. If the user accidentally adds an incorrect curve, it can be easily removed from the list by clicking on the ‘Remove Curve’ button. The list of the curves can be saved to the file and reloaded in the future by clicking on

two appropriately labeled buttons at the bottom of the dialog. Accepting the list by clicking on the ‘OK’ button returns the user to a main graphical output window shown in Figure 2.26.

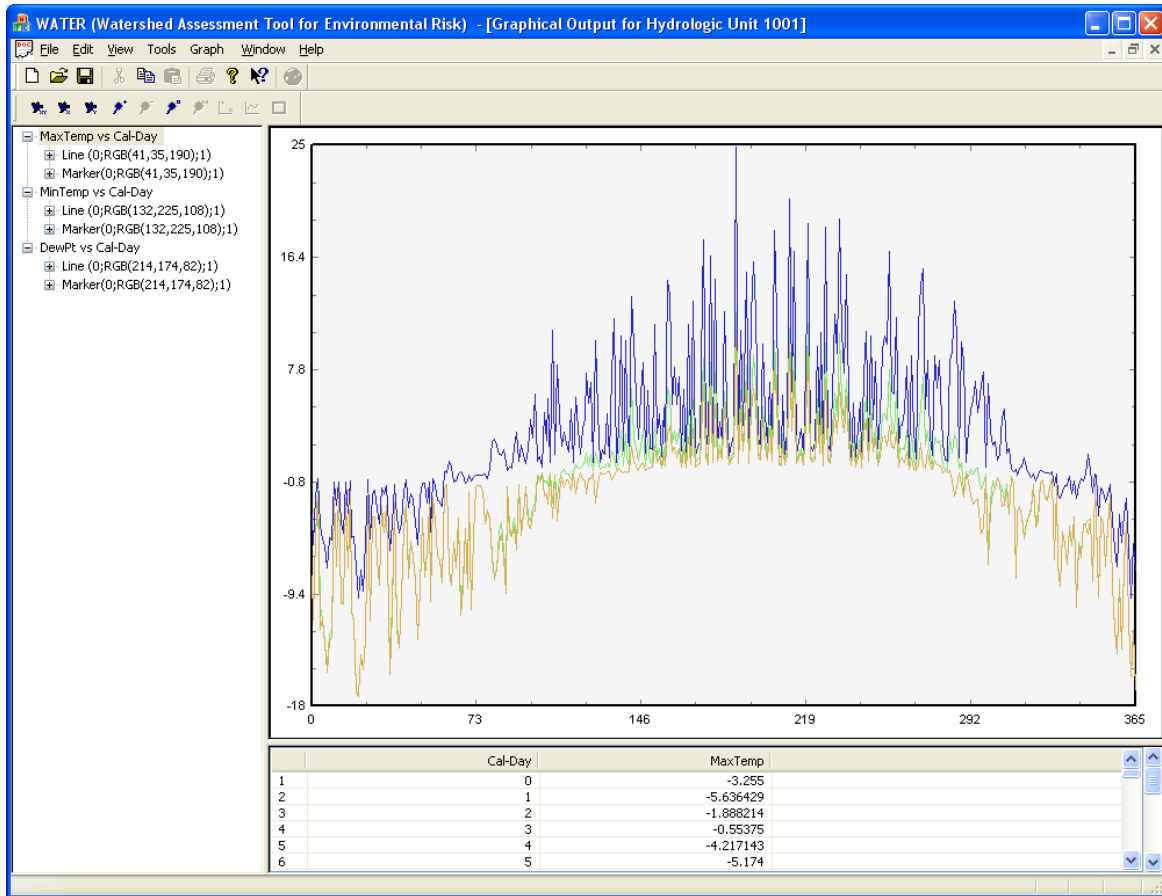


Figure 2.26. Main Graphical Output Window. Plotted Curves Can Be Added/Removed by Users.

The graphical window shown in Figure 2.26 is divided into three panes:

- Left pane with a tree structure of the uploaded curves selected in an Options dialog
- Bottom-right pane that presents data values of the selected curve
- Top-right pane of the main chart window that shows all the curves from the left pane and highlights the selected curve

Operations like zooming in and out, panning the plot, invoking the chart properties dialog, etc, can be called by clicking on menu items in a menu group called ‘Graph’ or button on the graph toolbar. The chart control properties window is presented in Figure 2.27 with several tabs with useful plotting options. The options for the ‘Elements’ tab is shown in Figure 2.27. Examples of properties on that tab include providing the user the option of changing the name of the curve and changing the attributes, such as a line type, line color, and width.

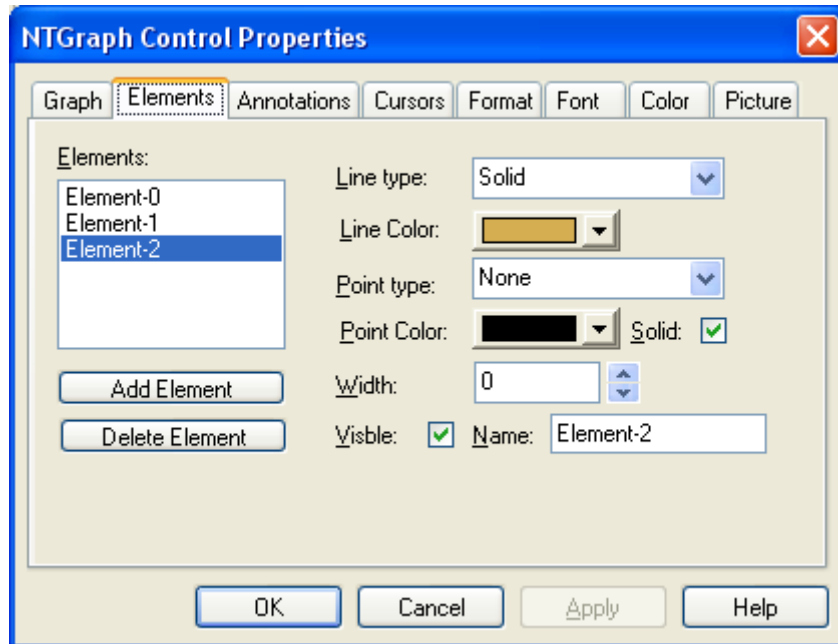


Figure 2.27. Plotting Options Control Window.

Simulate Multiple Land Uses

Impacts of construction activities at watershed scales typically need to combine flow and sediment from multiple land uses within the watershed. Most users of WATER will simulate the response for different land uses by changing the hydrologic and sedimentologic input parameters. Different modeling algorithms might also be selected by advanced users. After the response has been computed for each land use, the flows and sediment need to be routed through the fluvial network of channels and streams and combined to determine the overall response. Computational steps used in WATER to define the fluvial network and appropriate hydrographs and sedimentgraphs are given in this chapter. Details of the algorithms for generating the flows and sediment and for routing them through channels are given in Chapter 3. Details of the use of the graphical user interface for input and output have been previously explained.

An illustrative schematic of a watershed with multiple land uses is shown in Figure 2.28. Here five different land uses have been identified corresponding to the five separate subwatersheds. These different subwatersheds are referred to as Hydrologic Units (HU) with designators one through five (HU-1,..., HU-5). Each hydrologic unit has its own set of input parameters. Three channel reach segments are also shown in Figure 2.28 (R-1 through R-3). Each of these reaches has its own set of channel routing parameters. The circles corresponding to C-1, C-2, and C-3 are points in the watershed where flows and sediment are combined.

The user has the responsibilities of specifying the sequence of operations necessary to obtain

the total response of the watershed. Typically, there is not a unique sequence to simulate properly the watershed response. One straightforward approach for the watershed in Figure 1 is to first simulate the hydrologic and sedimentgraphs for each of the hydrologic units. The flow and sediment values are then available to be routed through the channel network and to be combined with flows from other areas. For example, the flow and sediment from UH-1 can be routed through R-1 to obtain a routed UH-1 hydrograph and sedimentgraph at C-1. These routed values can be combined with the runoff from UH-2 to obtain the response from the total drainage area upstream of C-1. These steps can be repeated for the other branch in Figure 1 consisting of UH-3 and UH-4. The hydrographs and sedimentgraphs at C-1 and C-2 can then be combined to obtain the total response at the confluence of the two branches (i.e., C-3). The final steps are to route the C-3 hydrograph and sedimentgraph through Reach R-3 and combine these routed values with the runoff from HU-5. These steps result in the total watershed response at C-4.

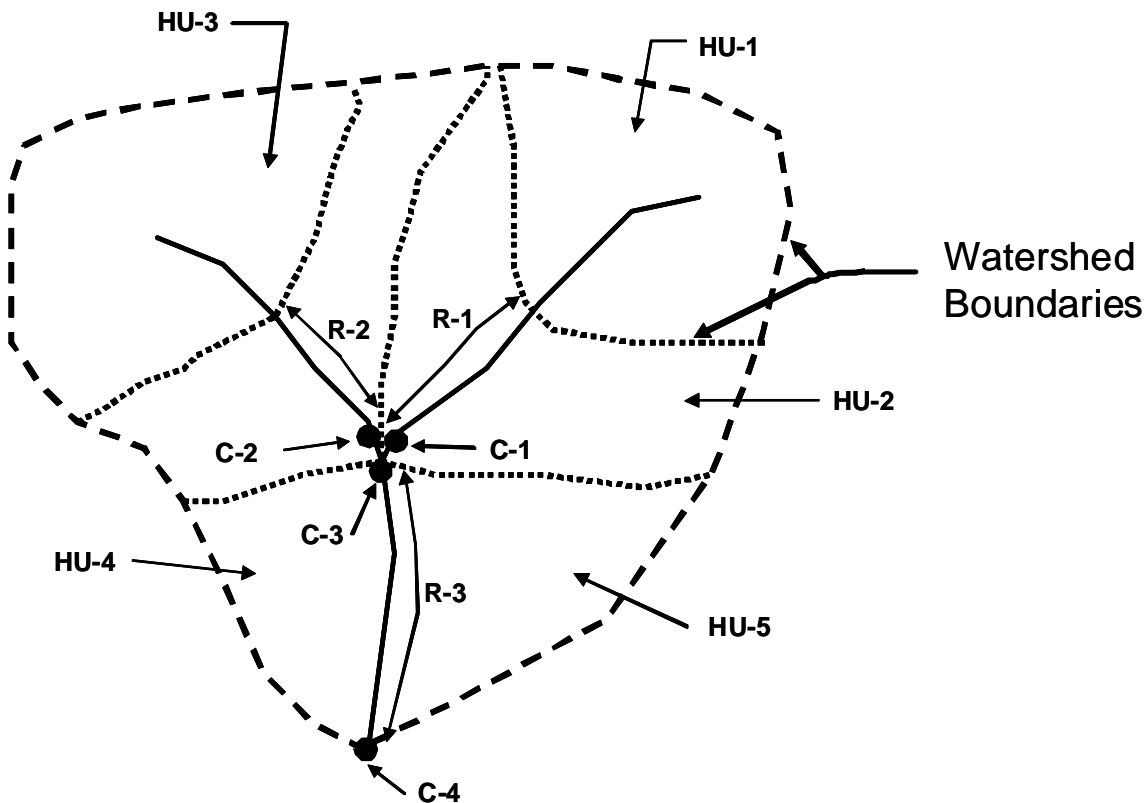


Figure 2.28. Illustrative Schematic of a Watershed with Multiple Land Uses.

GIS Viewer in WATER

Overview

The WATER model has capabilities of viewing GIS maps, editing shapefiles, and working with the geospatial characteristics of the GIS layers. These features are the first steps in creating hydrologic tools to delineate the watershed/drainage areas and to calculate main

geographical information, such as a watershed area, soil types, and topography parameters. The input parameters for the WATER model can be computed from this information.

The MapWinGIS ActiveX control discussed in details below is used as a set of base classes to create a GIS view window. The main class, called CGisData, has been developed to store the information of GIS layers, manipulate with the base MapWinGIS classes, and transfer the data to/from the GIS View class.

MapWindow Project and MapWinGIS Control

MapWindow project and its ActiveX control, MapWinGIS, is an open source geographic information system (GIS) and an application programming interface (API) distributed under the Mozilla Public License and built upon the Microsoft .NET Framework (same framework of the WATER model). MapWindow was developed by Dr. Daniel Ames and the team he leads at the Idaho State University. In 2005, the United States Environment Protection Agency (EPA) adopted MapWindow as the core GIS platform for its BASINS watershed analysis and modeling software.

- MapWindow is more than just a data viewer. It is an extensible geographic information system. This means that advanced users or developers can write plug-ins to add additional functionality (models, special viewers, hot-link handlers, data editors, etc) and pass these along to any number of the user's clients.
- MapWindow includes standard GIS data visualization features as well as DBF attribute table editing, shapefile editing, and data converters. Dozens of standard GIS formats are supported, including Shapefiles, GeoTIFF, ESRI, ArcInfo, ASCII, and binary grids.
- MapWindow also includes a complete ActiveX component which may be used to instantly add GIS capabilities to the user's existing software product.

To summarize, MapWindow is a mapping tool, a GIS modeling system, and a GIS API. The core MapWindow component is ActiveX control (MapWinGIS) that has been optimized for fast image and raster display including APIs for low-level access to spatial data. WATER utilizes MapWinGIS as a core component to display the layers of the map and uses its objects for data manipulation.

Objects in MapWinGIS


The MapWinGIS control has 19 class objects and 21 enumerations embedded in it. A brief description of these class objects and enumerations are given below. Not all of them have been implemented in the current version of WATER. Classes, such as Map, Shapefile, Point, Extents, Shape, and Utils, are used extensively to display maps, change layer properties, view attributes of the shapes, and calculate the distance. The classes are:

1. *ESRIGridManager* An ESRI grid manager object provides functions which facilitate using ESRI grids with MapWinGIS.
2. *Extents* Extents objects store information about other objects extents properties. Objects in MapWinGIS such as the Map, Shape, and Shapefile all have extents as a property. The extents properties tell us where in the map an object lies, what area is included in the

entire map, or where on the map the current map view is located. Extents can be used to set the zoom to include only a certain region specified by extents.

3. *Field*: A field object is used to store information about a field in a table.
4. *Grid*: A grid object is used to represent a grid which can be added to the map.
5. *GridColorBreak*: A grid color break object defines how a specified region of a grid will be colored using the grid color scheme containing the grid color break.
6. *GridColorScheme*: A grid color scheme defines how a grid will be colored. A grid color scheme may either contain grid color breaks created by the user, or may use a predefined color scheme.
7. *GridHeader*: A grid header object is used to hold the information contained in a grid's header.
8. *Image*: An image object is used to represent an image which may be added to the map.
9. *Map*: A map object represents a map which displays grids, images, and shapefiles. This is the cornerstone of the MapWinGIS ActiveX control.
10. *Point*: A point object represents a point with x, y, Z, and M values. Shapes created by adding point objects to the shape.
11. *Shape*: A shape object represents a geometric shape which can be added to a shapefile which is displayed in the map.
12. *ShapeNetwork*: A shape network is created from the shapes in a polyline shapefile which allows the developer to traverse the shapefile simulating water flowing in a watershed to a single outlet.
13. *Shapefile*: A shapefile object is an object containing shapes which define how it is to be displayed in the map.
14. *ShapefileColorBreak*: A shapefile color break object defines how a specified region of a shapefile will be colored using the the shapefile color scheme containing the shapefile color break.
15. *ShapefileColorScheme*: A shapefile color scheme defines how a shapefile will be colored. A shapefile color scheme contains shapefile color breaks which define how specified regions within the shapefile are colored.
16. *Table*: A table object is used to store information from the dbf file associated with a shapefile.
17. *Tin*: A tin object represents a tin which may be displayed in the map. A tin may be created from a grid, or opened from file.
18. *Utils*: A utils object provides access to a set of utility functions to perform a variety of tasks on other objects such as grids, images, points, shapes, shapefiles, tins, etc.
19. *Vector*: A vector object is used to represent the light source for a grid color scheme.

GIS Control

In WATER, the GIS viewer is offered as an alternative view of the main page. Clicking on the  button in the main toolbar switches the view from the main navigation window to the GIS viewer and back. While switching between the views, the information about the view data is stored in internal structures and immediately updated when the focus is back to the view so the user does not lose the work he/she has been working on. However, saving the project frequently is recommended.

The GIS viewer consists of two subwindows with a list of active/loaded map layers in the left pane and an actual map in the main pane. An example of the main pane is shown in Figure 2.29.

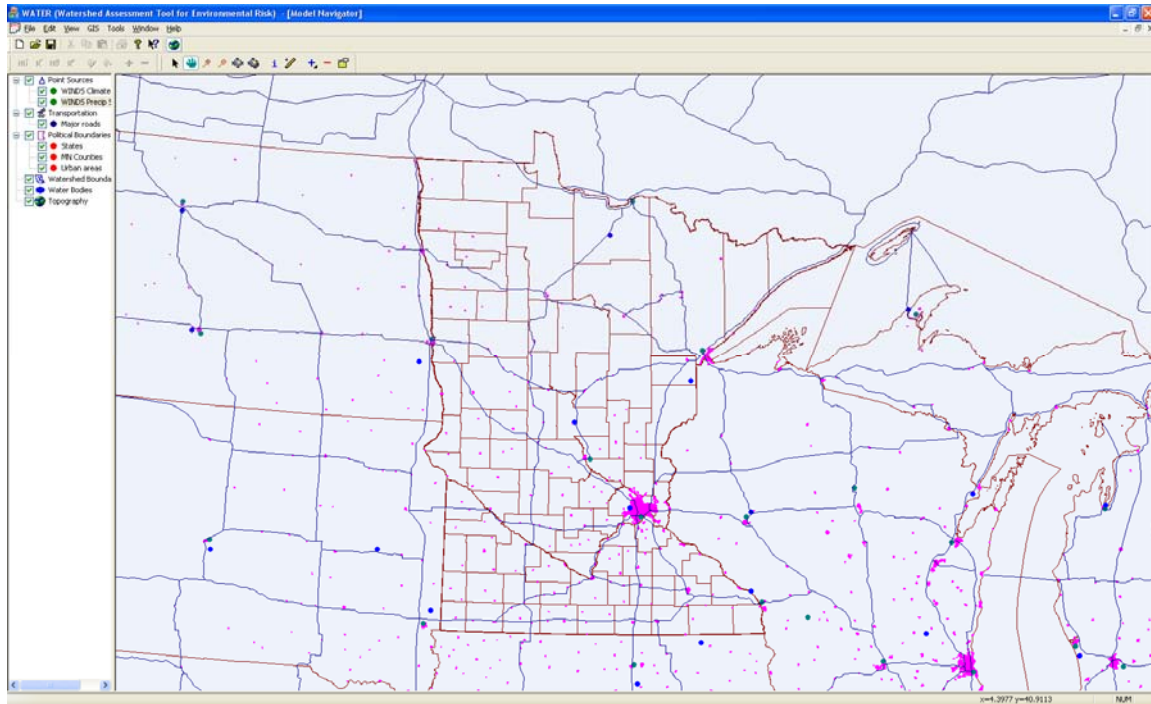
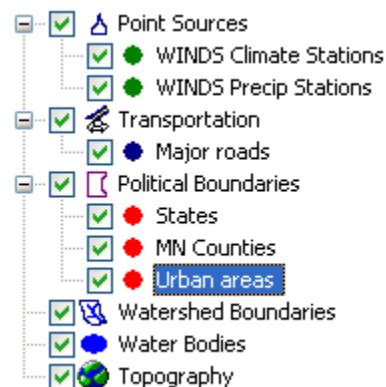


Figure 2.29. GIS Main Paine Window.

List of the layers is subdivided into the following categories with the layers loaded according to their physical meaning:

- Point sources
- Transportation
- Political boundaries
- Watershed boundaries
- Water bodies
- Topography




The user can move layers from one category to another and also move them forward and backward in the map to create a desirable view. It is recommended to have topography layers at the bottom of the layered list and point sources on top of it so all the layers stay visible. While the user hovers the mouse over the map, coordinates of the arrow pointed in the map are displayed in the status bar.

GIS Toolbar

To help the user manipulating with the view of the layers the GIS toolbar is created. It consists of 11 hot buttons, shown in Figure 2.30, clicking on which invokes a certain map operation or a map tool.



Figure 2.30. GIS Toolbar.

Viewing properties of the layer can be changed by clicking on the button  and using the pop-up modal dialog window. The available properties depend on the type of the layer whether it's a polygon type, a polyline type, or a point type. Shape labels can be set by clicking on the label details button.

The ruler tool shows the distance between two map points. The user has to invoke the dialog window first and then click on two points consequently. The dialog would show the coordinates of the two points and the distance between them in miles or kilometers.

The attribute dialog shows the characteristics of the selected shape. It consists of two columns with the field name to the right and the field value to the left. The list of field names is the same for all shapes in the layer while it may differ by selecting another layer. The field values of the shape attribute cannot be changed.

Chapter Three

Algorithms for Off-Site Practices and Channel Routing

Introduction

The original WATER model allowed only on-site practices, such as mulches and erosion-control blankets, to be evaluated as part of sediment control plans (Wilson et al., 2006). Many SWPPPs also need to use off-site sediment control practices to be successful. Routines have, therefore, been added to the WATER model to simulate the impact of off-site practices of rock check dams, vegetative filters, and detention ponds. The prediction of sediment removal by rock check dams is based on the approach used by Wilson et al. (1984) for surface mined lands. The sedimentation effectiveness of vegetative buffers is modeled by modifying the GRASSF model (Wilson et al., 1984). Routines to predict the response of detention ponds is based on the BASIN (Basin Analysis of Sediment-laden INflow) model developed by Wilson and Barfield (1985) and modified by Oolman and Wilson (2003). Particularly important changes in the BASIN model are made to allow rock and gravel infiltration filters to be included as an off-site practice. Development of the algorithms to model infiltration filters is given in Chapter 4. Description of the routines to simulate rock check dams, vegetative filters and detention ponds in general are given in the first section of this chapter.

Flow and sediment from different areas within a watershed need to be routed through channels and/or stream networks and to be combined to determine the overall response of the watershed. These processes were not included in the original WATER model. Volumetric flow rates are typically attenuated by their movement through fluvial channels. The WATER model has embedded code to route these flows through channels using the relatively simple Muskingum method and using the solution of one-dimensional equations for motion and mass balance (so-called St. Venant equations). The transport of eroded sediment through channels is also an important process for predicting watershed response. Sediment load between upstream and downstream points can either increase because of channel scour or decrease because of sediment deposition. Since the influent load for construction sites is usually large, sediment deposition is of greater interest for our modeling efforts. Rigorous analysis of sediment movement is beyond the scope of the project. In the WATER model, code has been added to route sediment movement through channels using a relatively simple delivery ratio approach and using a sediment transport relationship. These two modeling approaches are described in the final section of this chapter.

Off-Site Sediment Control Practices

Check Dams

The removal of sediment by rock check dams is modeled using the approach proposed by Hirschi (1981) and implemented by Wilson et al. (1984). With this approach, deposition is modeled over a longitudinal distance from a point that is 10% larger than normal depth to the outlet of the check dam. This longitudinal distance is computed using a single step

backwater curve. A simple triangular channel is assumed to represent the geometry of the channel. An important input parameter is the rock porosity. A critical assumption is that the outlet velocity through the check dam is equal to the product of the porosity and the velocity corresponding to the normal depth. Unsteady flow is represented by a series of step functions corresponding to the time increment of the inflow hydrograph.

Trap efficiency of the check dam is dependent on the detention time, fall distance and particle sizes of the influent sediment. Detention time of the check dam is obtained by dividing the longitudinal distance (from the backwater curve calculation) by the flow velocity. The flow velocity is approximated by the average of the normal velocity and the outlet velocity. Likewise, the fall distance is computed by the average of normal depth and the depth at the outlet. For a known detention time and fall distance, the trap efficiency is computed using a relationship similar to that given by Camp (1945).

Vegetative Filters and Buffers

A modified GRASSF code is used to simulate the sedimentation effectiveness of a vegetative buffer strip. GRASSF was developed from a series of studies investigating the ability of an erect media to trap sediment. The initial tests on erect media consisted of studies on metal pegs, but were later extended to grasses. Laboratory studies were used to develop predictive equations for bed load transport (Tollner et al., 1977) and for suspended load transport (Tollner et al., 1976). The application of these equations has been further modified by Hayes et al. (1979), Barfield and Hayes (1980) and Wilson et al. (1984). Changes in the GRASSF were necessary to accommodate the influent sediment characteristics of the WATER model.

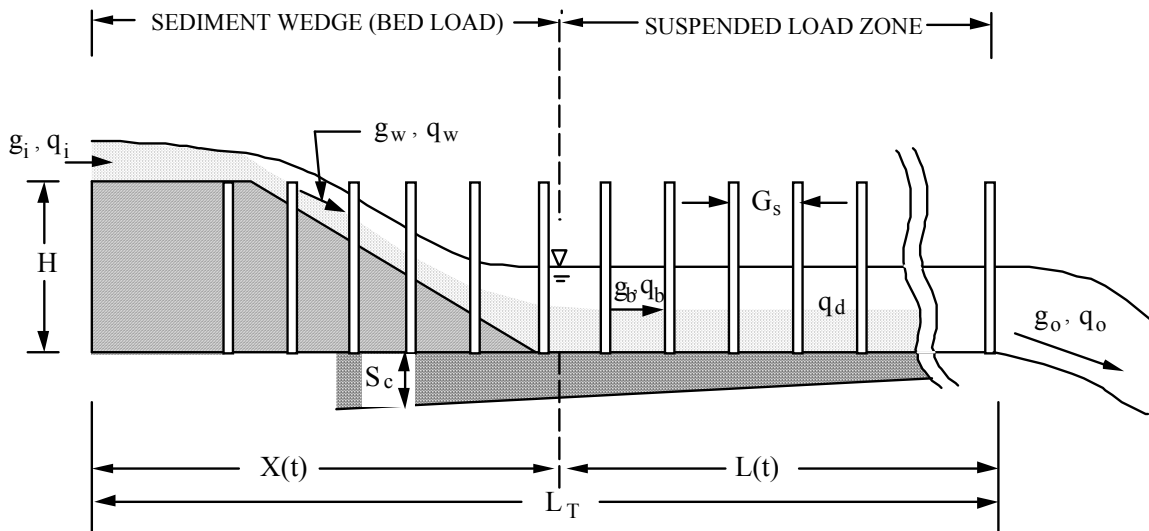


Figure 3.1. Schematic of a Vegetative Filter.

Experimental studies have found the general deposition pattern in vegetative filters as shown in Figure 3.1. As sediment laden flow impinges on the filter, a reduction in its velocity causes the transport capacity to be lowered, which allows sediment deposition to occur. In GRASSF, the bed load material is deposited in the sediment wedge. The suspended load is

trapped in the remaining portion of the filter

Einstein's bed load dimensionless parameters, calibrated using laboratory data, are used to calculate the transport capacity of bed material in the filter (Tollner et al., 1977). Bed load transport in a grass filter is predicted as

$$g_b = K \frac{(R_s S)^{3.57}}{d_p^{2.07}} \quad (3.1)$$

where

$$K = \frac{40367 SG}{(SG - 1)^{3.07}} \quad (3.2)$$

In the above expression, g_b is the bed load transport rate [N/m/s], R_s is the spacing hydraulic radius [m], and d_p is the diameter of the particle [m]. The characteristic hydraulic dimension is the spacing hydraulic radius and is defined by an analogy between the spacing of grass elements and a rectangular channel of the same width.

As shown in Figure 3.1, the suspended load zone extends from the base of the deposition wedge to the outlet of the filter. In contrast to the Einstein's bed-load dimensionless parameter used in the sediment wedge, the suspended load zone is analyzed using the dimensionless Reynolds' number (measure of turbulence) and the dimensionless fall number (measure of settling characteristics). Tollner et al. (1976) predicted the trap efficiency of the suspended load zone as

$$T_s = \exp \left[-0.00105 \frac{R_e^{0.82}}{N_f^{0.91}} \right] \quad (3.3)$$

where

$$N_f = \frac{L \omega_s}{V h} ; R_e = \frac{V R_s}{\nu} \quad (3.4)$$

and where T_s is the trap efficiency of suspended sediment, N_f is the particle fall number, R_e is the Reynolds' number, L is the length of the suspended sediment zone, ω_s is the settling velocity of the particle, V is the flow velocity, h is the flow depth, ν is the kinematic viscosity, and R_s is the spacing hydraulic radius. In Equation 3.3, the predicted trap efficiency increases with an increase in particle fall number and decreases with an increase in Reynolds' number.

The trap efficiency of sediment in the suspended zone is adjusted for accumulation of sediment on the bed and for infiltration losses. The accumulation of sediment on the filter bed reduces trap efficiency because the stools and grass indentations are filled. The infiltration losses increase trap efficiency because sediment particles are carried to the filter's bed with the downward movement of the transporting fluid.

The GRASSF model has been previously tested on observed data collected by Hayes (1979) on five vegetative strips located on the University of Kentucky experimental farm. Inflow hydrographs and sedimentgraphs were obtained by spraying an inclined platform containing spoil material. This procedure yielded a nonhomogeneous particle size distribution and an unsteady inflow sedimentgraph. The ability of GRASSF to predict effluent concentration is

very good (Wilson et al., 1984).

Detention Ponds

The removal of sediment by detention ponds is predicted using a modified BASIN (Basin Analysis of Sediment-laden INflows) model. This model is based on a mass balance for an infinitesimal layer using advection-diffusion processes. Although it has a relatively simple structure, it still accounts for most of the physical processes affecting sedimentation including turbulent diffusion and bed scour. In addition to modifications to be consistent within the framework of the WATER model, changes have been made to allow for rock and gravel infiltration filters. Most of the changes for rock infiltration filters are given in Chapter 4. Only those changes in the hydrologic routing will be given here.

In the BASIN model, the pond is divided into a series of chambers of equal volume, analogous to a series of reactors in chemical engineering literature. This concept is illustrated in Figure 3.2. Sediment mixing, settling, and resuspension are considered by subdividing the chamber into rectangular shaped layers. The mass balance for an infinitesimal layer can be derived as (Wilson and Barfield, 1985):

$$\frac{\partial C}{\partial t} = \frac{Q_{i-1}v_f}{EV_i} [C_p - C] + \omega_s \frac{\partial C}{\partial z} + \frac{\partial}{\partial z} \left(\epsilon_s \frac{\partial C}{\partial z} \right) \quad (3.5)$$

The symbols Q_{i-1} , EV_i , and AD represent discharge into the reactor chamber, effective reactor volume, and average reactor depth, respectively, C , ω_s , and ϵ_s are the sediment concentration, settling velocity and turbulent diffusion coefficient, respectively. In Equation 3.5, the first term on the right-hand side represents the advection rate of sediment into the reactor chambers. This term determines the residence time of the sediment particles. The second and third terms are used to predict the rate of sediment settling and the rate of turbulent diffusion, respectively. For numerical solution and for specification of boundary conditions, Equation 3.5 is more conveniently written as

$$\frac{\partial C}{\partial t} = \frac{Q_{i-1}v_f}{EV_i} [C_p - C] - \frac{\partial F}{\partial z} \quad (3.6)$$

where

$$F = -\omega_s C - \epsilon_s \frac{\partial C}{\partial z} \quad (3.7)$$

where F represents the net flux rate of sediment by turbulence and settling.

Equation 3.6 is a linear differential equation. Therefore the total concentration can be obtained by solving the concentration independently for different particle size classes. This is a necessary step because of the large variation in ω_s , with size class. In BASIN, a maximum of nine different particle size classes can be evaluated.

At the pond's bed, the net rate of scour or mass transfer rate at the boundary can be written as

$$F_b = S_f - \omega_s C \quad (3.8)$$

where F_b is the net flux rate at the pond's bed (i.e., net scour rate), S_f is the detachment rate per unit area, and other terms are as previously defined. In BASIN, the detachment rate from the pond's bed is predicted by modifying Wilson (1993) detachment theory.

The numerical solution for Equation 3.6 is obtained by modifying the hybrid difference scheme given by Dhamotharan et al. (1981). The solution can then be formulated in the following matrix solution

$$\mathbf{AC} = \mathbf{B} \quad (3.9)$$

where \mathbf{A} is a $n \times n$ tridiagonal matrix with known coefficients, \mathbf{C} is a column vector of unknown concentration values at each node point for the current time step, and \mathbf{B} is a column vector of known quantities from advection between reactors and from previous time step values. Equation 3.9 can be solved for \mathbf{C} by using simple numerical techniques as given by Wilson and Barfield (1984).

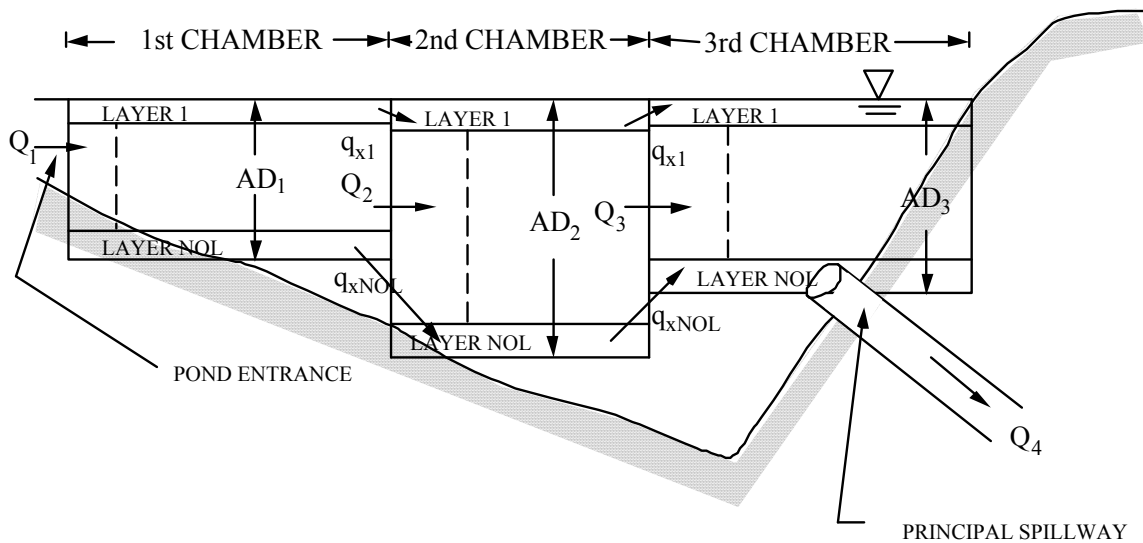


Figure 3.2. Cross-sectional View of a Hypothetical Pond.

Sediment detention ponds rarely have the ideal geometry as assumed in the model development. As is shown by Figure 3.2, the maximum distance that a particle must fall to become trapped varies between the inlet and outlet of the pond. In BASIN, this variation in depth is modeled using a volume-weighted depth for each reactor chamber. In Figure 3.2, the volume-weighted depth is represented by symbols AD_1 , AD_2 , and AD_3 . The volume-weighted depth varies with the changing water level in the pond.

A mass balance for the entire pond using a constant density fluid provides the foundation for determining the volumetric outflow rate. The mass balance equation is

$$I - O = \frac{dS}{dt} \quad (3.10)$$

where I is the volumetric inflow rate that is known from other computations in the WATER model, O is the unknown volumetric outflow rate, and S is the unknown storage volume in the pond. The solution to Equation 3.10 typically uses topographic areas for the pond and the hydraulics of pipes and open-channel flows to obtain relationships between O and elevation and between S and elevation. In the original BASIN model, these relationships were combined with Equation 3.10 to obtain the outflow rate using the Puls method (Wilson and Barfield, 1984). This method is reasonable when the outflow rate is constant for the same elevation of water in the pond. However for a rock infiltration filter, the outflow rate at the

same water elevation potentially changes with deposition. An alternative framework is to evaluate the mass balance equation as

$$\frac{I_i + I_{i-1}}{2} - \frac{O_i + O_{i-1}}{2} \approx \left(\frac{dS}{dEl}\right) \left(\frac{dEl}{dt}\right) \approx A_s \left(\frac{\Delta El}{\Delta t}\right) \quad (3.11)$$

where El is the water surface elevation, the average inflow and outflow rates are used for the numerical time step and the surface area (A_s) is defined as dS/dEl . The subscript “i” refers to the value at the end of the time step and “i-1” refers to the value at the beginning of the time step. By using Taylor series expansion for the outflow (using previous time step values), the outflow at the end of the time step can be written as

$$O_i = O_{i-1} + \left(\frac{dO}{dEl}\right)_{i-1} \Delta El + [\text{Higher Order Terms}] \approx O_{i-1} + \left(\frac{dO}{dEl}\right)_{i-1} \Delta El \quad (3.12)$$

By using this equation, the mass-balance equation can be written as

$$I_i + I_{i-1} - 2O_{i-1} - (dO/dEl)_{i-1} \Delta El = 2A_s \left(\frac{\Delta El}{\Delta t}\right) \quad (3.13)$$

from which the rate of change in elevation is defined as

$$\frac{\Delta El}{\Delta t} = b_{el,i} = \frac{I_i + I_{i-1} - 2O_{i-1}}{2A_{s,i-1} + (dO/dEl)_{i-1} \Delta t} \quad (3.14)$$

where, for simplicity, the surface area is based on the previous time step value. The elevation at the end of the time step is then defined as

$$El_i = El_{i-1} + b_{el,i} \Delta t \quad (3.15)$$

Outflow rate, storage volume, average settling depths, and surface area are computed from the elevation obtained from Equation 3.15.

The accuracy of BASIN has previously been compared to observed results gathered on two different pilot scale ponds. A total of twelve sediment laden runs were evaluated. The pond model did an excellent job of predicting the shape of the effluent sedimentgraphs. Relative to the peak influent concentration, the peak effluent concentration was predicted with reasonable accuracy. In general, the pond model tended to overpredict the effluent concentration for high influent concentration runs. The model was sensitive to possible errors in the particle size distribution.

Channel Routing of Flows and Sediment

Volumetric Flow Rates

St. Venant Equations

The St. Venant equations are based on a mass balance and an application of Newton’s equation of motion to infinitesimal cross-section of a channel reach. The control volume of interest is shown in Figure 3.3. The equation of motion is strictly based on one dimensional flow. Only an overview of the St. Venant equations is given here. More rigorous development is given by Chow et al. (1988), Chaudhry (1993) and others.

Total volumetric inflow rate into the cross-sectional control volume is the upstream flow rate and the lateral flow rate from the watershed between x and $x+\Delta x$. Storage volume can be

represented as the product of the average cross-sectional area (A) and Δx . For continuous function and for the limit of $\Delta x \rightarrow 0$, the conservation of mass is then defined for a constant density fluid as

$$\frac{\partial Q}{\partial x} + \frac{\partial A}{\partial t} = q_\ell \quad (3.16)$$

where Q is the volumetric flow rate and q_ℓ is the lateral flow rate per unit channel length, x is longitudinal location and t is time. Equation 1 provides one relationship for the two unknowns (assuming lateral flow is known) of Q and A . Therefore, at least one additional equation is needed to define a unique solution.

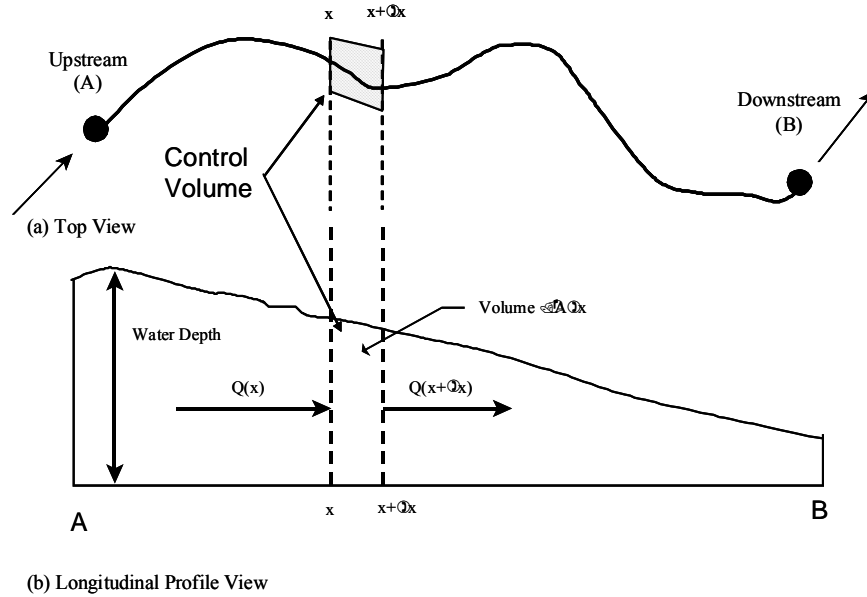


Figure 3.3. Cross-Section of Flow for Development of the St. Venant Equations.

Newton's equation of motion requires that the rate of change in the momentum of the control volume to equal the sum of the external forces acting on it. Key forces acting on the control volume in Figure 3.3 are bed shear stresses (friction force), gravity force (weight), pressure forces (including bank pressure), and expansion/contraction forces associated with bridges and other features of streams.

The equation of motion becomes easier to evaluate by relating the bed shear to the mean flow velocity or flow rate. The average bed shear can be related to mean flow velocity using Manning's equation. Average bed shear is then defined as

$$\tau_b = \frac{\rho V^2 n^2 g}{(1.49)^2 R^{1/3}} = \rho g K_o \left(\frac{V^2}{R^{1/3}} \right) = \rho g K_o \left(\frac{Q^2}{A^2 R^{1/3}} \right) \quad (3.17)$$

where $K_o = n^2 / (1.49)^2$ and where τ_b is the average bed shear, V is the mean flow velocity, n is Manning's roughness factor, ρ is the density of water, g is the acceleration of gravity and R is the hydraulic radius. These relationships are applicable to both uniform and nonuniform flows.

The rate of change in momentum can be evaluated by conducting a momentum balance for

the control volume of Figure 3.3. Let's consider a point velocity $u(z)$ and the momentum per unit volume of ρu . The total advected momentum (M) entering at x can then be evaluated as

$$M(x) = \int_0^{h(x)} (\rho u) u b(z) dz \quad (3.18a)$$

where h is the flow depth and b is the flow width. The momentum coefficient, or Boussinesq coefficient, is defined as

$$\beta = \left(\frac{1}{\rho A V^2} \right) \int_0^{h(x)} (\rho u) u b(z) dz \quad (3.18b)$$

and therefore the advected momentum at x can be obtained by

$$M(x) = \rho \beta A V^2 = \rho \beta V Q \quad (3.18c)$$

The advected momentum of lateral flow can be written as

$$M_\ell = \rho \beta_\ell U_\ell q_\ell \Delta x \quad (3.18d)$$

where U_ℓ is the downslope velocity corresponding to the lateral flow rate.

By using these relationships, the equation of motion allows us to conclude that (Chow et al., 1988)

$$\left[\begin{array}{c} \text{Rate of change} \\ \text{in Momentum} \end{array} \right] = \frac{\partial(\rho Q)}{\partial t} \Delta x + \frac{\partial(\rho \beta V Q)}{\partial x} \Delta x + M_\ell = \sum [\text{External Forces}] \quad (3.19a)$$

The above equation can be simplified by dividing by $\rho \Delta x$ and by using $R=A/WP$, or

$$\frac{\partial Q}{\partial t} + \frac{\partial(\beta V Q)}{\partial x} + \beta_\ell U_\ell q_\ell = -\frac{\tau_b A}{\rho R} + g A S_o - g A \frac{\partial h}{\partial x} - g A E_s \quad (3.19b)$$

where the first term on the right-hand side of the equation is friction force term, the second is a gravity force term, the third is a pressure force term, and the fourth is an expansion force term, where E_s is an gradient term corresponding to the expansion force. The bed shear is often related to friction slope defined as

$$\tau_b = \rho g R S_f = \rho g K_o \left(\frac{Q^2}{A^2 R^{1/3}} \right) \quad (3.19c)$$

The equation of motion can then be evaluated as

$$\frac{\partial Q}{\partial t} + \frac{\partial(\beta V Q)}{\partial x} + \beta_\ell U_\ell q_\ell + g A \frac{\partial h}{\partial x} + g A S_f - g A S_o + g A E_s = 0 \quad (3.19d)$$

where

$$\tau_b = \rho g R S_f = \rho g K_o \left(\frac{Q^2}{A^2 R^{1/3}} \right) \quad (3.19e)$$

By combining the mass-balance equation (i.e., Equation 3.16) with the equation of motion (i.e. Equation 3.19d), and for known lateral flow, expansion losses and Manning's n , we have two equation with four unknowns. The unknowns are Q , A , R , and h . To close the equation set, two additional equations can be obtained from channel cross-sectional information to relate area and hydraulic radius to flow depth.

Numerical methods are required to obtain solutions to the St. Venant equations. An excellent discussion of suitable methods is given by Chaudhry (1993). In the WATER model, code has been written to solve the equations using two explicit finite-difference methods schemes, frequently referred to as the diffusive scheme and MacCormack scheme. These schemes are relatively efficient but are not robust. As an alternative to these approaches, the implicit finite-difference scheme of Preissmann is also used (Chaudhry, 1993). This method provides

for more robust solutions but is computationally more demanding than the explicit schemes. Specification of upstream and downstream flow conditions is necessary to solve the St. Venant equations. Upstream condition is usually the inflow hydrograph.

Muskingum Storage Model

Routing flows through channels with the St. Venant equations generally require an experienced and knowledgeable user to be successful. Simple and robust modeling approaches are, therefore, also useful. These simpler approaches represent flow and storage relationships within a less rigorous and more conceptual framework. Their parameters are often calibrated to observed events. In the WATER model, code has been written to perform channel routing using the relatively simple Muskingum storage method.

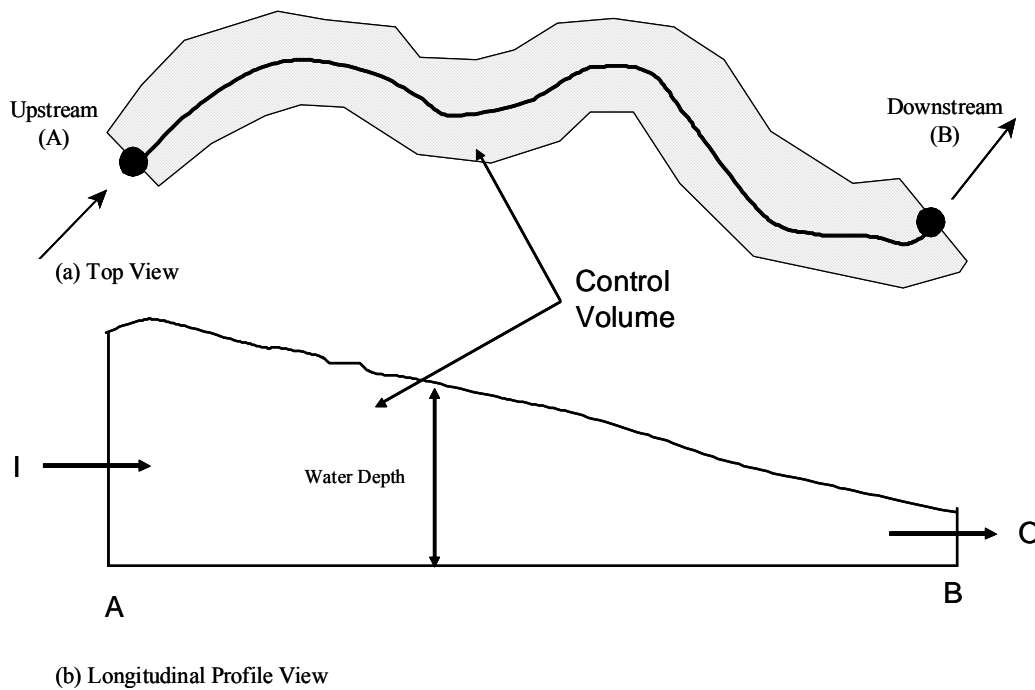


Figure 3.4. Control Volume for the Muskingum Method.

Figure 3.4 shows the control volume used in the Muskingum method. Instead of an infinitesimally small cross section of channel used by the St. Venant equations, the control volume here is the entire channel reach between the upstream and downstream points (A and B). The conservation of mass (for a constant density fluid) for this reach can be written as

$$[I + q_{\ell}L] - O = \frac{dS}{dt} \quad (3.20)$$

where I is the inflow volumetric flow rate, O is the outflow volumetric flow rate, S is storage, and L is the length between the inlet and outlet.

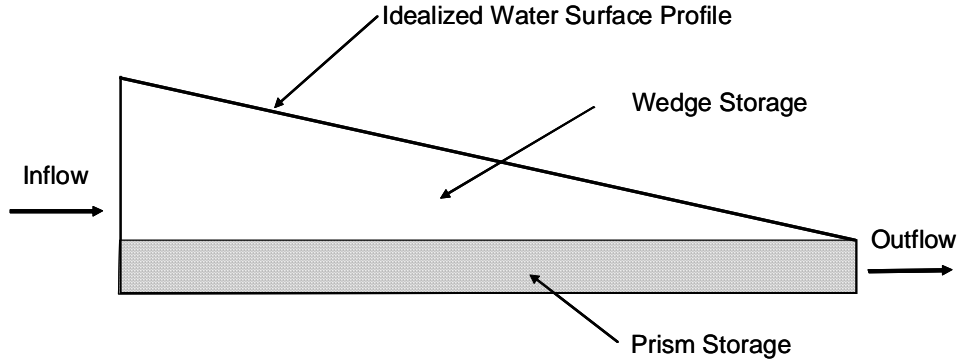


Figure 3.5. Idealized Storage of the Muskingum Method.

The use of Equation 3.20 provides us with one equation and two unknowns (outflow and storage). To close the equation set, an idealized storage representation shown in Figure 3.5 is assumed for the Muskingum method. Here total storage is divided into prism and wedge storage zones. Mathematically, total storage is then defined as

$$S = KO + K\theta(I - O) \quad (3.21)$$

where the first term on the left-hand side is the prism storage component, and the second term is the wedge storage component. The symbols of K and θ are parameters that are assumed to be independent of time.

By combining the mass balance (i.e., Equation 3.20) with the Muskingum storage relationship (i.e., Equation 3.21), we obtain

$$I - O = (K - K\theta) \frac{dO}{dt} + K\theta \frac{dI}{dt} \quad (3.22a)$$

where lateral flow has been neglected. Equation 3.22a can be evaluated numerically by using the average inflow and outflow flow volumes within a time step of Δt . We then obtain

$$\left(\frac{I_i + I_{i-1}}{2}\right)\Delta t - \left(\frac{O_i + O_{i-1}}{2}\right)\Delta t = (K - K\theta)(O_i - O_{i-1}) + K\theta(I_i - I_{i-1}) \quad (3.22b)$$

By rearranging terms, we obtain

$$O_i = C_o I_i + C_1 I_{i-1} + C_2 O_{i-1} \quad (3.22c)$$

where

$$C_o = \frac{-K\theta + 0.5\Delta t}{K - K\theta + 0.5\Delta t}, \quad C_1 = \frac{K\theta + 0.5\Delta t}{K - K\theta + 0.5\Delta t} \quad \text{and} \quad C_2 = 1 - C_o - C_1 \quad (3.22d)$$

To avoid negative flows, Δt should be approximately equal to K , which is often viewed as the travel time throughout the reach. In the WATER model, the reach is subdivided to maintain this condition.

If observed inflow and outflow hydrographs are available, the optimal values of K and θ values can be obtained by calibration (Chow et al., 1988). However, observed hydrographs are rarely available at construction sites. Fortunately, the Muskingum parameters can also be estimated using linearized forms of the equations of motion, with appropriate numerical approximations (see Wilson and Ruffini, 1988). This approach requires the selection of a representative flow rate (Q_o). The storage parameter K is then defined as the travel time for

water to pass from the upstream to the downstream point moving at the kinematic wave speed, or

$$K = \frac{L}{c_{ko}} = \frac{3L}{5V_o} \quad (3.23a)$$

where c_{ko} is the kinematic wave speed corresponding to the representative flow and V_o is the mean velocity corresponding to the representative flow. The wedge storage parameter is defined as

$$\theta = \frac{1}{2} \frac{h_o}{2m S_o L} \quad (3.23b)$$

where h_o is the flow depth corresponding to the representative flow and m is the relationship between friction slope and area defined by a rating curve. If Manning's equation is used, $m=5/3$.

Sediment

Delivery Ratio

Another important channel process is the routing of sediment from the subwatershed outlet through the channel to the outlet of the watershed. A simple approach used in the WATER model is the method developed by William (1975). William's method assumes that the rate of deposition is a function of initial sediment load and particle diameter as shown below:

$$\frac{dY}{dt} = -B Y \sqrt{d} \quad (3.24a)$$

where d is particle diameter, Y is the sediment load, t is time, B is a routing coefficient, and d is the sediment diameter. Equation 3.24a can be rearranged integrated between $t=0$ and the time required for the sediment to travel through the channel (t_t). For $t=0$, $Y=Y_o$ (load the upstream point of the reach) and for $t=t_t$, $Y=Y$ (load at the downstream point of the reach), we obtain

$$\int_{Y_o}^Y \frac{dY}{Y} = -B \sqrt{d} \int_0^{t_t} dt = -B \sqrt{d} t_t \quad (3.24b)$$

We therefore obtain

$$\frac{Y}{Y_o} = DR = \exp(-B \sqrt{d_{50}} t_t) \quad (3.25)$$

where DR is the delivery ratio, and d_{50} is the representative diameter corresponding to the median particle diameter.

Sediment Transport Capacity

Code has also been written to allow the WATER model to compute the deposition in channels using their sediment transport capacity. The transport capacity is predicted using Yang's total sediment load equation (1972, 1973). His equation is based on the assumption that unit stream power is the dominate factor in sediment transport. Data base for calibration was limited to bed-material load.

According to Yang, the dominate variables for sediment transport are:

$$C_m = f(VS, u_*, v, \omega_s, d) \quad (3.26a)$$

where C_m is the concentration in ppm by mass, the velocity-slope product (VS) is the unit stream power, u_* is the shear velocity, ν is the kinematic viscosity, ω_s is the settling velocity of the particle, and d is its diameter. Yang rearranged the independent variables into the following dimensionless groups

$$C_m = f\left(\frac{VS}{\omega_s} - \frac{V_c S}{\omega_s}, \frac{u_*}{\omega_s}, \frac{\omega_s d}{\nu}\right) \quad (3.26b)$$

where V_c is the critical velocity corresponding to the initiation of particle movement. Yang evaluated the critical velocity for hydraulically rough conditions ($70 < u_* d/\nu$) as $V_c/\omega_s = 2.05$. Sediment transport is zero if $V < V_c$. Otherwise, it is predicted using the following equation

$$C_m = \gamma + \beta \log\left(\frac{VS}{\omega_s} - \frac{V_c S}{\omega_s}\right) \quad (3.27)$$

Yang estimated γ and β as a function of u_*/ω_s and $\omega_s d/\nu$. By using data base consisting of 1093 laboratory flume data and 65 field data with a range in particle size of 0.15 mm to 1.71 mm, flow depth of 0.037 ft to 49.9 ft, channel width of 0.44 ft to 1746 ft, channel slope of 0.000043 to 0.0279, average velocity 0.75 ft/s to 6.45 ft/s, and concentrations of 10 ppm to 585,000 ppm, the following equations are used for γ and β

$$\gamma = 5.435 - 0.286 \log\left(\frac{\omega_s d}{\nu}\right) - 0.457 \log\left(\frac{u_*}{\omega_s}\right) \quad (3.28a)$$

and

$$\beta = 1.799 - 0.409 \log\left(\frac{\omega_s d}{\nu}\right) - 0.314 \log\left(\frac{u_*}{\omega_s}\right) \quad (3.28b)$$

Chapter Four

Algorithms for Rock and Gravel Infiltration Filters

Introduction

Construction activities and urbanization generally result in less vegetation and more impervious area. Stormwater runoff increases as a consequence of these land use changes. Increased stormwater can adversely impact the health of streams and other surface water. An increase in stormwater also corresponds to a decrease in ground recharge. A reduction in groundwater recharge can have undesirable impacts on water table levels and ground water flow. Therefore, much interest exists in reducing stormwater runoff by enhanced infiltration systems. Enhanced infiltration systems include the use of vegetal swales and rock and gravel infiltration trenches and basins. Algorithms used to predict the response of treatment options for rock and gravel infiltration filters are described in this chapter. These algorithms include the development and analysis of new relationships to represent rock and gravel filters.

Two different algorithms have been developed for the WATER model to predict the hydraulic response and removal of sediment in rock and gravel filters. One of the algorithms, referred to as the Protocol Method, is based on the evaluation of experimental data collected in a laboratory setting. This is a purely empirical method where the response of different rock filters is obtained from regression analyses of existing data or from measurements using standard protocols. The other algorithm, referred to as the Process-Based Method, is based on process-based relationships developed for porous media flow. It uses a fractal model to account for changes in permeability with sediment deposition. Removal efficiencies are predicted using process-based parameters developed from chemical and civil engineering work on the filtration characteristics of porous media. Two sets of laboratory experiments previously collected under the supervision of the lead investigator are used to evaluate the parameters and the accuracy of the two methods.

The first section of the chapter is used to establish basic relationships for representing flows and sediment deposition in porous media. This includes relationships for non-Darcian flow because of the relatively large flow velocities in rock filters and definitions for removal and trap efficiencies. An overview of the experimental studies used to evaluate the parameters is then given. A step-by-step description of algorithm for the Protocol Method is given, including a summary of equations used to determine parameter values. The Process-Based Method is presented in the final sections. It includes the development of the fractal model and the evaluation of parameters from observed data.

General Considerations for Porous Media Flow

Hydraulic Flow

Darcy Flow - Negligible Inertial Forces

A conceptual framework for flow through porous media can be obtained by considering the flow through interconnected idealized pores. For the special case of negligible inertial terms and laminar flow, the velocity of flow through the idealized pores can be evaluated as (McWhorter and Sunada, 1981)

$$U = - \frac{\rho g l^2}{C' \mu} \left(\frac{\Delta \Phi}{\Delta \ell} \right) \quad (4.1)$$

where U is the flow velocity in the direction of ℓ , l is a measure of pore size (width for pores of two flat plates or radius for circular pores), $\Delta \Phi$ is the change in pressure and gravity potential over a distance $\Delta \ell$, and C' is a geometry-related dimensionless parameter that is a function of media. Theoretical relationships for C' of cylindrical tubes and flat plates are 8 and 12, respectively.

Specific discharge is defined as the total flow rate per unit area. Assuming that flow rate is directly related to velocity, the specific discharge for non-inertia influenced flows can then be written as

$$q = - \frac{\rho g d^2}{C \mu} \left(\frac{\Delta \Phi}{\Delta \ell} \right) \quad (4.2a)$$

where d is the effective pore dimension for specific discharge and C is the equivalent of C' for specific discharge. The majority of experimental studies suggest a value of C between 0.5 and 0.6 (McWhorter and Sunada, 1981).

Intrinsic permeability (κ , unit L^2) is often defined as

$$\kappa = \frac{d^2}{C} \quad (4.2b)$$

and saturated conductivity (K , unit L/T) as

$$K = \frac{\rho g d^2}{C \mu} = \kappa \left(\frac{\rho g}{\mu} \right) \quad (4.2c)$$

Specific discharge can then be written in terms of Darcy equation, that is,

$$q = - \kappa \left(\frac{\rho g}{\mu} \right) \left(\frac{\partial \Phi}{\partial \ell} \right) = - K \left(\frac{\partial \Phi}{\partial \ell} \right) \quad (4.2d)$$

The Protocol and the Theoretical Methods both use relative permeability in their solution approach. Relative permeability is defined as

$$\kappa_r = \frac{\kappa}{\kappa_c} \quad (4.2e)$$

where κ_r is the relative permeability, κ is the permeability with sediment deposition in the media, and κ_c is the permeability without sediment deposition (clean).

Inertia Form

When inertia terms are significant, McWhorter and Sunada (1981) suggest the following dimensionless equation for specific discharge

$$\left(\frac{\mu}{\rho g \kappa} \right) q + \left(\frac{1}{g \sqrt{\kappa/C}} \right) q^2 = - \frac{\partial \Phi}{\partial \ell} \quad (4.3a)$$

where q^2 is the additional inertia term. Greater insight can be obtained by rearranging the above equation as

$$f = \frac{\mu}{\rho q \sqrt{\kappa C}} + 1 = - \left(\frac{g \sqrt{\kappa/C}}{q^2} \right) \frac{\partial \Phi}{\partial \ell} \quad (4.3b)$$

Since $\kappa = d^2/C$, the function f can be defined as

$$f = \frac{1}{R_e} + 1 \quad (4.3c)$$

where $R_e = \rho q d / \mu$ is the Reynolds number for porous media flow. Excellent fit to observed data is reported by McWhorter and Sunada (1981) using Equation 4.3c. For small R_e , $f \approx 1/R_e$ and Darcy's equation is obtained. For large R_e , $f \approx 1$, and the specific discharge for inertial-dominated flow is then obtained as

$$q = \sqrt{g \left(\frac{\kappa}{C} \right)^{1/2} \left(- \frac{\partial \Phi}{\partial \ell} \right)} \quad (4.3d)$$

The general solution for specific discharge can be obtained by rearranging Equation 4.3a as

$$\left(\frac{\sqrt{\kappa C}}{v} \right) q^2 + q - \frac{g \kappa}{v} \left(- \frac{\partial \Phi}{\partial \ell} \right) = 0 \quad (4.4a)$$

to solve for q as

$$q = \frac{-1 + \sqrt{1 + 4 g \kappa \sqrt{\kappa C} \left(- \frac{\partial \Phi}{\partial \ell} \right) / v^2}}{2 \sqrt{\kappa C} / v} \quad (4.4b)$$

The solution of Equation 4.4b is shown in Figure 4.1 (as circles). Also shown in this figure are the solutions obtained using Darcy's equation (i.e. Equation 4.2d), the inertia-dominated equation (i.e., Equation 4.3d) and power function defined below. These results were obtained using $v = 1.0 \times 10^{-6} \text{ m}^2/\text{s} = 3.6 \times 10^3 \text{ mm}^2/\text{h}$, acceleration of gravity as $g = 9.81 \text{ m/s}^2 = 1.272 \times 10^{11} \text{ mm/h}^2$, and $C = 0.6$. The intrinsic permeability was defined from the saturated conductivity using Equation 4.2c.

Specific discharge is linearly related to potential gradient for Darcian flow and to the square root of potential gradient for inertia-dominated flow. These trends suggest that a simpler equation, such as given by Equation 4.5, may be used to approximate Equation 4.4b:

$$q = \alpha K \left(- \frac{\partial \Phi}{\partial l} \right)^\eta \quad (4.5)$$

The “Power” line in Figure 4.1 corresponds to values predicted by Equation 4.5 with fitted coefficients of α and η . These results show that Equation 4.5 can be used as a good approximation to Equation 4.4b. Fitted coefficient values are shown in Figure 4.2. Both coefficients are reasonably represented by exponential functions.

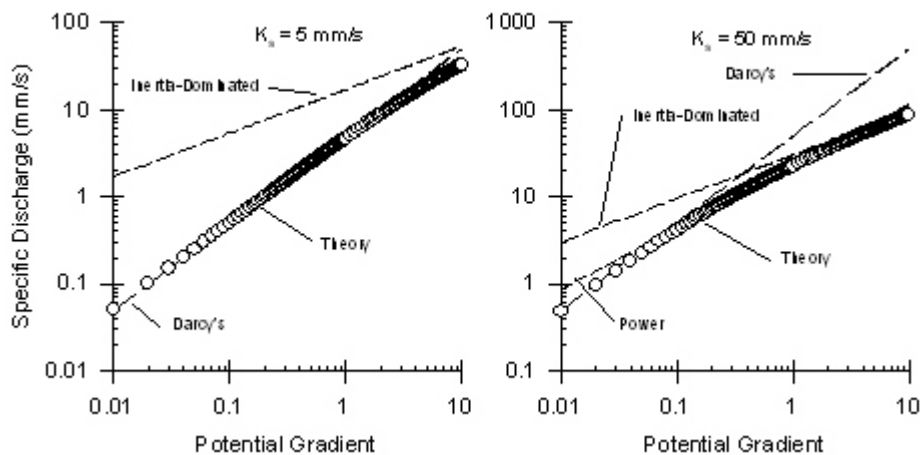


Figure 4.1. Evaluation of Representation of Specific Discharge.

Although rock and gravel infiltration rates are predicted by Equation 4.4b, the theoretical development of the process-based method is simplified using the consequence of a good representation obtained by Equation 4.5. For example, a consistent pore velocity with the specific discharge of Equation 4.5 is

$$U = - \alpha \frac{\rho g l^2}{C' \mu} \left(\frac{d \Phi}{d l} \right)^\eta \quad (4.6)$$

Equation 4.6 is used in the development of the Processed-Based Method.

Permeability from Observed Data

The determination of intrinsic permeability, with and without sediment deposition, from observed data is necessary to estimate the parameters for the rock and gravel infiltration algorithms. The numerical approach used to determine observed intrinsic permeability is given here. For this application, the specific discharge (q) and the potential gradient of

Equation 4.4a have been measured and are used to solve for the unknown intrinsic permeability. A C value of 0.6 is assumed, and therefore, any use of the derived intrinsic permeability in a later application also needs to use C=0.6. Equation 4.4a is a nonlinear function of intrinsic permeability and iterative solution is needed.

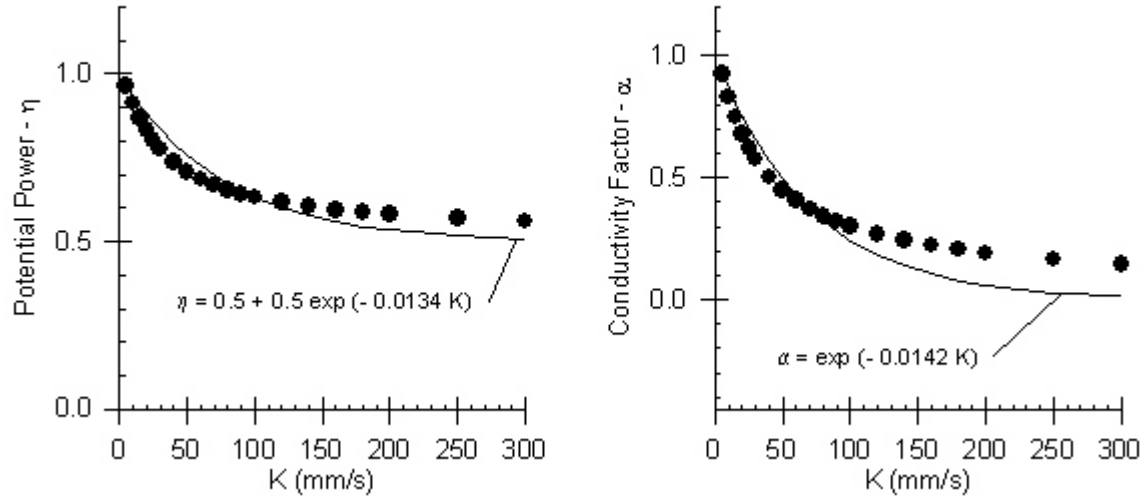


Figure 4.2. Trends in Power Function Coefficients for Predicting Specific Discharge.

An initial estimate of intrinsic permeability, κ_o , is obtained from Equation 4.5 using the exponential functions shown in Figure 4.2. The next estimate is obtained using a Taylor series expansion to the flow rate relationship of Equation 4.4a. In general, Taylor series can be written in the following form

$$f(x) = f(x_o) + (x - x_o) f'(x_o) + \frac{(x - x_o)^2}{2} f''(x_o) + \dots \quad (4.7a)$$

where $f(x)$ is defined here as

$$f(x) = \left(\frac{\sqrt{x} C}{v} \right) q^2 + q - \frac{g x}{v} (-\partial \Phi / \partial \ell) \quad (4.7b)$$

where x is the unknown intrinsic permeability, and x_o is the initial estimate. By setting $f(x) = 0$ and by neglecting third-order terms, the value of x can be obtained by using the quadratic equation as

$$x - x_o = \frac{-f'(x_o) \pm \sqrt{[f'(x_o)]^2 - 2 f''(x_o) f(x_o)}}{f''(x_o)} \quad (4.7c)$$

Only feasible solutions to Equation 4.7c are obtained if the positive square root is used. We then obtain

$$x = x_0 - \frac{f'(x_0)}{f''(x_0)} + \sqrt{\left(\frac{f'(x_0)}{f''(x_0)}\right)^2 - 2 \frac{f(x_0)}{f''(x_0)}} \quad (4.7d)$$

Evaluations of derivatives are tedious but straightforward and are given below. The reader uninterested in the algebra can simply go directly to Equation 4.7m. The first derivative can be evaluated directly from Equation 4.4a as

$$f' = \left(\frac{1}{2 x^{1/2}}\right) \left(\frac{q^2 \sqrt{C}}{v}\right) - \frac{g}{v} (-\partial\Phi/\partial\ell) \quad (4.7e)$$

and the second derivative as

$$f'' = -\left(\frac{1}{4 x^{3/2}}\right) \left(\frac{q^2 \sqrt{C}}{v}\right) \quad (4.7f)$$

Let's now evaluate the function

$$\frac{f'(x_0)}{f''(x_0)} = -2x_0 + 4gx_0^{3/2} \left(\frac{-\partial\Phi/\partial\ell}{q^2 \sqrt{C}}\right) \quad (4.7g)$$

and

$$\frac{f(x_0)}{f''(x_0)} = -4x_0^2 - \frac{4x_0^{3/2} v}{q\sqrt{C}} + \frac{4x_0^{5/2} g (-\partial\Phi/\partial\ell)}{q^2 \sqrt{C}} \quad (4.7i)$$

We then conclude that

$$\left(\frac{f'(x_0)}{f''(x_0)}\right)^2 = 4x_0^2 - 16gx_0^{5/2} \left(\frac{-\partial\Phi/\partial\ell}{q^2 \sqrt{C}}\right) + 16g^2 x_0^3 \left(\frac{-\partial\Phi/\partial\ell}{q^4 C}\right)^2 \quad (4.7j)$$

and

$$\left(\frac{f'(x_0)}{f''(x_0)}\right)^2 - 2 \frac{f(x_0)}{f''(x_0)} = 16g^2 x_0^3 \left(\frac{-\partial\Phi/\partial\ell}{q^4 C}\right)^2 - 24 \frac{x_0^{5/2} g (-\partial\Phi/\partial\ell)}{q^2 \sqrt{C}} + 12x_0^2 + 8 \frac{x_0^{3/2} v}{q\sqrt{C}} \quad (4.7k)$$

which can be rearranged as

$$\left(\frac{f'(x_0)}{f''(x_0)}\right)^2 - 2 \frac{f(x_0)}{f''(x_0)} = \left(4 \frac{x_0^{3/2} g (-\partial\Phi/\partial\ell)}{q^2 \sqrt{C}} - 3x_0\right)^2 + 3x_0^2 + 8 \frac{x_0^{3/2} v}{q\sqrt{C}} \quad (4.7l)$$

We therefore conclude that

$$x = x_0 + 2x_0 - 4gx_0^{3/2} \left(\frac{-\partial\Phi/\partial\ell}{q^2 \sqrt{C}}\right) + \sqrt{\left(4 \frac{x_0^{3/2} g (-\partial\Phi/\partial\ell)}{q^2 \sqrt{C}} - 3x_0\right)^2 + 3x_0^2 + 8 \frac{x_0^{3/2} v}{q\sqrt{C}}} \quad (4.7m)$$

The ability to obtain a good estimate of the intrinsic permeability using a single iteration based on Equation 4.7m is quite good. Percent errors are typically less than 2%. Although this error is small, it was decided that even a smaller error should be used in the study. Therefore, Equation 4.7m is applied repeatedly, where $x_0 = x$ in the next iteration, until the x_0

is virtually constant.

Sediment Removal

Definitions

The trap efficiency of the filter is an important design parameter. Sediment deposited in the media will eventually plug the filter. In general, trap efficiency is defined as

$$T_e = \frac{\text{Mass In} - \text{Mass Out}}{\text{Mass In}} = \frac{\text{Mass Deposited}}{\text{Mass In}} \quad (4.8)$$

The removal efficiency is defined for this study as

$$e = \frac{dM_D}{dM_I} \approx \frac{C_{in} Q_{in} \Delta t - C_{out} Q_{out} \Delta t}{C_{in} Q_{in} \Delta t} \approx 1 - \frac{C_{out}}{C_{in}} \quad (4.9)$$

where the last term is valid for equal inflow and outflow rates corresponding to a saturated porous media and an incompressible fluid.

Cumulative trap efficiency is defined as

$$E_f = \frac{\int_0^{M_D(t)} dM_D}{\int_0^{M_I(t)} dM_I} = \frac{M_D(t)}{M_I(t)} \quad (4.10a)$$

By using the definition for the removal efficiency (Equation 4.9), we obtain

$$E_f = \frac{\int_0^{M_I(t)} e dM_I}{M_I} \quad (4.10b)$$

Sediment Removal using Relative Permeability

Experimental data discussed in the next section are analyzed using relationships between sediment removal and relative permeability. These relationships are based on the assumption that relative permeability decreases exponentially with cumulative inflow mass. This assumption is also used in the Protocol Method and in analyzing sediment deposition in the experimental data sets. Key relationships for these analyses are developed here.

A key assumption in this section is that permeability ratio can be represented as

$$\kappa_r = \frac{\kappa}{\kappa_c} = \exp \left[- \xi \left(\frac{M_I}{M_{0.3I}} \right) \right] \quad (4.11)$$

where $M_{0.3I}$ is the inflow mass corresponding to $\kappa_r = 0.3$, and therefore κ_r equals one and 0.3 for M_I of zero and $M_{0.3I}$, respectively. We then conclude that

$$M_I = \left(- \frac{M_{0.3I}}{\xi} \right) \ln(\kappa_r) \quad (4.12a)$$

and therefore

$$dM_I = \left(- \frac{M_{0.3I}}{\xi} \right) \left(\frac{d\kappa_r}{\kappa_r} \right) \quad (4.12b)$$

By using these relationships, the cumulative trap efficiency of Equation 4.10b is defined as

$$E_f = \frac{\left(- \frac{M_{0.3I}}{\xi} \right) \int_1^{\kappa_r(t)} e \left(\frac{d\kappa_r}{\kappa_r} \right)}{\left(- \frac{M_{0.3I}}{\xi} \right) \ln(\kappa_r)} = \left(\frac{1}{\ln(\kappa_r)} \right) \int_1^{\kappa_r(t)} \left(\frac{e}{\kappa_r} \right) d\kappa_r \quad (4.13a)$$

In the analysis of experimental data, interest lies in a solution for e of the following form:

$$e = b_0 + b_1 \kappa_r \quad (4.13b)$$

By using this relationship, cumulative trap efficiency is defined as

$$E_f = \left(\frac{1}{\ln(\kappa_r)} \right) \int_1^{\kappa_r(t)} \left(\frac{b_0}{\kappa_r} + b_1 \right) d\kappa_r = \frac{b_0 \ln(\kappa_r) + b_1 (\kappa_r - 1)}{\ln(\kappa_r)} \quad (4.13c)$$

If we perform a regression analysis on observed data, using cumulative trap efficiency as the dependent variable, of the form

$$E_f = b_0 + b_1 \left(\frac{\kappa_r - 1}{\ln(\kappa_r)} \right) \quad (4.13d)$$

then the regression parameters for b_0 and b_1 correspond to those of the linear representation for e given by Equation 4.13b.

As discussed in the analysis of observed data, sediment deposition is computed by interpolation using observed estimates of removal efficiency and relative permeability. The equation for interpolation is based on the difference in cumulative trap efficiencies defined as

$$\Delta E_f = \frac{\Delta M_D}{\Delta M_I} = \frac{- \frac{M_{0.3I}}{\kappa} \int_{\kappa_{r,i-1}}^{\kappa_{r,i}} e \left(\frac{d\kappa_r}{\kappa_r} \right)}{- \frac{M_{0.3I}}{\kappa} [\ln(\kappa_{r,i}) - \ln(\kappa_{r,i-1})]} = \frac{\int_{\kappa_{r,i-1}}^{\kappa_{r,i}} e \left(\frac{d\kappa_r}{\kappa_r} \right)}{\ln(\kappa_{r,i}) - \ln(\kappa_{r,i-1})} \quad (4.14a)$$

For the condition of $e = b_0 + b_1 \kappa_r$, we obtain

$$\Delta E_f = \frac{b_o [\ln(\kappa_{r,i}) - \ln(\kappa_{r,i-1})] + b_1 [\kappa_{r,i} - \kappa_{r,i-1}]}{\ln(\kappa_{r,i}) - \ln(\kappa_{r,i-1})} \quad (4.14b)$$

Deposition mass is then defined from cumulative trap efficiency difference as

$$\Delta M_D = \Delta E_f \Delta M_I \quad (4.15a)$$

or outflow mass using

$$\Delta M_O = (1 - \Delta E_f) \Delta M_I \quad (4.15b)$$

In contrast b_o and b_1 as constant parameters in a predictive relationship as originally defined in Equation 4.13b, they are computed directly from observed data to determine ΔE_f and vary between two sets of observations. For the first (or only) measured data point, insufficient information is available to evaluate both b_o and b_1 . Therefore for the first point, the interpolation coefficient is defined as $b_o = e_{obs,1}$ and $\kappa_{r,i-1} = 1$ so that $E_f = b_o$. For all subsequent data, the interpolation coefficients are defined as

$$b_1 = \frac{e_{obs,i} - e_{obs,i-1}}{\kappa_{r,obs,i}^* - \kappa_{r,obs,i-1}^*} \quad \text{and} \quad b_o = e_{obs,i} - b_1 \kappa_{r,obs,i} \quad (4.16)$$

As discussed in the next section, the overall trap efficiency is available for many of the observed cores by using the weight of the cores before and after the end of the test as well using measurements of influent and effluent concentrations during the test. The overall trap efficiencies, however, correspond to different final relative permeabilities among the cores. It is desirable to convert them to a standard value for analyses of $\kappa_{r,std} = 0.3$. The conversion factor is developed here. For known regression b_o and b_1 values, we can use

$$\frac{E_{fstd}}{E_f} = B = \frac{b_o + b_1 \left(\frac{\kappa_{r,std} - 1}{\ln(\kappa_{r,std})} \right)}{b_o + b_1 \left(\frac{\kappa_r - 1}{\ln(\kappa_r)} \right)} \quad (4.17a)$$

Therefore the conversion from the overall trap efficiency at the end of the test to a standard value corresponding to $\kappa_{r,std} = 0.3$ is obtained as

$$E_{fstd} = B E_f \quad (4.17b)$$

where E_f is the measured overall trap efficiency at the end of the test and E_{fstd} is the trap efficiency at the standard relative permeability.

Process-based Dimensionless Parameters

Removal of contaminants by porous media in air or water is of great practical interest in a variety of different disciplines. It is therefore not surprising that considerable research has been done to study the process (Tien, 1989). Important dimensionless parameters obtained from this work are summarized below:

$$\gamma = (1 - \phi)^{1/3} \quad (4.18a)$$

$$A_s = [\text{Stream Function Parameter}] = \frac{2(1 - \gamma^5)}{2 - 3\gamma + 3\gamma^2 - 2\gamma^6} \quad (4.18b)$$

$$N_{vw} = [\text{van der Waals Dimensionless Parameter}] = \frac{4H}{9\pi\mu d_p^2 q} \quad (4.18c)$$

$$D_R = [\text{Interception Number (Sediment - Filter Diameter Ratio)}] = \frac{d_p}{d_m} \quad (4.18d)$$

$$C_N = [\text{Contact Number (Velocity Ratio)}] = \frac{\omega_s}{U} = \frac{\omega_s}{q/\phi} \quad (4.18e)$$

where ϕ is the porosity, H is the Hamaker constant (approximately 10^{-14} ergs for suspended particles in aqueous media), μ is the dynamic viscosity, d_p is the diameter of the incoming sediment, d_m is the diameter of the media, q is the inflow rate per unit area, and ω_s is the settling velocity of sediment.

Analysis of Observed Data

Description of Data Sets

Minnesota Department of Agriculture's Study

Two sets of experimental data were collected by the lead investigator on previous projects and are used to estimate parameters for the rock and gravel infiltration algorithms. The first set of experimental data was collected for a study funded by the Minnesota Department of Agriculture (MDOA) (Wilson et al., 1999). The primary goal of this study was to investigate the use of rock filters as a possible replacement for surface tile inlets in agricultural fields. Sediment was delivered to a test chamber using a vibrating sloped feeder, the slope of which could be changed to increase or decrease the rate. The maximum rate of sediment delivery for this system was, however, unable to plug the media for the large rock filter. Water flow was controlled to maintain an approximately constant pressure head. The test chamber was constructed using PVC pipe of 15 cm inside diameter. A metal mesh was used to support the media at the bottom of the module. The cylinder was filled with media to a depth of approximately 30 cm.

Three different gravel mixtures were used in the test chambers corresponding to fine (Camas #7), medium (Camas #67), and coarse (Camas #6) particle sizes. The gravel was obtained from the Camas Company, which is a large sand and gravel company in the Twin Cities area. The gravel mixtures are therefore readily available and could be used in field installation. The medium mixture was created by mixing particles from Camas #7 and Camas #6. The particle size distributions for the three gravel mixtures were determined using standard sieve

analysis techniques. Only one type of influent sediment was used for the laboratory experiments. The particle size distributions were obtained using standard sieve and hydrometer methods.

Porosity and flow rate using clean water were determined prior to the start of the sediment laden inflow. Sediment-laden flows were then introduced into the core for 10 minutes. Effluent concentrations were obtained at 2-minute intervals. After the media and deposited soil had dried, the 10-minute runs were repeated until the flow rate was roughly 10% of that obtained for clean water or until the maximum sediment load rate was used and no change in permeability.

Oveson's Master of Science (MS) Project

Additional data on reduction of permeability with sediment-laden flows were collected with a more extensive experimental design done by Kris Oveson as part of her MS work (Oveson, 2001). This project was funded by the Minnesota Pollution Control Agency, the University of Minnesota Water Resources Center, and the University of Minnesota Agricultural Experiment Station. The impact of three variables was considered in her experimental design: media size, sediment size, and sediment loading rate. The experimental procedures were similar to those of the MDOA's study. Each rock core was constructed from 15 cm diameter PVC pipe with a metal mesh or screen installed at the bottom of the pipe to support the test media. The core was filled with media to a total depth of 33 cm. A brass barred reducer was installed in each core approximately 1 cm above the rock media.

An important difference from the MDOA's study was the sediment feeder apparatus. A conveyor belt system was used to deliver sediment to the core. This system allowed a large influent concentrations to be delivered to the cores. During each 10-minute run of a test, four effluent 250 ml samples were collected to determine the effluent sediment concentrations. At the end of the 10-minute run, the four samples were combined to determine an average effluent concentration for that 10 minutes of the test. Each test lasted from 20 to 60 minutes

Three rock media sizes were investigated, referred to as University of Minnesota Standard (UMS) #1, UMS #2 and UMS #3. These rock media varied more than those used in the MDOA's study. Four different types of sediment were investigated. Based on the primary particle sizes, they were classified as a fine sand, two types of silt loams, and a clay. Tests were originally planned to be conducted until the permeability of the rock core was less than 10% of its clean water value. After the test, the rock core was placed in a drying oven to determine the total mass of sediment deposition.

Summary of Tests

Particle size distributions of the media and influent sediment for the two sets of data are summarized in Figures 4.3 and 4.4. As shown by these figures, the range of sizes between the different types of rock media and the range of size between the different types of influent sediment were reasonably large.

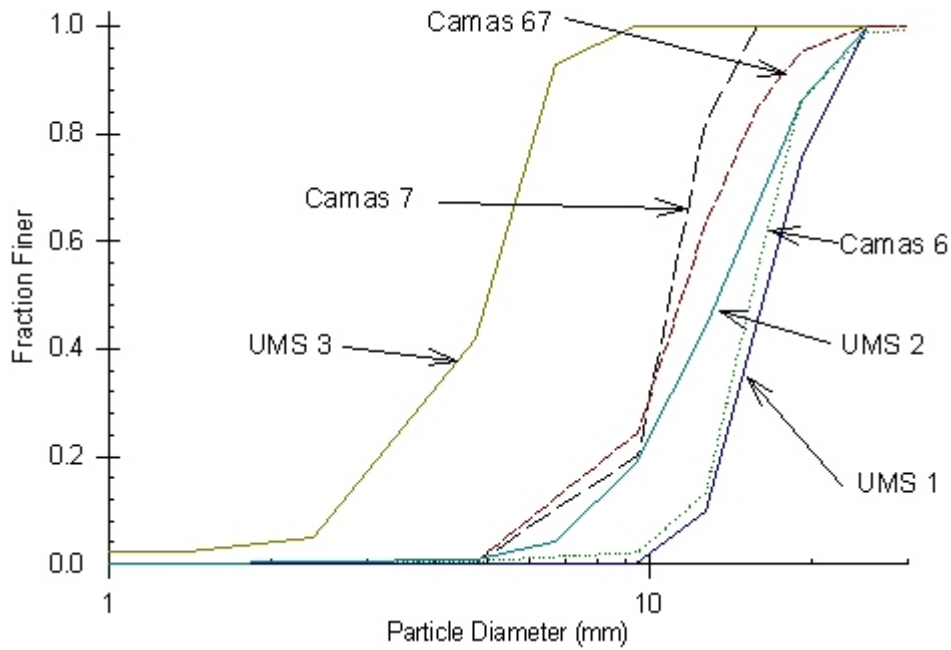


Figure 4.3. Particle Size Distributions for the Rock Media.

Table 4.1. Summary of Characteristics of Data Sets.

Variables	Porosity (ϕ) m^3/m^3	κ_c mm^2	κ_r mm^2/mm^2	Conc mg/l	Mass In kg	Deposition kg	ϕ_f m^3/m^3
Observations	50	50	50	50	50	33	33
Mean	0.396	0.140	0.2553	24160	36.0	1.47	0.250
Std Deviation	0.023	0.158	0.3692	40320	28.1	1.18	0.199
Maximum	0.450	0.613	1.0000	246700	124.8	4.53	0.766
Minimum	0.357	0.002	0.0005	3220	0.4	0.05	0.009

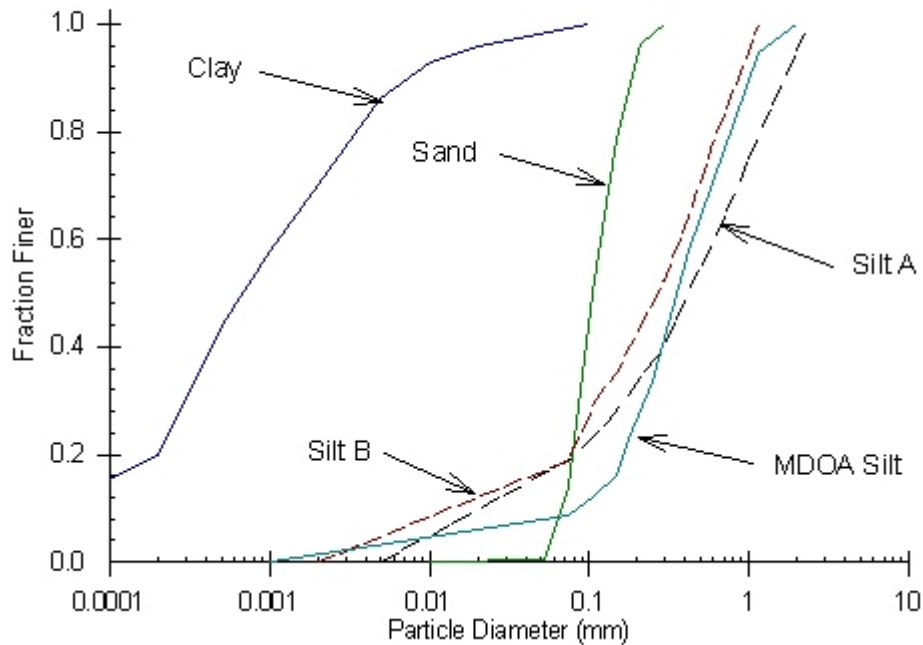


Figure 4.4. Particle Size Distributions for the Influent Sediment.

A summary of the key variables for the tests of the combined data sets is shown in Table 4.1. The combined data from the two studies provided a nice range in characteristics of the media and sediment. The last column, ϕ_f , is the fraction of the total porosity of the filled corresponding to the sediment volume deposited at the end of the test. The number of observations are different for the total deposition and ϕ_f because of the cores that were not plugged with sediment during the test.

Analysis of Permeability Data

Clean Permeability

A predictive relationship for the permeability of the media using sediment-free water (clean) was examined for the six types of rock media of the combined data set. Each rock media was represented by the harmonic mean of replicates. Two possible predictive relationships were chosen. The simplest is only a function of the diameter corresponding to the 50% finer value. The best fit regression equation and its accuracy are shown in Figure 4.5. The second model also included a ratio of the diameters of the 75% and 25% values. The results and predictive accuracy of this model are shown in Figure 4.6. The second model provides a reasonable good fit to the data.

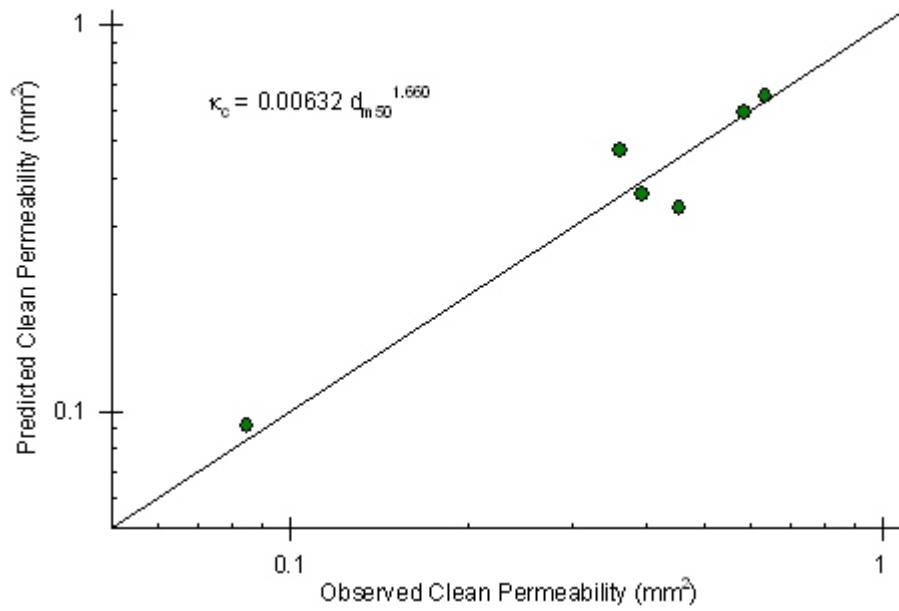


Figure 4.5. Prediction of Clean Media Permeability Using Median Diameter.

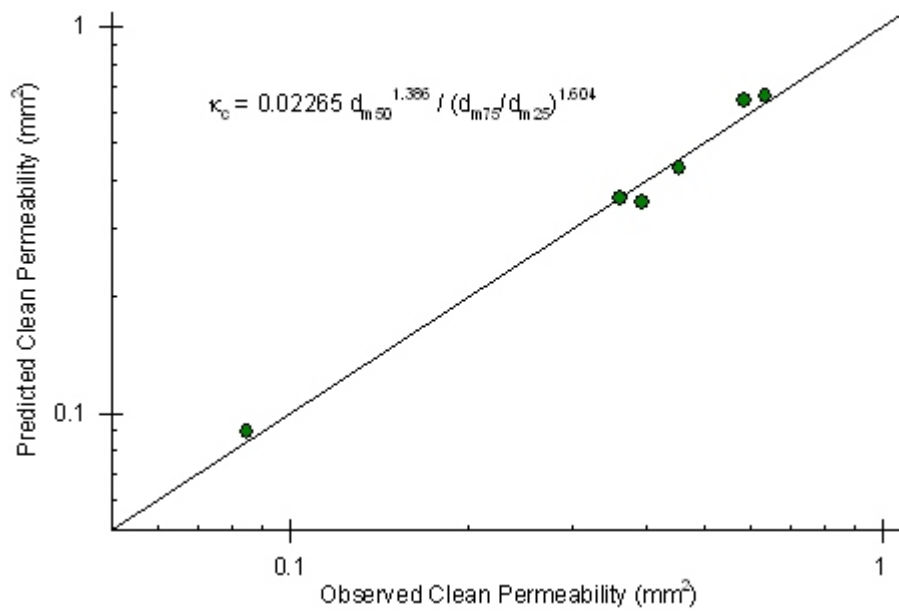


Figure 4.6. Prediction of Clean Media Permeability Using Median Diameter and the Ratio of Diameters of 75% and 25% Values.

Observed Trends in Relative Permeability

Observed trends in the changes in permeability with cumulative inflow mass are shown in Figure 4.7 for Camas 7 and Figure 4.8 for Camas 6. Intrinsic permeability decreased consistently with an increase in inflow mass. However, the relatively large Camas 6 media was unable to obtain a permeability of one-tenth of the clean media value for one of the replicates. A larger mass loading rate was needed for this test, a rate that exceeded the delivery potential of the sediment feeder. The sediment feeder was therefore redesigned for the Oveson study. In general, the permeability increased initially after drying and the re-start of the test.

Observed trends in intrinsic permeability with cumulative inflow mass for the UMS media are shown in Figures 4.9, 4.10, and 4.11. In general, the trends are similar to those of the Camas media. However, none of the three media types showed significant decrease in intrinsic permeability for sand as the influent sediment. This is particularly noticeable for the smallest media of UMS 3. This media was not plugged with sand even with a concentration of influent concentration greater than 200,000 mg/l. This is particularly surprising because even the clay-sized sediment resulted in a decrease in permeability for some of the tests. Apparently, the lack of cohesiveness, or stickiness of the influent sediment, was the primary reason for this result.

The non-plugging of the media with sand suggests that an adjustment is needed for non-cohesive sediment. The logistic function of Equation 4.19 is used to represent the sticking coefficient. It gives sticking coefficient values close to one for percent-sand less than or equal to 50% and near zero values for percent-sand greater than 80%. A function that has these properties is shown below.

$$\alpha = \frac{T_{E,noncohesive}}{T_E} = 1 - \exp \{ - \exp [- 0.30 (\text{Percent Sand} - 65)] \} \quad (4.19)$$

where the percent sand is for non-aggregated sand.

Analysis of Relative Permeability

One of the goals of this work is to evaluate the representation of the change in relative permeability as a function of variables that are readily simple to measure or to predict. The cumulative inflow mass is one of the most reliable variables in the observed data set. An exponential model of the following form is suggested from observed trends in intrinsic permeability given in Figures 4.7 through 4.11:

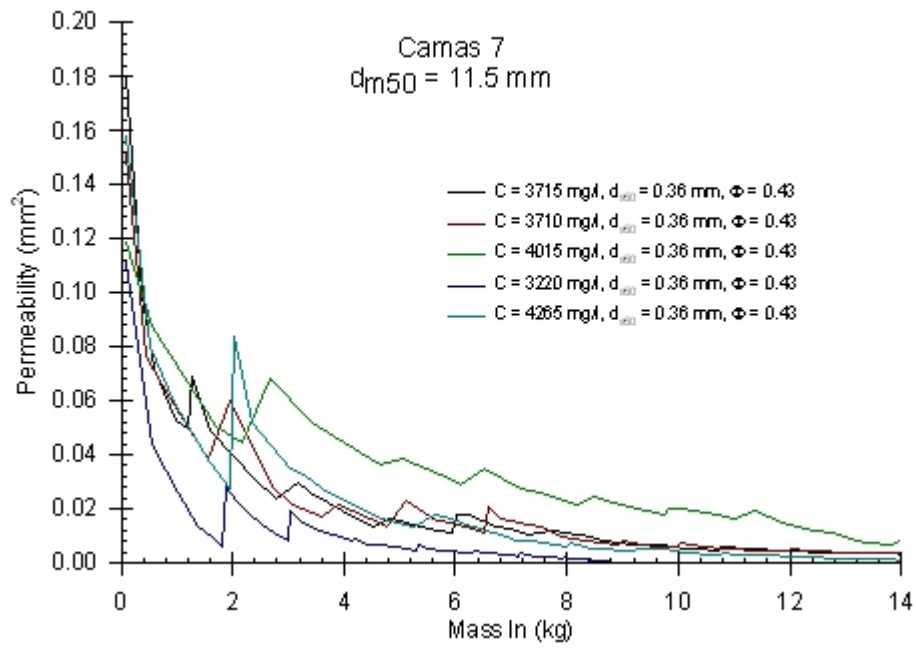


Figure 4.7. Change in Permeability with Inflow Mass for Camas 7 Rock Media.

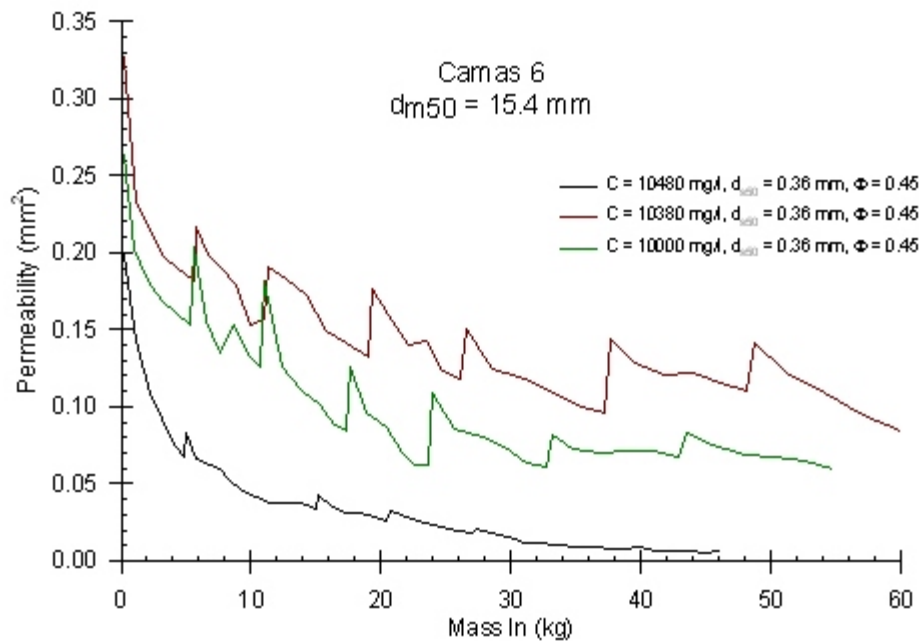


Figure 4.8. Change in Permeability with Inflow Mass for Camas 6 Rock Media.

$$\kappa_r = \frac{\kappa}{\kappa_c} = \exp \left[- \xi \left(\frac{M_I}{M_{0.31}} \right) \right] \quad (4.20)$$

where $M_{0.31}$ is the inflow mass corresponding to a relative permeability of 0.3. Theoretically, the value of ξ is 1.204 for $\kappa_r=0.3$ when $M_I/M_{0.31}=1$. The best least-square fit using log-transformed data for ξ is 0.2973. This value reflects the many small κ_r values for the Camas data.

A comparison of observed relative permeability and that predicted by Equation 4.20 with two different values of ξ is shown in Figures 4.12 through 4.17. Overall, the data are fairly well represented by using $\xi = 1.204$, especially for relative permeability values greater than 0.3.

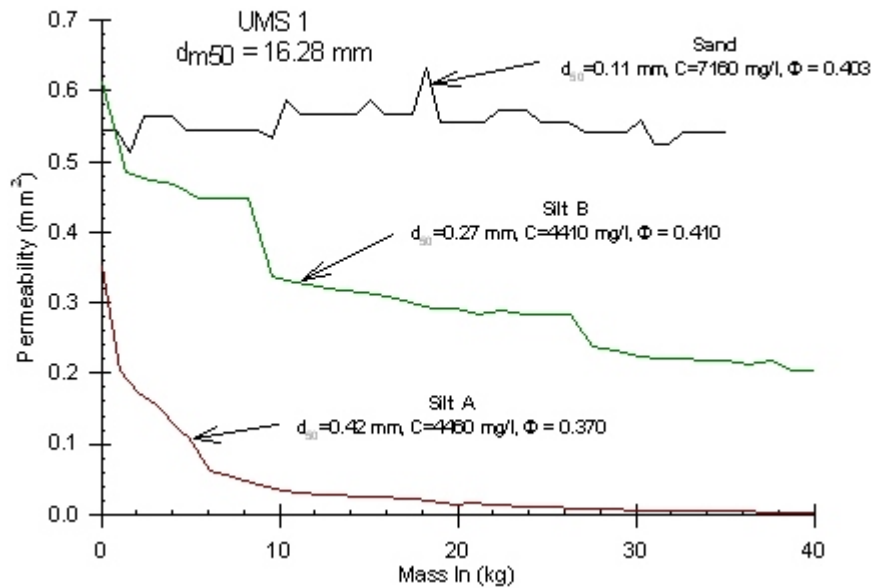


Figure 4.9. Change in Permeability with Inflow Mass for UMS 1 Rock Media.

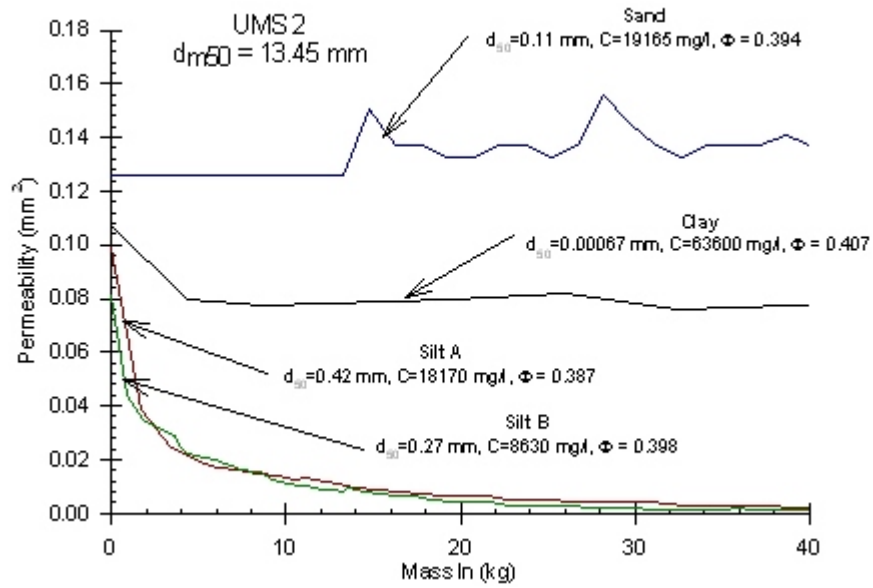


Figure 4.10. Change in Permeability with Inflow Mass for UMS 2 Rock Media.

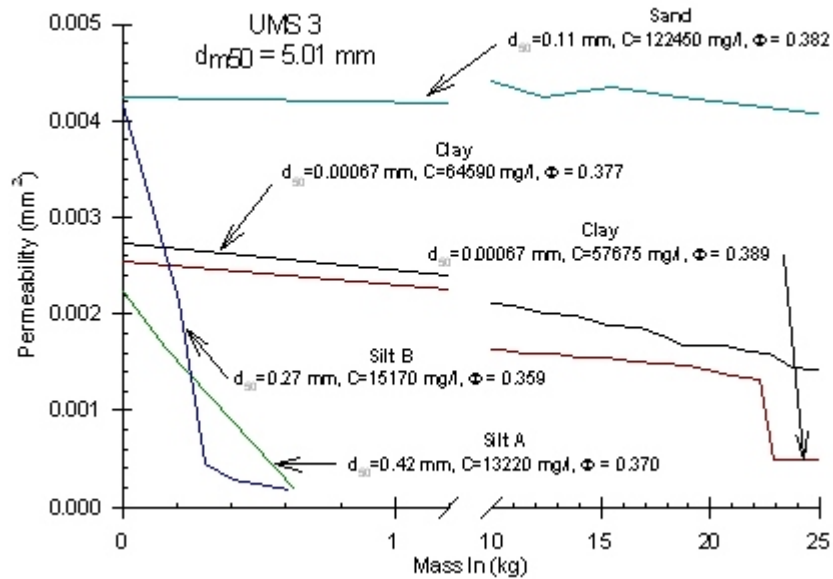


Figure 4.11. Change in Permeability with Inflow Mass for UMS 3 Rock Media.

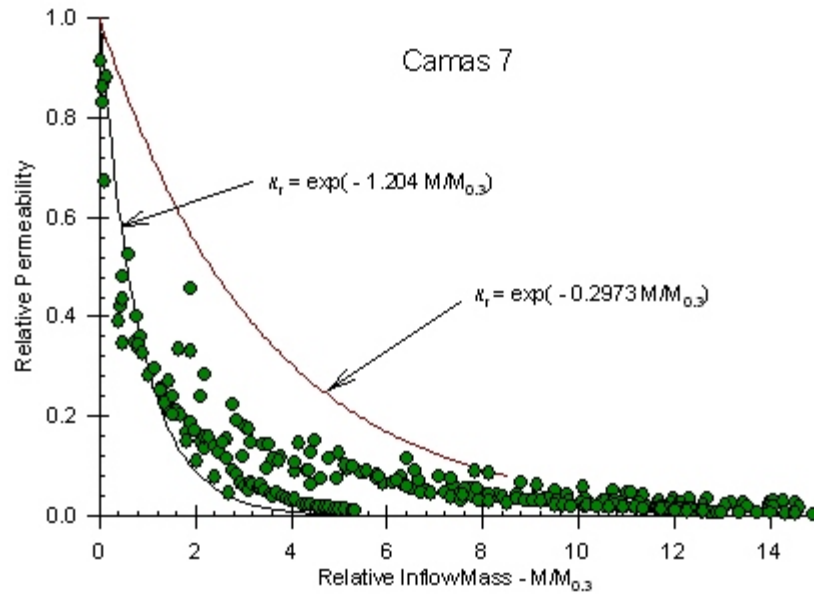


Figure 4.12. Exponential Models of Relative Permeability for Camas 7.

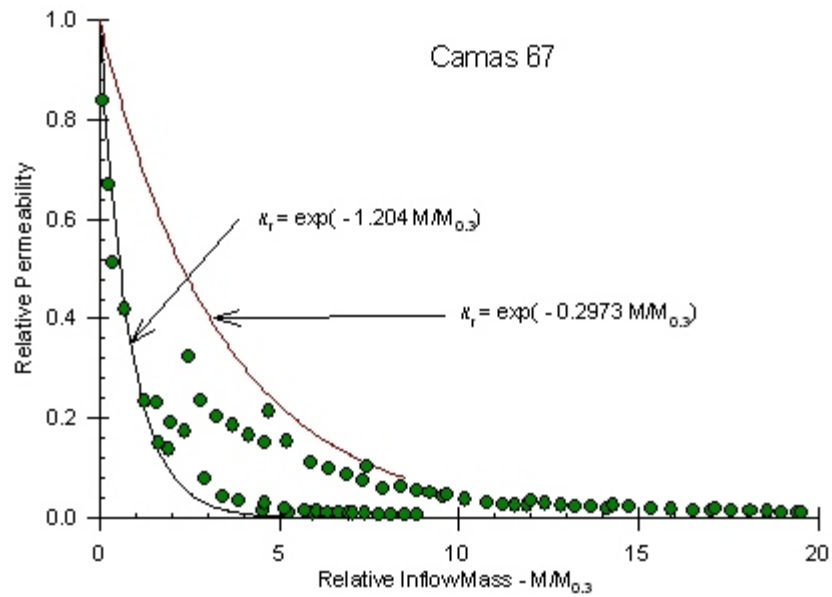


Figure 4.13. Exponential Models of Relative Permeability for Camas 67.

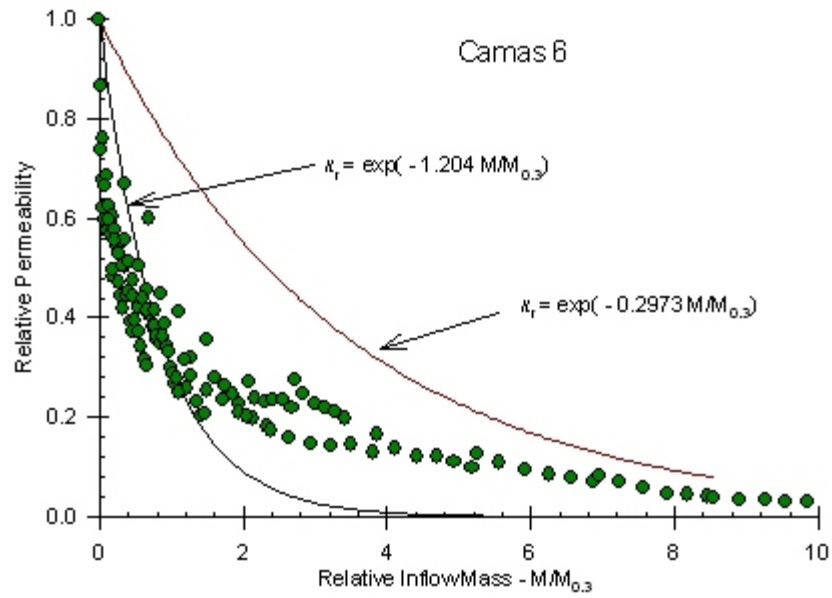


Figure 4.14. Exponential Models of Relative Permeability for Camas 6.

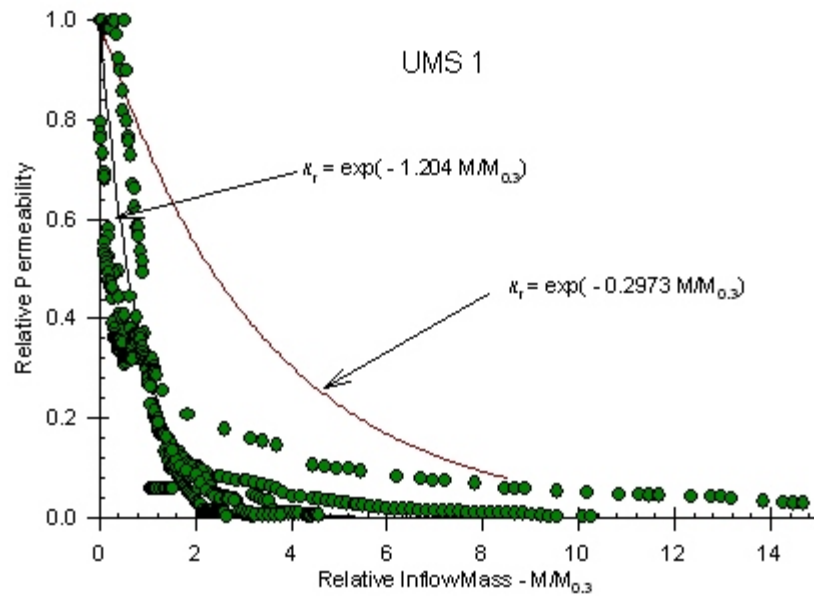


Figure 4.15. Exponential Models of Relative Permeability for UMS 1.

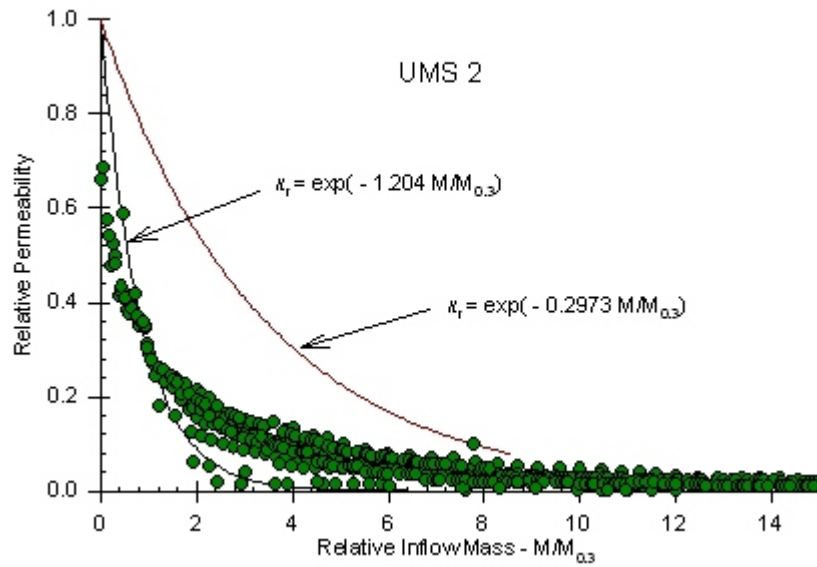


Figure 4.16. Exponential Models of Relative Permeability for UMS 2.

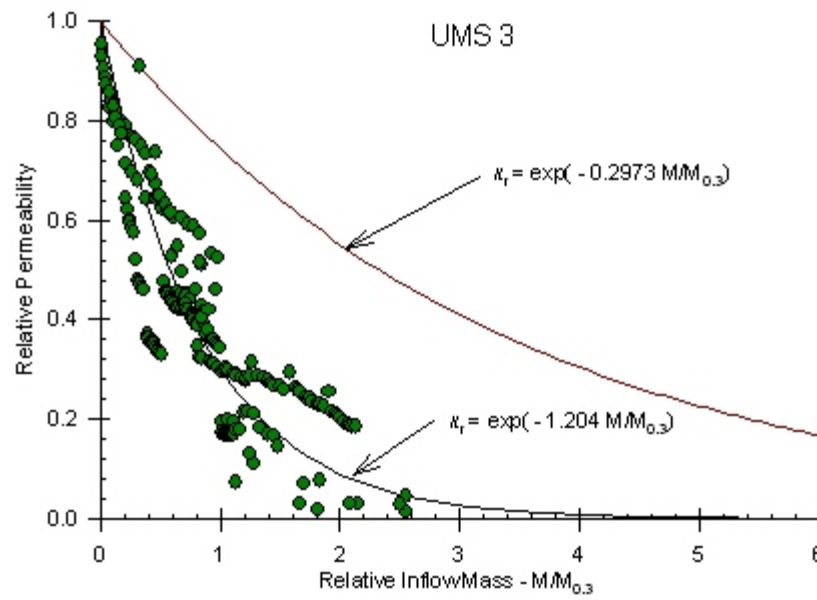


Figure 4.17. Exponential Models of Relative Permeability for UMS 3.

Analysis of Removal Efficiencies

As given by Equation 4.9, removal efficiency is simply defined as the difference between influent and effluent concentration relative to the influent concentration. Examples of observed influent and effluent concentration for the Camas 7 and UMS 2 rock media are shown in Figures 4.18 and 4.19. These concentrations fluctuate with time. Since influent and effluent concentrations are similar, small fluctuations can result in large variations in observed removal efficiencies. Effluent concentrations were occasionally larger than the influent concentrations. The removal efficiency is then negative. Negative removal efficiencies were not included in the data analysis. Problems with fluctuations with influent and effluent concentrations were more troublesome with the UMS rock media where relatively few effluent concentrations were gathered. More sophisticated analyses using cumulative trap efficiencies were done to address these issues. In general, statistical analyses of removal efficiency are biased toward the Camas data set because more data were collected for these rock filters.

Estimates of removal efficiencies were also explored using the cumulative trap efficiency equations given by Equation 4.13b, 4.13c, and 4.13d. With this approach, the cumulative deposition of mass in the media is needed. Because of the large number of effluent concentration for the Camas rock filter, the cumulative mass deposition is reliably estimated using inflow and outflow mass integrated with time. Only a relatively small number of effluent concentrations were measured for the UMS rock filters. Therefore deposition was estimated with respect to relative permeability using Equation 4.15b. Further adjustments were made so that total deposition correspond to that measured directly from the core at the end of the run.

Observed removal efficiencies plotted as function of relative permeability are shown in Figure 4.20. A large scatter of values is apparent, especially for low relative permeabilities. The best fit linear equation is shown by the unbracketed equation. Although the fit is not strong, the slope term is still significantly different than zero at the 1% level. This suggests that the trap efficiency of the media increases with increasing deposition (decreasing relative permeability). As discussed later, the bracket equation is the best fit using cumulative efficiency data.

The first attempt to reduce the scatter of observations in Figure 4.20 was to normalize the removal efficiency data by the overall trap efficiency at $\kappa_r = 0.3$. This trap efficiency was estimated using the Equation 4.17a. Unfortunately, this normalization method does not substantially improve the representation of the removal efficiency data and was not used in subsequent data analysis.

The analysis of cumulative trap efficiency is shown in Figure 4.21. In comparison to the analysis of removal efficiency, the scatter appears to be smaller with this formulation. The predicted trends obtained with this approach are therefore preferred. The best fit equation, using the form suggested by Equation 4.13d, is shown on the figure. The bracketed equation

shows the trend using the original removal efficiency data.

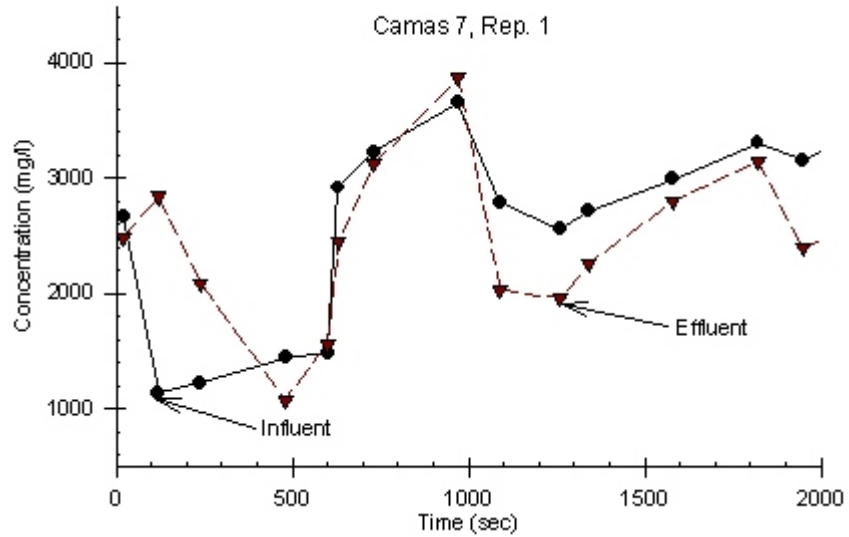


Figure 4.18. Observed Influent and Effluent Concentrations for Camas 7.

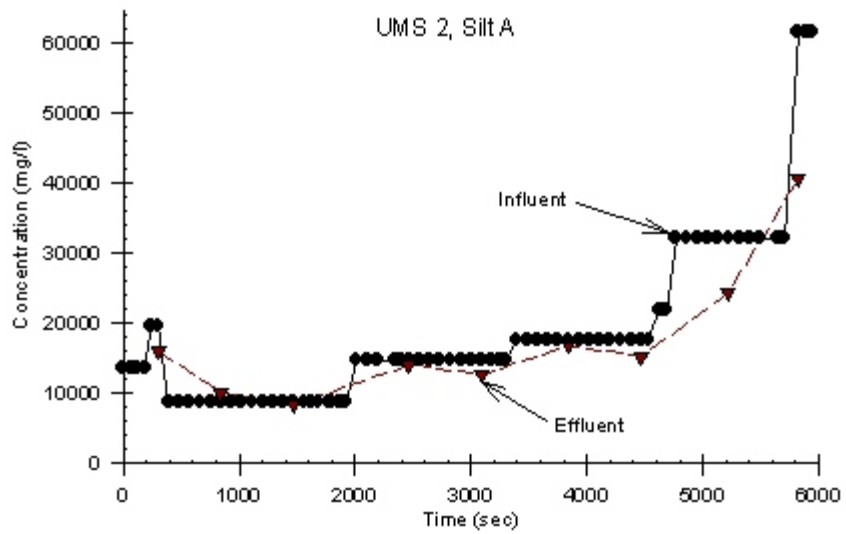


Figure 4.19. Observed Influent and Effluent Concentrations for UMS 2.

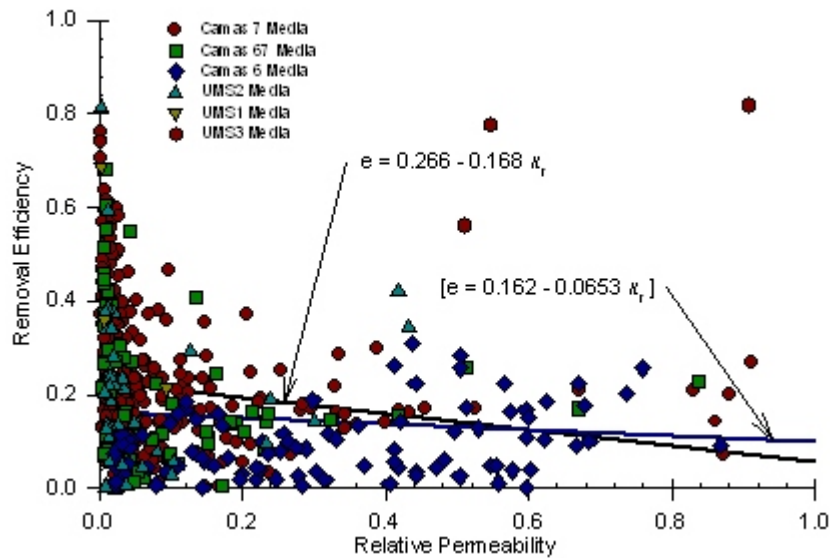


Figure 4.20. Removal Efficiency as a Function of Relative Permeability.

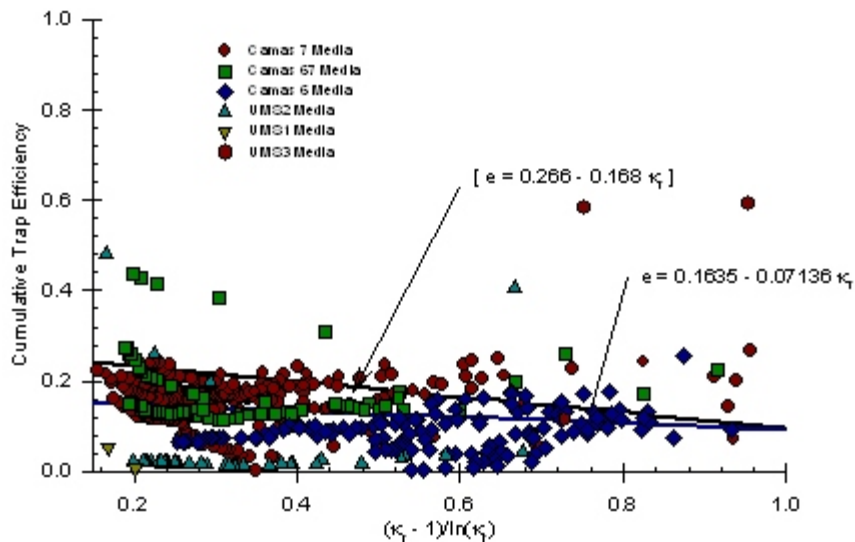


Figure 4.21. Cumulative Trap Efficiency as a Function of Weighted Relative Permeability.

Analyses were also performed on the removal efficiency using the process-based parameters as previously given by Equations 4.18a through 4.18e. These analyses were done using removal efficiency defined from changes in deposition mass and inflow mass, where the deposition mass was estimated using the same general procedures as given for the cumulative

trap efficiency.

Settling velocity in these process-based parameters is estimated using WATER model relationships (Wilson et al., 2006). To select the appropriate diameters of sediment and media, parameters were evaluated for selected diameters between 10% to 90% finer values and the goodness-of-fit was evaluated for each of the combination of diameters. This analysis suggested that a diameter of sediment corresponding to the 25% finer value and the median diameter of the media are good estimates.

Two different statistical models were explored to represent the observed data. The first model used a log-linear model (power model). The two most significant variables were the diameter ratio and the contact number. The second model was based on the work done for the filtration of aerosol and hydrosol by chemical engineering (Tien, 1987). This work suggests the prediction of removal efficiency using a relationship of the form

$$e = b_0 + b_1 X_1 + b_2 X_2 \quad (4.21)$$

where

$$X_1 = \gamma^2 A_s N_{Lo}^{1/8} D_R^{15/8} \quad (4.22a)$$

and

$$X_2 = \gamma^2 A_s C_N^{1.2} D_R^{-0.4} \quad (4.22b)$$

where parameters are as previously defined.

A comparison of predicted and observed removal efficiency using the process-based parameters is shown in Figures 4.22 and 4.23. The data are roughly clustered into values corresponding to small (largest removal efficiency), medium and large (smallest removal efficiency) diameters of the rock filters. Neither model represented the observed data well. As previously discussed, there are inherent problems in the observed removal efficiencies that likely contributed to the poor fit. The power model is simpler and is therefore preferred.

Evaluation of Data for $0.3 \kappa_c$

The exponential decay model (see Equation 4.20) is used in the Protocol Method. It requires an estimate of the inflow mass at $0.3 \kappa_c$ (i.e., $M_{0.31}$). This value could be estimated directly from experimental studies similar to those done here. If the user doesn't have the resources to perform these studies, they may wish to estimate this parameter from our data using a regression equation. Therefore, a regression analysis of log-transformed data was done to develop potential predictive relationships for $M_{0.31}$ as a function of media diameter, sediment diameter, average influent concentration and core porosity. The data were limited to only those cores where the final κ_t was less than or equal to 0.3.

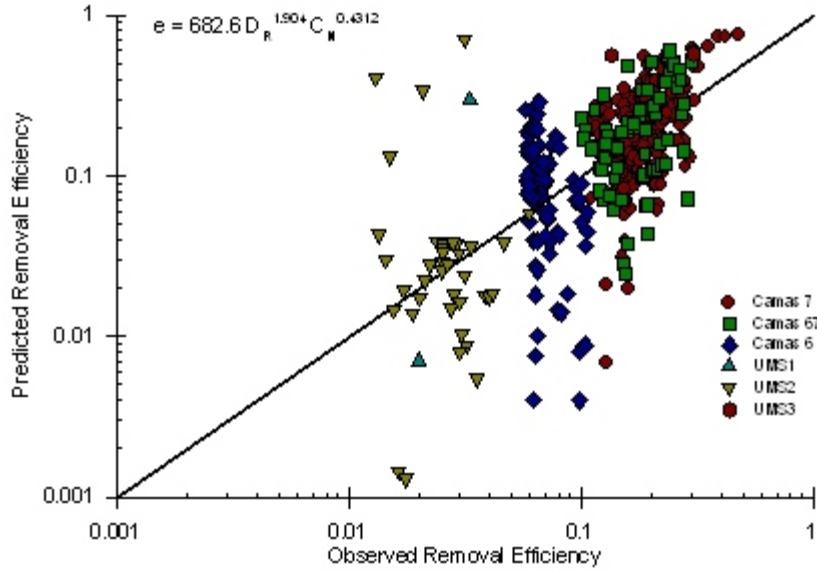


Figure 4.22. Predicted and Observed Removal Efficiencies Using Power Model of Process-based Parameters.

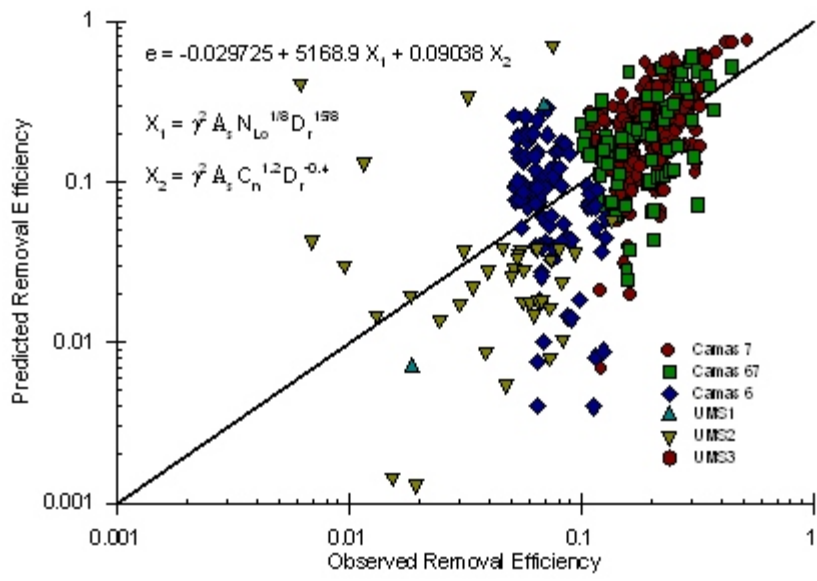


Figure 4.23. Predicted and Observed Removal Efficiencies Using Additive Model of Process-based Parameters.

The results of the regression analysis are shown in Figure 4.24. Average concentration and

porosity were not significant regression variables. Selected combinations of diameters corresponding to 10% through 90% finer values were examined in the regression model. Median diameters were selected to sediment and media size characteristics. Also shown in the figure are the results from the cores that were not plugged with sediment. Here the observed $M_{10,3}$ was taken as the total mass into the core (an underestimation) and predicted values were those obtained with the use of the stickiness coefficient given by Equation 4.19. The predicted results are substantially greater than those observed non-plugged values, which is desirable.

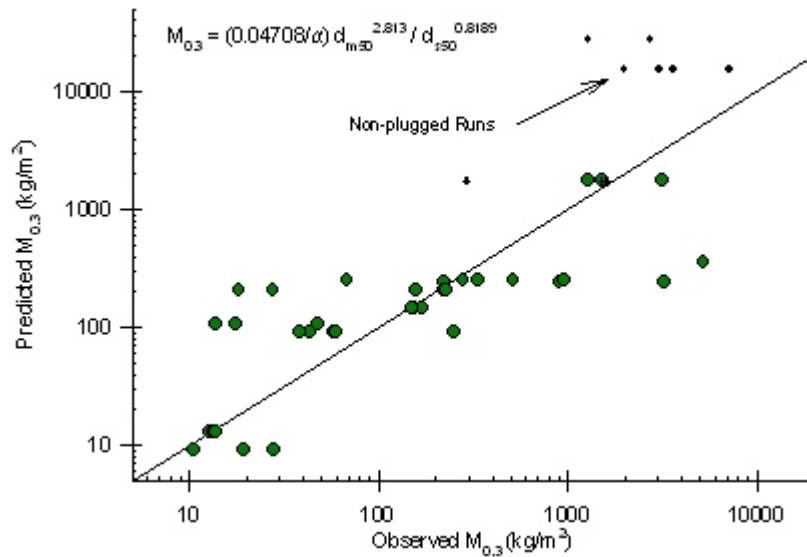


Figure 4.24. Predicted and Observed Cumulative Inflow Mass at $0.3\kappa_c$.

In addition to $M_{10,3}$, the corresponding deposition mass is also of interest. The deposition mass can be obtained as the product of the cumulative trap efficiency and inflow mass at $\kappa_r = 0.3$. The cumulative trap efficiency at $\kappa_{rstd} = 0.3$ was estimated using Equation 4.17a.

Regression analysis was performed to investigate the overall trap efficiency at $\kappa_r = 0.3$. The results are shown in Figures 4.25 and 4.26. Median sediment and media diameters were once again found to be good representative values for the size of influent sediment and the rock filter. Average concentration was a significant variable, but didn't substantially improve the overall representation of trap efficiency.

A summary of core characteristics at $\kappa_r = 0.3$ is given in Table 4.2. In comparison to the results in Table 4.1, which corresponds to the characteristics at the end of the test, the inflow mass, deposition mass, and fraction of porosity are substantially smaller. A possible explanation is that deposition corresponding to $\kappa_r = 0.3$ occurs mainly in the top portion of the core.

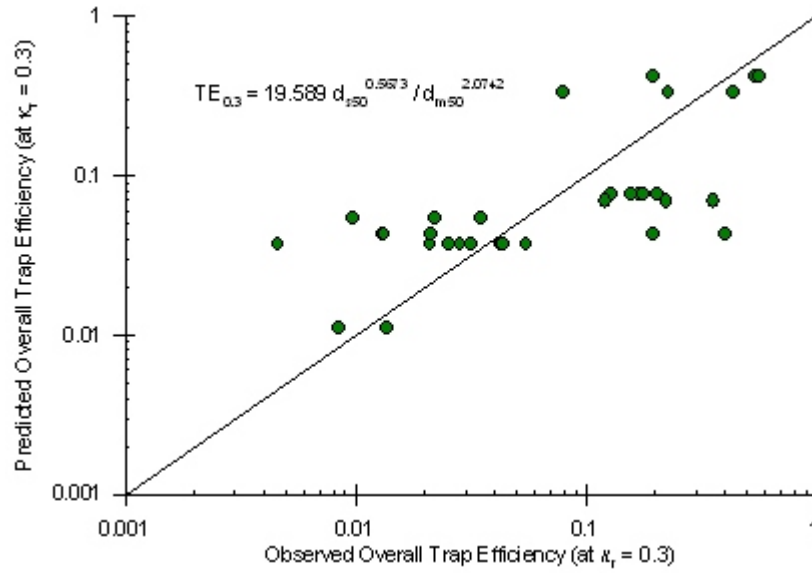


Figure 4.25. Predicted and Observed $T_{e0.30}$ Using Sediment and Media Sizes.

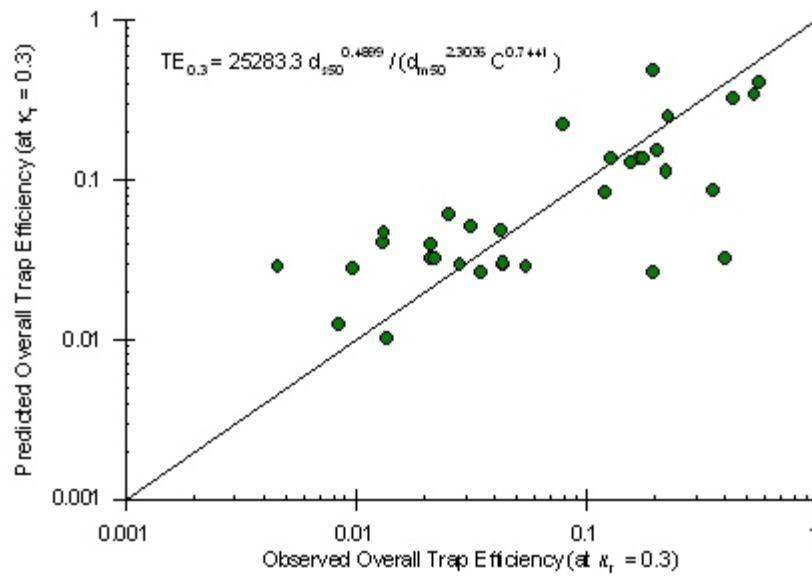


Figure 4.26. Predicted and Observed $T_{e0.30}$ Using Particle Sizes and Influent Concentration.

Table 4.2. Summary of Characteristics of Data Sets at $\kappa_r = 0.3$.

Variables	$M_{10.3}$ kg	$T_{E0.3}$ kg/kg	$M_{Dep0.3}$ kg	$\phi_{10.3}$ m^3/m^3
Observations	36	34	34	34
Mean	9.81	0.136	0.181	0.0308
Std Dev	19.65	0.157	0.173	0.0287
Maximum	92.31	0.568	0.700	0.1179
Minimum	0.19	0.005	0.019	0.0035

Protocol Method

Description

One of the rock filters options available in the WATER model is the Protocol Method. In concept, this method is based on experimentally-derived parameters using a standard protocol. The protocol currently available corresponds to the experimental steps used by Oveson's study. However, additional research could be done to improve or modify her approach to establish a new standard.

Conceptually, the user of the Protocol Method would send the rock or gravel media of interest to laboratory. The laboratory would perform a series of flow rate tests for clean water and sediment-laden flows with different influent sediment size to obtain the parameters for the Protocol Method. These parameters would then be used to simulate the response of the filter as part of a sediment control plan. Parameters of the Protocol Method are porosity (ϕ), clean media permeability (κ_c), inflow mass ($M_{10.3}$) and overall trap efficiency ($T_{E0.3}$) at which $\kappa_r = 0.3$. Inflow mass is relatively easy to measure in tests. A simple method for determining the overall trap efficiency is to estimate the change in the mass of the test chamber, if measured carefully. Trap efficiency is then obtained from the measured inflow and deposition masses.

If users do not have the resources to perform a series of tests for their media, the WATER model has the option of estimating the parameters from some basic characteristics of the media. These estimates are obtained from regression equation developed as part of this study.

Algorithm

A step by step algorithm for the protocol method is given below.

- Step #1:* Select dimension of the rock filter. Determine total volume.
- Step #2:* Determine porosity (ϕ), clean water permeability (κ_c) and mass inflow ($M_{10.3}$) and trap efficiency ($T_{E0.3}$) at $\kappa_r = 0.3 = 0.3$ for rock filter. Use method a or b given below.
- (a) Estimate porosity (ϕ), κ_c , $M_{10.3}$, and $T_{E0.3}$ from standard protocol procedures.

- (b) Determine the porosity (ϕ), d_{m50} , and d_{m75} for the rock filter. The d_{s50} , and percent non-aggregated sand for the influent sediment is computed directly from other components in the WATER model. It can be entered directly for stand alone simulations. A single representative sediment diameter is used for the entire simulation. Compute the κ_c , $M_{10.3}$, and $T_{E0.3}$ using

$$\kappa_c = 0.022647 \left(\frac{d_{m50}^{1.3857}}{(d_{m75}/d_{m25})^{1.6043}} \right)$$

$$M_{10.3} = \left(\frac{0.04708}{\alpha} \right) \left(\frac{d_{m50}^{2.813}}{d_{s50}^{0.8189}} \right)$$

$$T_{E0.3} = (19.588) \alpha \left(\frac{d_{s50}^{0.5673}}{d_{m50}^{2.0749}} \right)$$

$$\alpha = 1 - \exp\{ - \exp[- 0.30 (\text{Percent Sand} - 65)] \}$$

where $M_{10.3}$ has units of kg, diameters of media (subscript m) and influent sediment (subscript s) has unit of mm.

- Step #3:* Adjust the $M_{10.3}$ for non-ideal conditions using an input safety factor (S_F). The $M_{10.3}$ is then computed as

$$M_{10.3} = \frac{M_{10.3}}{S_F}$$

- Step #4:* Adjust $M_{10.3}$ and trap efficiency for potentially unrealistic values. Compute mass deposited, volume deposited, and fraction of porosity as

$$M_{D0.3} = T_{E0.3} M_{10.3}$$

$$V_{D0.3} = \frac{M_{D0.3}}{(2.6) 1000 \text{ kg/m}^3}$$

$$f_{\phi 0.3} = \frac{V_{D0.3}/V_T}{\phi}$$

$$M_{Dmax} = 0.5 * \phi * V_T * 1000.0 * 2.6$$

The maximum deposition assumes a maximum fraction of the porosity filled by deposition at $\kappa_r = 0.3$ is 50% (substantially larger than that observed with the experimental data set). If $M_{Dmax} < M_{D0.3}$, the predicted values of $M_{10.3}$ and $T_{E0.3}$ are reduced using the equation given below. Since the inflow mass was more reliably measured in the experiments, a greater reduction is given to the trap efficiency.

$$M_{10.3} = M_{10.3} \left(\frac{M_{Dmax}}{M_{D0.3}} \right)^{1/3} \quad \text{and} \quad T_{E0.3} = T_{E0.3} \left(\frac{M_{Dmax}}{M_{D0.3}} \right)^{2/3}$$

Step #5: Estimate permeability and specific discharge as

$$\kappa_r = \frac{\kappa}{\kappa_c} = \exp \left[- 1.204 \left(\frac{M_I}{M_{0.3I}} \right) \right]$$

$$\kappa = \kappa_r \kappa_c$$

$$q = \frac{-1 + \sqrt{1 + 4g\kappa\sqrt{\kappa C} (-\partial\Phi/\partial\ell) / v^2}}{2\sqrt{\kappa C} / v}$$

where $C=0.6$. For units of κ of mm^2 , g of mm^2/h , v of mm^2/h , specific discharge has units of mm/h .

Step #6: Estimate removal efficiency in the media using ($\kappa_{r,\text{std}} = 0.3$)

$$\frac{e}{E_{\text{std}}} = e^* = \frac{b_o + b_1 \kappa_r}{b_o + b_1 \left(\frac{\kappa_{r,\text{std}} - 1}{\ln(\kappa_{r,\text{std}})} \right)} = \frac{b_o + b_1 \kappa_r}{b_o + 0.5814 b_1}$$

where $b_o = 0.1629$ and $b_1 = -0.0653$. We therefore obtain

$$e = e^* T_{E0.3}$$

Step #7: Repeat steps 5 and 6 throughout the simulation.

Development of Process-Based Model

Pore-Scale Approach

General Concepts

Specific discharge is defined as the volumetric flow rate divided by the total cross sectional area. Solution approaches discussed thus far have been at a Darcian scale that does not consider flow processes within individual pores. The process-based model is developed within a framework at the pore scale. Differences between representation at the Darcian scale and the pore scale are shown in Figure 4.27. The pore scale framework considers flow in individual pores as the product of the pore velocity and the pore area. Total flow is obtained by adding all of the contributing pores to flow. Specific discharge is obtained by dividing the total flow rate by the total cross sectional area.

Representation of the number and distribution of pores is obviously important for the pore-scale approach. The media are represented as a collection of interconnected pores of varying radii. The domain of these pore radii, r , lies between R_{min} and R_{max} and is described as a pore distribution function $f(r)$, which is media dependent. These concepts are shown in Figure 4.28.

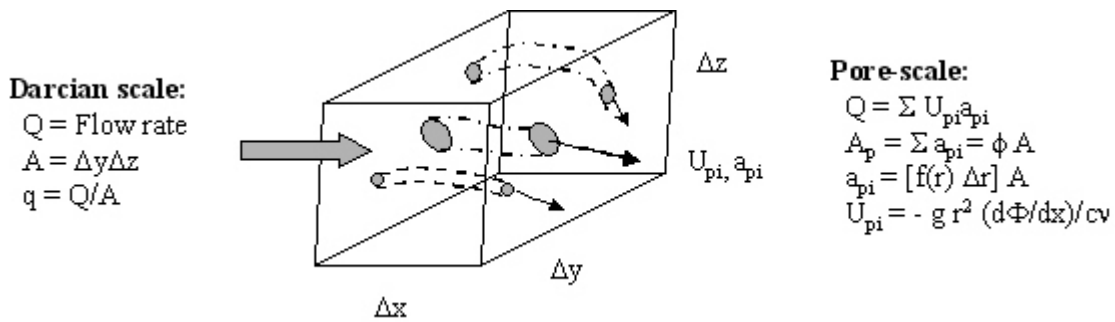


Figure 4.27. Concepts for Darcian Scale and Pore Scale Representation of Flow.

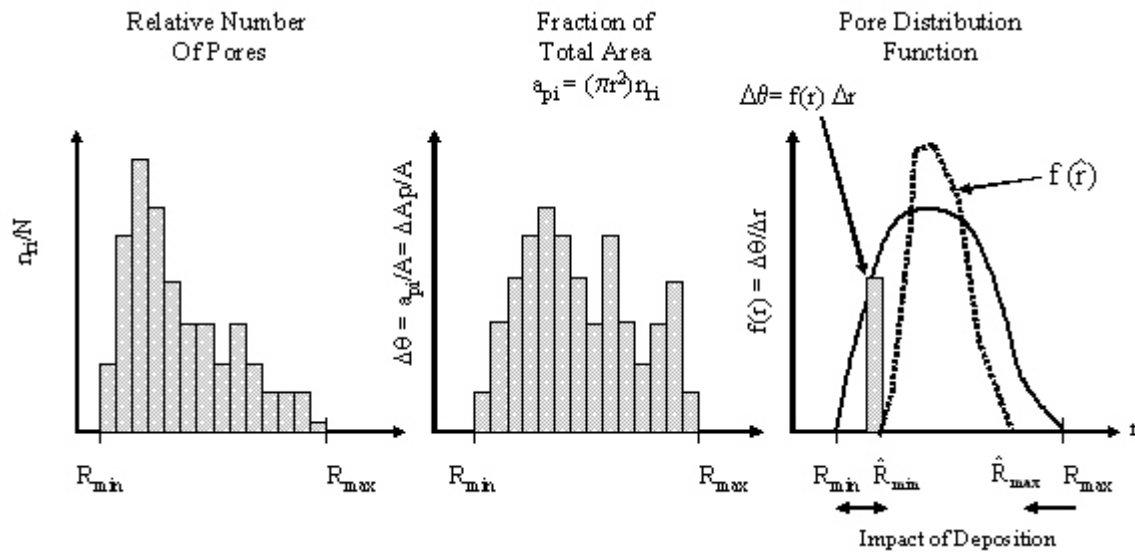


Figure 4.28. Hypothetical Representation of the Pores in Rock Filters.

In Figure 4.28, the number of pores that corresponds to a particular pore radius is shown in the left figure. This number is clearly dependent on the media type. For example, sand has more pores of smaller radii than gravel. However, a more useful representation is the distribution of pore surface areas relative to the total surface area (voids and soil). This concept is shown in the middle figure and can be, conceptually, computed from the number of pores and the area of these pores. For an areal definition of moisture content, changes in moisture content by filling (or draining) pores corresponding to a particular radius are those values given by the bar graph. The pore distribution is used to capture this concept for a continuous function and is defined $f(r) = \Delta\theta/\Delta r$ for the limit of $\Delta r \rightarrow 0$. Any incremental change in moisture content requires a corresponding change in water-filled radii, or

$$d\theta = f(r) dr = \frac{dA_p}{A} \tag{4.23a}$$

where A_p is the cumulative pore area with pore radius. It follows directly from the above equation that the moisture content is defined as

$$\theta = \int_{R_{\min}}^R f(r) dr \quad (4.23b)$$

Two special integration limits are: $R = R_{\min} \rightarrow$ Lowest Moisture Content = θ_{\min} and $R = R_{\max} \rightarrow$ Saturated Moisture Content = θ_s .

Of particular importance to the process-based model is the change in characteristics with sediment deposition. Hypothetical changes are shown in the right figure. Deposition could possibly (1) decrease or even increase the size of the smallest pore, (2) decrease the size of the largest pore and/or (3) change the pore distribution function. Variables that change as the result of deposition will be represented by the hat symbol. Direct measurement of pore distribution function is not possible. An indirect measure, however, can be obtained using fractal relationships.

Specific Discharge Using Pore Velocity and Area

By following widely used concepts for Darcian flow through porous media (Brooks and Corey, 1964; Mualem, 1976), specific discharge can be determined by the sum of the product of velocity and area of discharge for individual pores divided by the total cross sectional area. The pore area between r_i and r_i+dr is defined from the pore distribution function as

$$a_{pi} = dA_p = A f(r) dr \quad (4.24)$$

As previously discussed (i.e., Equation 4.6), the velocity in an idealized pore can be approximated as.

$$U_i = - \alpha_i \frac{g r_i^2}{C'v} \left(\frac{d\Phi_i}{dx} \right)^{\eta_i} \quad (4.25a)$$

where $d\Phi_i/dx$ is the potential gradient for pore radii of r_i . To account for non-ideal pores, a tortuosity factor (T) for the complex flow path between two faces and an adjustment factor (ζ) for irregular shaped pores. The velocity is then estimated as

$$U_i = - \alpha_i (T \zeta) \left(\frac{g r_i^2}{C'v} \right) \left(\frac{d\Phi_i}{dx} \right)^{\eta_i} \quad (4.25b)$$

By using Equations 4.24 and 4.25b, the incremental change in specific discharge is defined as

$$dq_i = \frac{U dA_p}{A} = - \alpha_i (T \zeta) \left(\frac{g r_i^2}{C'v} \right) \left(\frac{d\Phi_r}{dx} \right)^{\eta_i} f(r_i) dr \quad (4.26a)$$

where α and η can conceptually vary with pore radius. The total flow from all water conducting pores less than or equal to R is then obtained as

$$q = - \left(\frac{g}{C'v} \right) \int_{R_{\min}}^R \alpha_r (T \zeta) r^2 \left(\frac{d\Phi_r}{dx} \right)^{\eta_r} f(r) dr \quad (4.26b)$$

Tortuosity and other non-ideal factors are assumed to be a power function of the difference between the moisture content and the lowest moisture content. Mathematically, these factors are represented as

$$\Omega = \frac{\int_{R_{\min}}^R \alpha_r (T \zeta) r^2 \left(\frac{d\Phi_r}{dx} \right)^{\eta_r} f(r) dr}{\alpha \left(\frac{d\Phi}{dx} \right)^{\eta} \int_{R_{\min}}^R r^2 f(r) dr} \quad (4.26c)$$

where α , η , and $d\Phi/dx$ are the effective values for all conducting pores, that is, these parameters correspond to values for the media, and Ω is the combined adjustment factor for non-ideal flow.

By using the adjustment factor, the pore-scale specific discharge for *clean (sediment-free) condition* is defined as

$$q_c = - \alpha_c \Omega_c \left(\frac{d\Phi}{dx} \right)^{\eta_c} \left(\frac{g}{C'v} \right) \int_{R_{\min}}^{R_{\max}} r^2 f(r) dr \quad (4.27)$$

where the subscript c is used to indicate media without any sediment deposition.

Fractal Representation of Porous Media

Background

The Sierpinski carpet is a useful model to illustrate fractal concepts for porous media and will be used to illustrate important features of fractals (Mandelbrot, 1977). These features are then generalized for other types of fractal surfaces.

The Sierpinski carpet is shown in Figure 4.29 for four level of recursion (the blocks are squares). We start with an original filled surface area of side length b_0 . We then insert a pore space corresponding to a pore of side length $b_1=b_0/3$. At the next smaller scale, a pore space of side length $b_2=b_1/3=b_0/9$ is placed in the center of the remaining eight areas. This approach is used for the next two iterations for subsequent subregions using smaller boxes of length $b_3=b_2/3=b_0/3^3$ and then using boxes of lengths of $b_4=b_3/3=b_0/3^4$.

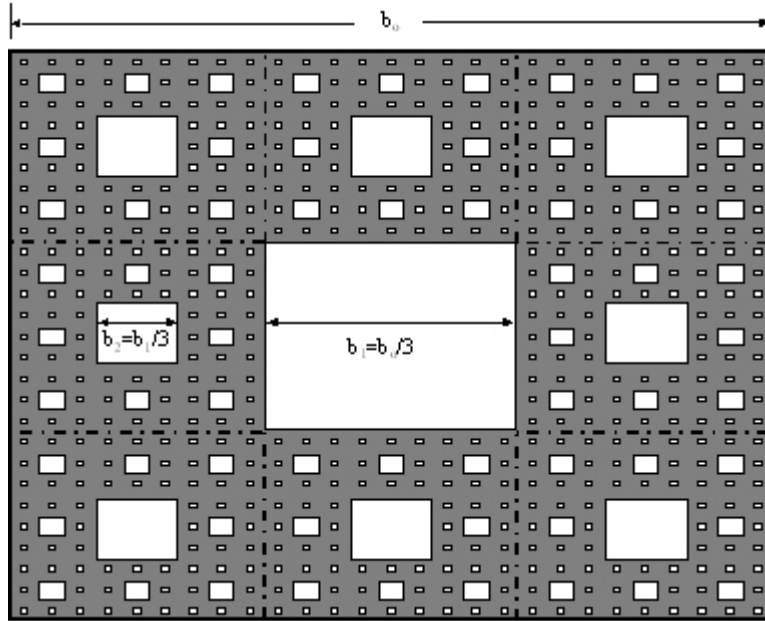


Figure 4.29. Sierpinski Carpet to Illustrate Fractal Concepts for Porous Media.

The fractal nature of the solid surface and pore surface may be of interest. The fractal dimensions using the box counting method for the solid and pore surface can be defined as (Mandelbrot, 1977)

$$D_s = \frac{\log(n_{i+1}/n_i)}{\log(\epsilon_i/\epsilon_{i+1})} = \frac{\log(n_i)}{\log(\lambda_i)} \quad \text{and} \quad D_v = \frac{\log(N)}{\log(1/\epsilon)} = \frac{\log(N_{i+1}/N_i)}{\log(\lambda)} \quad (4.28a)$$

where D_s and D_v are the fractal dimensions of the solid and pore surfaces, respectively, n_i and N_i are the number of boxes of size (width) ϵ_i needed to cover the solid and pore space, respectively. For porous media, we are typically interested in the number of pores corresponding to different pore widths. By using the box width as measure of scale, we can readily define the number of pores as

$$N_{i+1} = N_i \left(\frac{b_i}{b_{i+1}} \right)^{D_v} \quad (4.28b)$$

Recursive relationships and number of boxes to cover the pore and solid surfaces for the Sierpinski carpet are shown in Table 4.3. Two sets of equations are given for the solid surface. The first equation is obtained by computing the total number of boxes to cover the total surface and then subtracting the number of boxes used to cover the pore surface. The second equation is based on computing the number of boxes necessary to cover solid surface within each of the major subareas. The number of boxes is easily computed for each of the major subareas and then adding the number of boxes to cover the large pore in the center of the surface.

The fractal dimension of the solids is easily defined as

$$D_s = \frac{\log(n_i)}{\log(\lambda_i)} = \frac{\log(\lambda_i^2 - N_i)}{\log(\lambda_i)} \approx 1.893 \quad (4.29)$$

where the first relationship is based on the second recursive relationship in the table and the second equality on the first. The number of pore space boxes can now be directly related to the fractal dimension of the solids as

$$N_i = \lambda_i^2 - \lambda_i^{D_s} \quad (4.30)$$

Table 4.3. Box-Counting Relationships for Defining Fractal Numbers.

Scale	Number of Boxes for Pore Surface		Number of Boxes for Solid Surface	
	Equation	Value (N)	Equation	Value (n)
$\epsilon_1 = b_1 = b_0/3$ $\lambda_1 = 3$	1	$N_1 = 1$	$3^2 - N_1 = \lambda_1^2 - N_1$	$n_1 = 8$
$\epsilon_2 = b_2 = b_1/3 = b_0/\lambda_2$ $\lambda_2 = 3^2$	$8 N_1 + 3^2$	$N_2 = 17$	$(3^2)^2 - N_2 = \lambda_2^2 - N_2$ or $(3^2 - 1) n_1 = n_1^2$	$n_2 = 64$
$\epsilon_3 = b_3 = b_2/3 = b_0/\lambda_3$ $\lambda_3 = 3^3$	$8 N_2 + (3^2)^2$	$N_3 = 217$	$(3^3)^2 - N_3 = \lambda_3^2 - N_3$ or $(3^2 - 1) n_2 = n_1^3$	$n_3 = 512$
$\epsilon_4 = b_4 = b_3/3 = b_0/\lambda_4$ $\lambda_4 = 3^4$	$8 N_3 + (3^3)^2$	$N_4 = 2465$	$(3^4)^2 - N_4 = \lambda_4^2 - N_4$ or $(3^2 - 1) n_3 = n_1^4$	$n_4 = 4096$

Areal Porosity and Moisture Content

Tyler and Wheatcraft (1990) used the Serpinski carpet results to estimate the areal porosity as a function of pore size. Since areal porosity is defined as the area of pore surface divided by the total area, the porosity for each pore size is defined as

$$\phi(b_i) = \frac{N_i b_i^2}{b_0^2} = \frac{N_i (b_0/\lambda_i)^2}{b_0^2} = \frac{N_i}{\lambda_i^2} \quad (4.31a)$$

where $\theta(b_i)$ is the areal porosity corresponding to pore of size b_i . By using the relationship between number of pores (N_i) and the fractal dimension of solids (D), we obtain

$$\phi(b_i) = \frac{\lambda_i^2 - \lambda_i^{D_s}}{\lambda_i^2} = 1 - \lambda_i^{D_s-2} \quad (4.31b)$$

The above relationship presumes a fractal surface. Only pores greater than the pore of interest are used to compute porosity. Pores smaller than this size are not discernable for the

scale of measurement.

As discussed later, it is mathematically convenient for us to have the areal porosity approximated as a continuous function and to consider the media as circular pore. Square pores are converted in an equivalent pore radius using equal surface area. We then obtain

$$\pi r_i^2 = b_i^2 = \left(\frac{b_o}{\lambda_i} \right)^2 \quad \text{and therefore} \quad r_i = \frac{1}{\sqrt{\pi}} \left(\frac{b_o}{\lambda_i} \right) \quad (4.32)$$

Let's consider the maximum radii for conducting water as $r = R_{\max}$, We then can obtain

$$b_o = \sqrt{\pi} \lambda_1 R_{\max} \quad (4.33a)$$

where R_{\max} and λ_1 are constants. We can now define

$$\lambda_i = \lambda_1 \left(\frac{R_{\max}}{r} \right) \quad (4.33b)$$

from which we obtain areal porosity as

$$\phi(r) = 1 - \lambda_1^{D_s-2} \left(\frac{R_{\max}}{r} \right)^{D_s-2} \quad (4.33c)$$

Approximating the discrete fractal surface using a continuous range of pore radii, the change in areal porosity with pore radius is simply

$$d\phi = (D_s - 2) \lambda_1^{D_s-2} \left(\frac{R_{\max}}{r^2} \right) \left(\frac{R_{\max}}{r} \right)^{D_s-3} dr = f(r) dr \quad (4.34a)$$

where $f(r)$ is the pore distribution function that has been previously defined (see Figure 4.27). The pore distribution function is then defined as

$$f(r) = (D_s - 2) \lambda_1^{D_s-2} \left(\frac{R_{\max}}{r^2} \right) \left(\frac{R_{\max}}{r} \right)^{D_s-3} \quad (4.34b)$$

If we integrate between $r = R_{\max}$, to $r = R_i$, we can determine the increase in areal porosity between these radii. Mathematically, we obtain

$$\Delta \phi(R_i) = \lambda_1^{D_s-2} (D_s - 2) \int_{R_{\max}}^{R_i} \left(\frac{R_{\max}}{r^2} \right) \left(\frac{R_{\max}}{r} \right)^{D_s-3} dr \quad (4.34c)$$

which can be easily integrated using $u = R_{\max}/r$, $du = -R_{\max}/r^2 dr$. We then obtain

$$\Delta \phi(R_i) = \lambda_1^{D_s-2} \left[1 - \left(\frac{R_{\max}}{R_i} \right)^{D_s-2} \right] \quad (4.34d)$$

The total porosity is then defined as

$$\phi(R_i) = \phi(R_{\max}) + \Delta \phi(R_i) = 1 - \lambda_1^{D_s-2} + \lambda_1^{D_s-2} \left[1 - \left(\frac{R_{\max}}{R_i} \right)^{D_s-2} \right] = 1 - \lambda_1^{D_s-2} \left(\frac{R_{\max}}{R_i} \right)^{D_s-2} \quad (4.35)$$

which is equal to the definition of porosity previously given.

The moisture content for a particular size is defined as the area (or volume) of pores *filled* with water for sizes less than or equal to b . This can be obtained by subtracting the porosity for b from the total porosity from the smallest pores ($b \rightarrow 0, \lambda \rightarrow \infty$). Areal moisture content is then defined as

$$\theta(b_i) = \text{Total Porosity} - \text{Porosity for } b_i$$

or

$$\theta(b_i) = \phi(b \rightarrow 0) - \phi(b_i) = \left[\lim_{\lambda \rightarrow \infty} (1 - \lambda^{D_s-2}) \right] - \left[1 - \lambda_i^{D_s-2} \right] \quad (4.36a)$$

Since $D_s < 2$, the $\lambda^{D_s-2} \rightarrow 0$ as $\lambda \rightarrow \infty$. We then obtain

$$\theta(b_i) = \lambda_i^{D_s-2} \quad (4.36b)$$

By using the relationship between λ_i and radii given by Equation 4.33b, we obtain

$$\theta(r) = \lambda_1^{D_s-2} \left(\frac{R_{\max}}{r} \right)^{D_s-2} \quad (4.37)$$

Fractal Representation with Sediment Deposition

Let's define D_{sc} as the fractal dimension of solids corresponding to the clean media (no deposition) and D_s as the fractal number corresponding to the media with deposition. By using trap efficiencies or other methods, the cumulative mass deposited, and therefore cumulative deposition volume, in the media is known. The fraction of the total effective volume can then be computed as

$$\theta_{\text{dep}} = \frac{\text{Volume of deposited sediment}}{f_{\text{vol}} (\text{Total volume})} \quad (4.38)$$

where f_{vol} is an adjustment factor for non-uniform deposition with depth within the rock filter. For example, a value of 0.1 corresponds to deposition in the top 10% of the media.

Let's define β as the fraction of deposited volume (θ_{dep}) that fills the smallest pores in the media. We then obtain the fractional volume in these pores as

$$\theta_t = \beta \theta_{\text{dep}} \quad (4.39a)$$

This effectively shifts the smallest fractal scale so that $R_{\min} = R_t$ in the clean media pore distribution function. The unfilled, available porosity for radii greater than R_t as,

$$\phi_{\text{ac}} = \phi_T - \theta_t \quad (4.39b)$$

The sediment deposited in pores greater than R_t is also of interest. It is defined as

$$\Delta \theta_{\text{dep}} = (1 - \beta) \theta_{\text{dep}} \quad (4.40a)$$

The available porosity that remains after accounting for this deposition is simply

$$\phi_{ad} = \phi_{ac} - \Delta\theta_{dep} \quad (4.40b)$$

After the parameter β is selected, we can compute θ_{dep} , θ_t , ϕ_{ac} , $\Delta\theta_{dep}$ and ϕ_{ad} from the trap efficiency models and specific gravity of sediment. They are considered to be known values for the fractal model.

For equal areal and volumetric porosity, the available porosity for clean media is defined as

$$\phi_{ac} = 1 - \lambda_{1c}^{D_{sc}-2} \left(\frac{R_{max}}{R_t} \right)^{D_{sc}-2} \quad (4.41a)$$

which can be rearranged as

$$\frac{R_{max}}{R_t} = \frac{(1 - \phi_{ac})^{\frac{1}{D_{sc}-2}}}{\lambda_{1c}} \quad (4.41b)$$

For the special case when $\theta_t = 0$ (i.e., $\beta = 0$ with sediment deposition), the parameters in Equation 4.41b are defined as $R_{t,c} = R_{min,c}$ and $\phi_{ac} = \phi_T$.

Likewise for deposition in pores greater than R_t (but none of the pores is completely filled with sediment), the available porosity after deposition can be defined as

$$\phi_{ad} = 1 - \lambda_{1d}^{D_s-2} \left(\frac{\hat{R}_{max}}{\hat{R}_t} \right)^{D_s-2} \quad (4.40a)$$

where the hat symbol refers to the modified radii with deposition. Once again, $\theta_t = 0$ (i.e., $\beta = 0$ with sediment deposition), $R_t = R_{min}$.

We will assume that the radii ratio of maximum to smallest water conducting pore is equal for clean media and media with deposition. We then have

$$\frac{\hat{R}_{max}}{\hat{R}_t} \approx \frac{R_{max}}{R_t} = \frac{(1 - \phi_{ac})^{\frac{1}{D_{sc}-2}}}{\lambda_{1c}} \quad (4.40b)$$

By using this condition, ϕ_{ad} can be evaluated as

$$1 - \phi_{ad} = \left(\frac{\lambda_{1d}}{\lambda_{1c}} \right)^{D_s-2} (1 - \phi_{ac})^{\frac{D_s-2}{D_{sc}-2}} = \lambda_*^{D_s-2} (1 - \phi_{ac})^{\frac{D_s-2}{D_{sc}-2}} \quad (4.40c)$$

where λ_* equals the ratio of the λ_{1d} and λ_{1c} . We now have two parameters, λ_* and D_s , that can be used to solve for ϕ_{ad} . A unique solution is possible if another condition is specified. For example if we assume $D_s = D_{sc}$, we can then solve for λ_* as

$$\hat{\lambda}_* = \left(\frac{1 - \phi_{ad}}{1 - \phi_{ac}} \right)^{\frac{1}{D_{sc}-2}} \quad (4.40d)$$

The solution given by Equation 4.40d corresponds to only a change in the scaling factor with

deposition. This solution is not preferred because we know that the fractal dimension is two for a completely plugged filter (i.e., $\phi_{ad}=0$). To allow the fractal dimension to vary also with deposition, the following function is used

$$\lambda_* = \left(\frac{1 - \phi_{ad}}{1 - \phi_{ac}} \right)^{\frac{K}{D_{sc}-2}} \quad (4.40e)$$

where K is an adjustment factor that allows deposition to be shifted between scaling factor and fractal dimension. A value of one corresponds to a constant fractal dimension of the clean media. A value of K=0.2 was selected for our analyses. By using the above equation for λ_* , we can now evaluate Equation 4.40c as

$$(1 - \phi_{ad})^{D_{sc}-2} = \left(\frac{1 - \phi_{ad}}{1 - \phi_{ac}} \right)^{K(D_s-2)} (1 - \phi_{ac})^{D_s-2} \quad (4.40f)$$

and solve for D_s as

$$D_s = 2 + \frac{(D_{sc} - 2) \ln(1 - \phi_{ad})}{K \ln(1 - \phi_{ad}) + (1 - K) \ln(1 - \phi_{ac})} \quad (4.41)$$

The above equation results in the theoretical correct solution of $D_s = 2$ for a completely plugged media ($\phi_{ad}=0$). Let's also consider the condition where deposition only fills the smallest pores. This corresponds to $\beta = 1$ and $\phi_{ac} = \phi_{ad}$. We again obtain the desired result of $D_s = D_{sc}$, that is, there is no change in the pore size distribution for radii greater than R_t .

The computation of the Interception Number for computing trap efficiency requires a representative media diameter. Statistical analyses previously given suggested that the median diameter be used to represent rock filters. This diameter would conceptually increase with deposition. Let's assume the increase in representative diameter is directly proportional to the increase in the fraction of surface area of solids. We then obtain

$$\frac{\hat{d}_m}{d_m} = \frac{1 - \phi_{ad}}{1 - \phi_T} \quad (4.42)$$

Fractal Model of Relative Permeability

Theoretical Representation

Let us consider the intrinsic permeability for pores with deposition to that of clean water. By using the definitions of intrinsic permeability, we obtain

$$\kappa_r = \frac{\kappa}{\kappa_c} = \frac{K (v/g)}{K_c (v/g)} = \frac{q / [\alpha (\frac{d\Phi}{dx})^n]}{q_c / [\alpha_c (\frac{d\Phi}{dx})^{n_c}]} = \left(\frac{\alpha_c (d\Phi/dx)^{n_c}}{\alpha (d\Phi/dx)^n} \right) \left(\frac{q}{q_c} \right) \quad (4.43)$$

The ratio of q/q_c is evaluated using the pore-scale relationships given by Equations 4.26b and 4.27. For sediment deposition, there is a potential change in the minimum and maximum

radii of the media as well as a change in the distribution of pores. These changes are represented by a “hat” symbol. By using Equations 4.26b and 4.27, we obtain

$$\kappa_r = \left(\frac{\alpha \hat{\Omega} \left(\frac{d\hat{\Phi}}{dx} \right)^\eta \left(\frac{g}{C'v} \right)}{\alpha_c \Omega_c \left(\frac{d\Phi}{dx} \right)^{\eta_c} \left(\frac{g}{C'v} \right)} \right) \frac{\int_{\hat{R}_i}^{\hat{R}_{\max}} r^2 \hat{f}(r) dr}{\int_{R_{\min}}^{R_{\max}} r^2 f(r) dr} \quad (4.44)$$

Since from Equation 4.23a $d\theta = f(r)dr$, the relative permeability can be evaluated with respect to moisture content. The corresponding integration limits for clean media are $r = R_{\min} \rightarrow \theta = \theta_{\min} \approx 0$ and $r = R_{\max} \rightarrow \theta = \phi_T$. The upper integration limit for media with deposition corresponds to $\theta = \hat{\phi}_T = \phi_T - \Delta\theta_{\text{dep}}$. The lower integration limit corresponds to $\theta = \theta_i$. By using these concepts, we obtain

$$\kappa_r = \left(\frac{\alpha \hat{\Omega} \left(\frac{d\hat{\Phi}}{dx} \right)^\eta \left(\frac{g}{C'v} \right)}{\alpha_c \Omega_c \left(\frac{d\Phi}{dx} \right)^{\eta_c} \left(\frac{g}{C'v} \right)} \right) \frac{\int_{\theta_i}^{\hat{\phi}_T} r(\hat{\theta})^2 d\hat{\theta}}{\int_0^{\phi_T} r(\theta)^2 d\theta} \quad (4.45)$$

where the relationship between radii and moisture contents is defined using our fractal relationships.

Fractal analysis was used to derive a relationship between areal moisture content and radius (see Equation 4.37). For simplicity, we assume that volumetric porosity and moisture contents are approximately equal to areal values. We then obtain

$$\theta(r) = \lambda_1^{D_s-2} \left(\frac{R_{\max}}{r} \right)^{D_s-2} = \left(\frac{1}{\lambda_1 R_{\max}} \right)^{1/b} r^{1/b} \quad (4.46a)$$

where

$$b = - \frac{1}{D_s - 2} \quad (4.46b)$$

and therefore

$$r = \lambda_1 R_{\max} \theta^b \quad (4.46c)$$

Relative permeability is then defined as

$$\kappa_r = \left[\frac{\alpha \hat{\Omega} \left(\frac{d\Phi}{dx} \right)^\eta \left(\frac{g}{C'v} \right) \lambda_{1d}^2 \hat{R}_{\max}^2}{\alpha_c \Omega_c \left(\frac{d\Phi}{dx} \right)^{\eta_c} \left(\frac{g}{C'v} \right) \lambda_{1c}^2 R_{\max}^2} \right] \frac{\int_{\theta_l}^{\hat{\Phi}_T} \theta^{2b} d\theta}{\int_0^{\hat{\Phi}_T} \theta^{2b_c} d\theta} \quad (4.47)$$

By following approaches used in unsaturated flow (Mualem, 1976), the non-ideal flow and other characteristic are represented by a power function of

$$\left(\frac{(\Phi_T - \Delta\theta_{dep}) - \theta_l}{\Phi_T} \right)^p = \left(\frac{\Phi_{ad}}{\Phi_T} \right)^p = \frac{\alpha \hat{\Omega} \left(\frac{d\Phi}{dx} \right)^\eta \left(\frac{g}{C'v} \right) \lambda_{1d}^2 \hat{R}_{\max}^2}{\alpha_c \Omega_c \left(\frac{d\Phi}{dx} \right)^{\eta_c} \left(\frac{g}{C'v} \right) \lambda_{1c}^2 R_{\max}^2} \quad (4.48a)$$

We then obtain

$$\kappa_r = \left(\frac{\Phi_{ad}}{\Phi_T} \right)^p \frac{\int_{\theta_l}^{\hat{\Phi}_T} \theta^{2b} d\theta}{\int_0^{\hat{\Phi}_T} \theta^{2b_c} d\theta} = \left(\frac{\Phi_{ad}}{\Phi_T} \right)^p \left[\frac{\left(\frac{1}{2b+1} \right) \left[\theta^{2b+1} \right]_{\theta_l}^{\hat{\Phi}_T}}{\left(\frac{1}{2b_c+1} \right) \left[\theta^{2b_c+1} \right]_{\Phi_T}^0} \right] \quad (4.48b)$$

or

$$\kappa_r = \left(\frac{\Phi_{ad}}{\Phi_T} \right)^p \left(\frac{2b_c+1}{2b+1} \right) \left[\frac{\hat{\Phi}_T^{2b+1} - \theta_l^{2b+1}}{\Phi_T^{2b_c+1}} \right] \quad (4.48c)$$

Since $2b+1 = (D_s - 4)/(D_s - 2)$, we can rearrange the above equation to obtain

$$\kappa_r = \left(\frac{\Phi_{ad}}{\Phi_T} \right)^p \left(\frac{D_s - 2}{D_{sc} - 2} \right) \left(\frac{D_{sc} - 4}{D_s - 4} \right) \left[\frac{\Phi_T^{(D_s-4)/(D_s-2)} - \theta_l^{(D_s-4)/(D_s-2)}}{\Phi_T^{(D_{sc}-4)/(D_{sc}-2)}} \right] \quad (4.49)$$

The key parameters for using the fractal model is the determination of an appropriate p , β , and D_{sc} . Procedures to estimate these parameters from the observed data set are given in the next section.

Estimating Fractal Model Parameters from Observed Data

The following iterative steps can be used to estimate the best set of parameters for each test of the observed data set with measured relative permeabilities with time.

- (1) General media information: Clean media permeability (κ_c), clean media porosity (ϕ_T), and total volume of the core.
- (2) Iterative loop for f_{vol} for values between 0.2 and 1.0.
- (3) Iterative loop for β for values between 0.0 and 1.0.
- (4) Iterative loop for p for values between 0.0 and 3.5.
- (5) Iterative loop for D_{sc} for values between 1.25 and 1.85.
- (6) For each time, estimate the cumulative deposition mass using the methodology previously given to determine cumulative trap efficiency. Compute

$$\text{Cumulative Deposition Volume} = \frac{\text{Mass In} - \text{Mass Out}}{SG \rho_w}$$

$$\text{Fraction of Total Volume} = \theta_{dep} = \frac{\text{Volume of deposited sediment}}{f_{vol} (\text{Total volume})}$$

$$\text{Deposition Volume Fraction for Smallest Pore} = \theta_t = \beta \theta_{dep}$$

$$\text{Available Non-filled-Pores Porosity} = \phi_{ac} = \phi_T - \theta_t$$

$$\text{Deposition Fraction for Non-filledPores} = \Delta \theta_{dep} = (1 - \beta) \theta_{dep}$$

$$\text{Available Porosity After Depositon} = \phi_{ad} = \phi_{ac} - \Delta \theta_{dep}$$

- (7) Estimate the fractal dimension of the media with sediment deposition using (for $K=0.2$)

$$D_s = 2 + \frac{(D_{sc} - 2) \ln(1 - \phi_{ad})}{K \ln(1 - \phi_{ad}) + (1 - K) \ln(1 - \phi_{ac})}$$

- (8) Calculate fractal model relative permeability and the difference between the corresponding observed value, that is

$$\kappa_r = \left(\frac{\phi_{ad}}{\phi_T} \right)^p \left[\frac{(D_{sc} - 4)/(D_{sc} - 2)}{(D_s - 4)/(D_s - 2)} \right] \left[\frac{(\phi_T - \Delta \theta_{dep})^{(D_s - 4)/(D_s - 2)} - \theta_t^{(D_s - 4)/(D_s - 2)}}{\phi_T^{(D_{sc} - 4)/(D_{sc} - 2)}} \right]$$

$$\varepsilon = \kappa_{r,obs} - \kappa_r$$

- (9) For each combination of f_{vol} , β , p , and D_{sc} , compute mean square error

$$\text{MSE} = \frac{1}{n} \sum_{i=1}^n \epsilon_i^2$$

where n is the number of estimates of ϵ for a given run.

(10) Select optimal f_{vol} , β , p, and D_{sc} using minimal MSE

(11) Examine trends in parameters with media and sediment characteristics.

Analyses of Fractal Model Parameters

Direct Estimate of Deposition

The parameters of the fractal model were first evaluated using observed estimates of sediment deposition obtained from cores available at the end of the test. Estimate of deposition within the test was obtained using the relationship given by Figure 4.22. Iterative values for f_{vol} varied by increments of 0.1, by increments of 0.05 for β , by increments of 0.1 for p, and by increments of 0.05 for D_{sc} .

Optimal values of parameters and the corresponding mean square errors are shown in Table 4.4. The optimal parameters varied for the different tests. Optimal parameters range from the allowable minimum value to the allowable maximum value. The optimal value of D_{sc} was the most consistent result.

A comparison between observed and predicted relative permeability, using the optimal parameter set for each test, is shown in Figure 4.30. The calibrated fractal model overpredicted observed relative permeabilities for some tests and underpredicted the relative permeabilities for other tests. Overall, the fractal model was able to represent the observed values with reasonable accuracy.

Predicted Estimate of Deposition

For application at construction sites, field measurements of observed deposition are impractical, and sediment deposition will need to be predicted. In addition, the parameters for the fractal model cannot be optimized based on observed deposition as done for good results shown in Figure 4.30. Analyses to determine these parameters for field application are done in this section.

Table 4.4. Optimal Parameter Values for the Fractal Model.

Run	Optimal β	Optimal p	Optimal D_{sc}	Optimal f_{vol}	Optimal MSE
Camas 7, Rep 1	0.10	3.1	1.85	0.4	0.00064
Camas 7, Rep 2	0.45	3.5	1.85	1.0	0.00283
Camas 7, Rep 3	0.85	3.0	1.85	1.0	0.00117
Camas 7, Rep 4	0.10	3.5	1.85	1.0	0.00177
Camas 7, Rep 5	0.00	3.5	1.85	0.9	0.00173
Camas 67, Rep 1	0.25	3.1	1.85	1.0	0.00308
Camas 67, Rep 2	0.00	3.1	1.85	0.6	0.00173
Camas 67, Rep 3	0.00	3.1	1.85	0.4	0.00008
Camas 6, Rep 1	0.70	3.5	1.85	1.0	0.00411
Camas 6, Rep 2	0.90	0.0	1.85	1.0	0.00881
Camas 6, Rep 3	0.95	1.3	1.85	1.0	0.02630
UMS1, SiltA, Load2, Rep3	0.20	2.1	1.85	0.2	0.00001
UMS2, SiltA, Load1, Rep2	0.00	0.0	1.25	0.2	0.00469
UMS2, SiltB, Load1, Rep2	0.00	0.3	1.35	0.2	0.00077
UMS2, SiltB, Load1, Rep2	0.00	0.3	1.35	0.2	0.00077
UMS2, SiltB, Load2, Rep3	0.00	0.0	1.25	0.2	0.00727
UMS3, SiltA, Load1, Rep2	0.80	0.0	1.30	0.2	0.00441
UMS3, SiltB, Load1, Rep2	0.90	1.6	1.30	1.0	0.00000

The fractal model is evaluated using predicted deposition in the cores. The predicted deposition was obtained from the removal efficiency using a power model of process-based parameters that is shown below

$$e = 682.6 \alpha D_R^{1.904} C_N^{0.4312} \quad (4.50)$$

where D_R and C_N are interception number and contact number as previously defined and α is the adjustment for high percentage of sand given by Equation 4.19. Equation 4.50 is used to predict deposition for observed increments of inflow mass. This deposition is cumulated to obtain the total deposition in the core with time (or cumulative inflow mass).

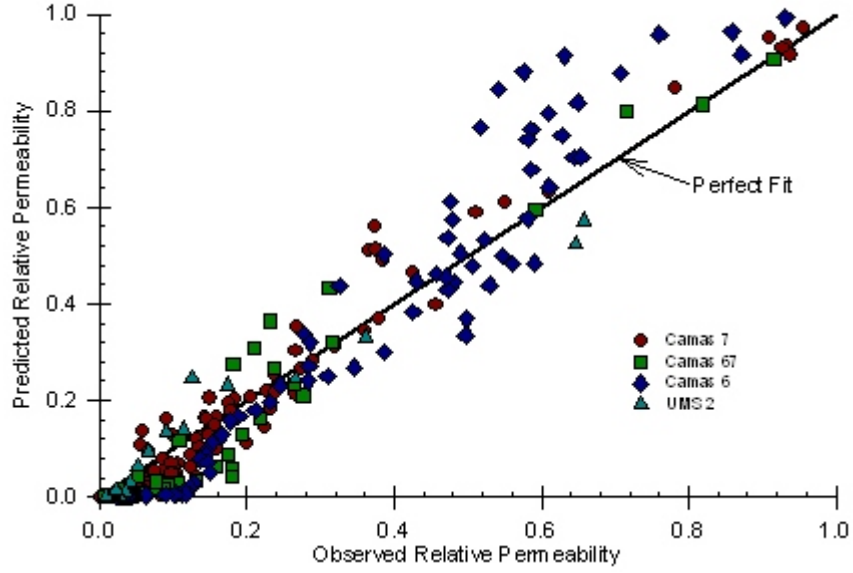


Figure 4.30. Predicted Relative Permeability Using the Best Fit Fractal Model.

The framework to estimate parameters is also modified to vary f_{vol} within the test to account for sediment deposited in the upper part of the filter. This sediment may later be transported downward into the rock filter with subsequent flows. To account for this process, f_{vol} is represented as

$$f_{vol} = 1 - (1 - f_{vol,min}) \exp(-\xi \theta_{dep}) \quad (4.51a)$$

where the $f_{vol,min}$ is the minimum value for the fraction of total volume taken as 0.2 and θ_{dep} is as defined by Equation 4.38. To make the coefficient ξ more physically meaningful, its value is related to a fraction of porosity by using $\xi \theta_{dep,0.9} = \psi \phi$ for $f_{vol} = 0.9$, where ψ is a fraction of porosity. The value of ξ is then defined as

$$\xi = - \frac{\ln[(1 - 0.9) / (1 - f_{vol,min})]}{\psi \phi} \quad (4.51b)$$

Possible values for ψ was explored by using different estimates and by examining its impact on the mean square error. The value appeared to vary (weakly) with media size. As part of a general predictive algorithm, the value is related to the ratio of the median particle size of influent sediment and media as

$$\psi = 1.0 - (1 - 0.1) \exp\left[-35 \left(\frac{d_{s50}}{d_{m50}}\right)\right] \quad (4.52c)$$

For very large media (say, $d_{m50} \rightarrow \infty$), ψ equals a small value of near 0.1. Therefore, a relatively small value of $\theta_{dep,0.9}$ is required to obtain a value of $f_{vol} = 0.9$, corresponding to deposition in most of the filter. For very small media (say, $d_{m50} \rightarrow 0$), ψ equals a large value of near one. Deposition occurs in most of the filter depth (as represented by $f_{vol} = 0.9$) when

$\theta_{\text{dep},0.9} = \phi$. Since the filter is completely plugged for this condition, f_{vol} will be small for the most of the prediction, which corresponds to deposition in only the upper part of the filter.

In addition to estimate of f_{vol} using the above equations, values need to be selected for the other parameters in the fractal model. A value of $p=2$ was selected for the non-ideal flow parameter. This value is consistent with values used in unsaturated flow theory for non-ideal flow (see Brooks and Corey, 1964; Mualem, 1976). Based on the results in Table 4.4, values of $\beta=0.1$ and $D_{\text{sc}}=1.85$ were also selected. By using these values, Equation 4.50 for removal efficiency and observed inflow mass, and Equations 4.51 for f_{vol} , predicted relative permeability is predicted for each of the observed values in the tests.

The parameters of the previous paragraph and the prediction of deposition given by Equation 4.50 have been used to predict the relative permeabilities of the MDOA's and Oveson data. Observed and predicted relative permeabilities are shown in Figures 4.31 and 4.32 for the Camas 7 and UMS 2 rock media. For the Camas 7 media, the predicted relative permeabilities are generally smaller than those observed. For the UMS 2, the model overpredicted relatively permeabilities for some of the tests and underpredicted them for other tests. Differences in predicted and observed values are a consequence of potential errors in predicting both the removal efficiencies and in the relative permeability itself. For example, the predicted permeabilities for influent sediment of clay are greater than observed because, in part, the removal efficiency predicted by Equation 4.50 is smaller than that observed.

Trends in predicted and observed relative permeabilities with inflow mass are shown in Figures 4.32 and 4.33, respectively, for the MDOA silt influent sediment for the Camas rock filters and the Silt A influent sediment for the UMS rock filters. As shown by these figures, the predicted relative permeabilities are sometimes greater than and sometimes less than those observed. Overall, given the complexity of predicting both removal efficiency and relative permeability and the variability in optimal parameters, the fractal model performed reasonably well in predicting the observed relative permeabilities.

Process-Based Method

Description

In addition to the Protocol Method, the user of the WATER model has the option of using the Process-Based Method to simulate the response of rock and gravel filters. The Process-Based Method is based on a conceptual framework to predict sediment deposition in these filters and corresponding changes in their relative permeabilities. Parameters are evaluated using the same data base used to determine the parameters for the Protocol Method. The Process-Based Method has the advantage of providing insight into the filtration process and therefore provides a better framework for incorporating additional research into prediction of the response of rock and gravel infiltration filters.

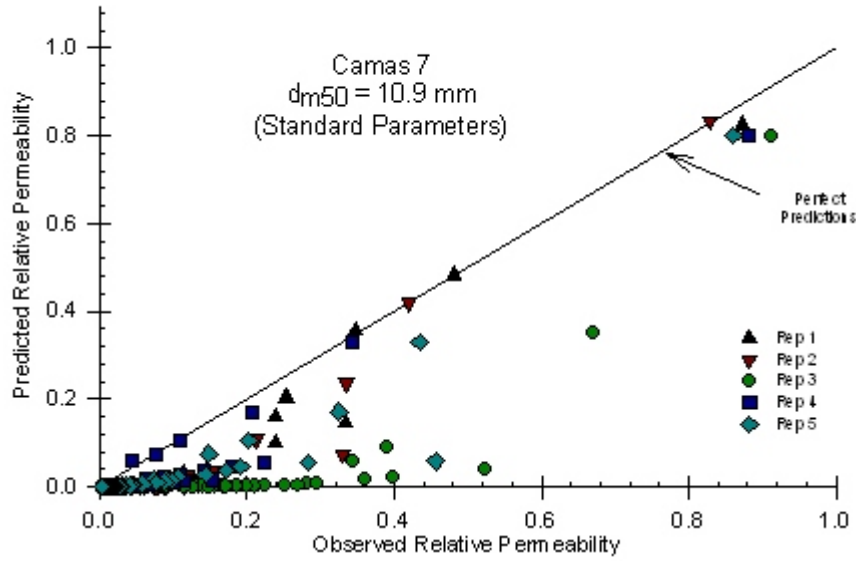


Figure 4.31. Predicted Relative Permeability Using Field Parameters and Deposition for the Camas 7 Rock Media.

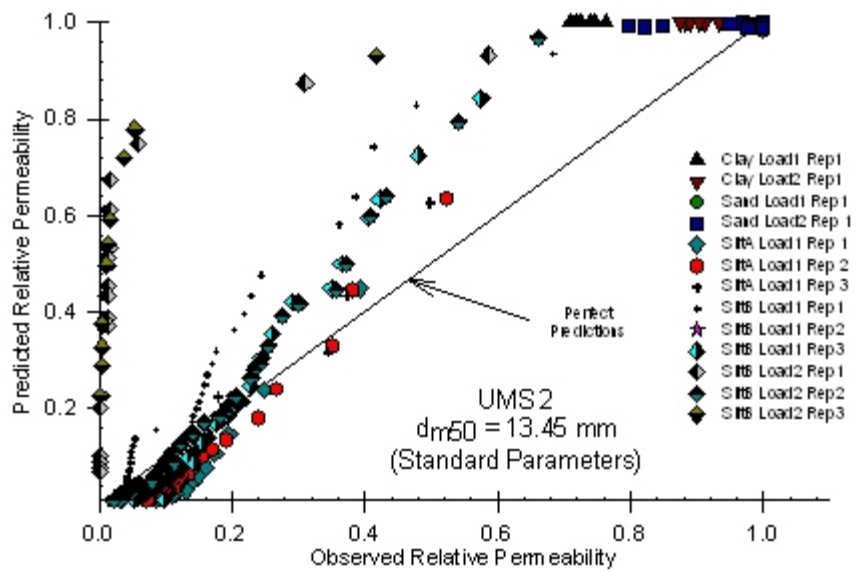


Figure 4.32. Predicted Relative Permeability Using Field Parameters and Deposition for the UMS 2 Rock Media.

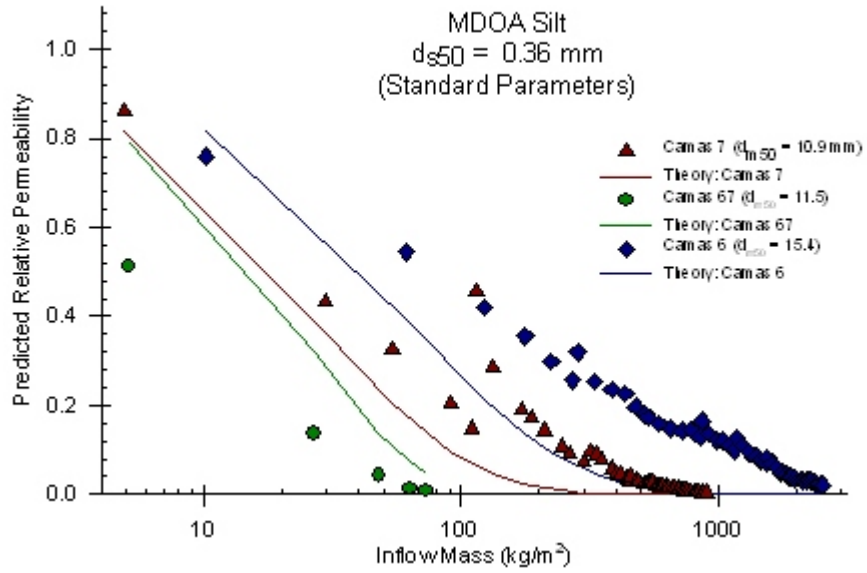


Figure 4.33. Selected Tests of Predicted and Observed Relative Permeability for the MDOA Silt.

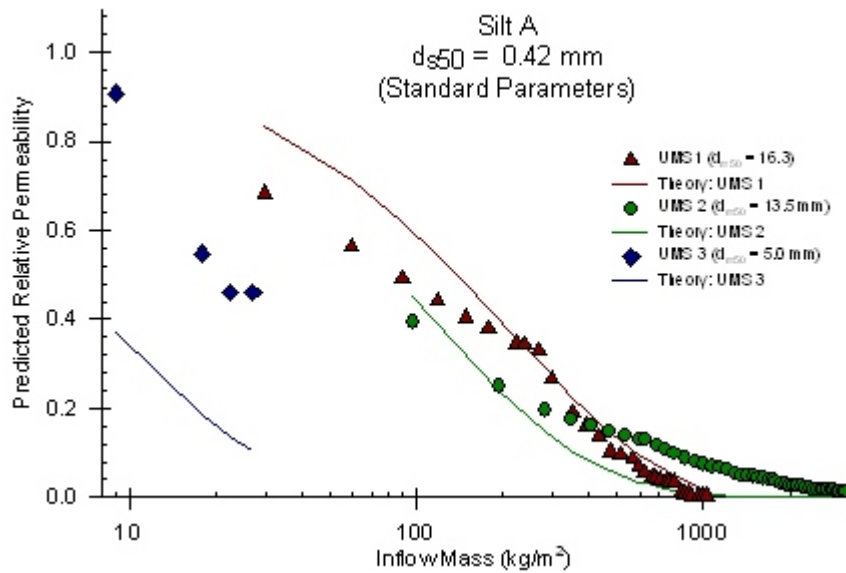


Figure 4.34. Selected Tests of Predicted and Observed Relative Permeability for the Silt A.

Algorithm

A step-by-step description of the process-based method is given below.

Step #1: Select dimension of the rock filter. Determine total volume.

Step #2: Determine porosity (ϕ_T), clean water permeability (κ_c) and the median diameter of the media ($d_{m50,in}$).

Step #3: Select the parameters of the fractal model. Default values are $p = 2.0$, $\beta = 0.1$, $D_{sc} = 1.85$, $f_{vol,min} = 0.2$, and $d_{s50,fvol} = 0.25$ mm. Estimate coefficients for fraction of rock media filling with sediment

$$\psi = 1.0 - (1 - 0.1) \exp \left[-35 \left(\frac{d_{s50,fvol}}{d_{m50,in}} \right) \right]$$

$$\xi = - \frac{\ln [(1 - 0.9) / (1 - f_{vol,min})]}{\psi \phi_T}$$

Step #4: Adjust parameters for non-ideal conditions using an input safety factor (S_F) as

$$f_{vol,min} = \frac{f_{vol,min}}{S_F} \quad \text{and} \quad \xi = \xi S_F$$

Step #5: Initialize deposition parameters:

$$\theta_{dep} = \theta_t = \Delta \theta_{dep} = 0$$

$$\phi_{ac} = \phi_{ad} = \phi_T$$

Step #6: Estimate influent mass and sediment size using BASIN routines. Cumulate influent mass and compute percent sand and diameter (d_{s25} in mm) corresponding to 25% finer and corresponding settling velocity (ω_{s25}). Also the flow rate at the beginning of the time step (initial value obtained using clean water conductivity).

Step #7: Estimate and cumulate sediment deposition using the following equations:

$$\alpha = 1 - \exp \{ - \exp [-0.30 (\text{Percent Sand} - 65)] \}$$

$$d_{m50} = d_{m50,in} \left(\frac{1 - \phi_{ad}}{1 - \phi_T} \right)$$

$$D_R = \frac{d_{s25}}{d_{m50}}$$

$$C_N = \frac{\omega_{s25}}{q_{in} / \phi_{ad}}$$

$$e = 682.6 \alpha D_R^{1.904} C_N^{0.4312}$$

$$\Delta m_d = e [M_I(t) - M_I(t-\Delta t)]$$

$$M_d(t) = M_d(t-\Delta t) + \Delta m_d$$

$$V_d(t) = \frac{M_d(t)}{S_g \rho_w}$$

Step #8: Estimate fractal model deposition terms

$$f_{vol} = 1 - (1 - f_{vol,min}) \exp(-\xi \theta_{dep})$$

$$\text{Fraction of Total Volume} = \theta_{dep} = \frac{V_d(t)}{f_{vol} V_T}$$

$$\text{Deposition Volume Fraction for Smallest Pore} = \theta_l = \beta \theta_{dep}$$

$$\text{Available Non-filled-Pores Porosity} = \phi_{ac} = \phi_T - \theta_l$$

$$\text{Deposition Fraction for Non-filledPores} = \Delta \theta_{dep} = (1 - \beta) \theta_{dep}$$

$$\text{Available Porosity After Depositon} = \phi_{ad} = \phi_{ac} - \Delta \theta_{dep}$$

$$D_s = 2 + \frac{(D_{sc} - 2) \ln(1 - \phi_{ad})}{K \ln(1 - \phi_{ad}) + (1 - K) \ln(1 - \phi_{ac})}$$

Step #9: Estimate permeability and specific discharge as

$$\kappa_r = \left(\frac{\phi_{ad}}{\phi_T} \right)^p \left[\frac{(D_{sc} - 4)/(D_{sc} - 2)}{(D_s - 4)/(D_s - 2)} \right] \left[\frac{(\phi_T - \Delta \theta_{dep})^{(D_s - 4)/(D_s - 2)} - \theta_l^{(D_s - 4)/(D_s - 2)}}{\phi_T^{(D_{sc} - 4)/(D_{sc} - 2)}} \right]$$

$$\kappa = \kappa_r \kappa_c$$

$$q = \frac{-1 + \sqrt{1 + 4g\kappa\sqrt{\kappa C}(-\partial\Phi/\partial\ell)/v^2}}{2\sqrt{\kappa C}/v}$$

where $C=0.6$. For units of κ of mm^2 , g of mm^2/h , v of mm^2/h , specific discharge has units of mm/h .

Step #10: Repeat steps 6 through 9 with time for flows through the rock filter.

Chapter Five

Summary and Conclusions

The Minnesota Pollution Control Agency requires that stormwater pollution prevention plans be developed for construction activities that disturb an area that is equal to or greater than one acre. Different strategies, including a combination of practices, can be used to develop these plans. Simulation models are valuable tools that can be used to assess the effectiveness of different sediment control practices. They are also useful in transferring recent research information into the hands of engineers and scientists, which can then be incorporated into field designs.

A previous project funded by the Minnesota Local Road Research Board and Minnesota Department of Transportation supported the development of a risk simulation tool called the WATER (Watershed Assessment Tool for Environmental Risk) model. This model focused on the impact of highly variable weather conditions on the runoff and erosion for a single construction site. Widely used off-site practices, such as detention ponds, were not included and need to be added to meet the sediment control goals of most construction sites. Integration of the impact of sediment control plans at the watershed scale is also of value to field practitioners. Improved interface and input routines are needed to utilize readily available spatial data bases. The WATER model is therefore expanded in this study to consider off-site practices, to include processes at the watershed scale, and to allow spatial data sets to be integrated into the simulation framework.

The WATER model has been expanded to consider five different types of modeling projects: risk assessment for a single construction site, multiple land uses within a watershed, stand-alone modules for off-site processes, feedlot runoff, and statistical tools. The feedlot runoff module was developed from a companion project funded by the Minnesota Pollution Control Agency. The WATER model can retrieve and edit input data, proceed with continuous simulations, view output results graphically, and work with GIS layers. The file structure has been organized so that each modeling project retrieves input parameters and stores output results into a project folder with appropriate subdirectories. Both input and output data are formatted in a simple ASCII text format.

Routines have been added to the WATER model to simulate the impact of off-site practices of rock check dams, vegetative filters, and detention ponds. Rock check dams are modeled using the approach proposed by Hirschi (1981) and implemented by Wilson et al. (1984) for surface-mined lands. It is based on a single-step backwater curve with trap efficiency predicted by a relationship similar to that given by Camp (1945). The sediment removal of vegetative filters and buffers is modeled by modifying the GRASSF model (Wilson et al., 1984). This model divides the removal processes into two components: (1) deposition of sediment load at the inlet of the filter because of a reduction in the transport capacity of flow and (2) settling of suspended sediment in the remaining portion of the filter. Routines to predict the response of detention ponds is based on the BASIN (Basin Analysis of Sediment-laden INflow) model developed by Wilson and Barfield (1985) and modified by Oolman and Wilson (2003). This model divides the pond into a series of chambers of equal volume. A

mass balance in the vertical direction is evaluated for each of the chambers. It considers settling of velocity of sediment, turbulent diffusion, and scour at the bed of the pond.

Particularly important changes in the BASIN model are made to allow rock and gravel infiltration filters to be included as an off-site practice. Two different algorithms have been implemented in the WATER model. One of the algorithms, referred to as the Protocol Method, is a purely empirical method based on the evaluation of experimental data collected in a laboratory setting using measurements obtained from standard protocols. The other algorithm, referred to as the Process-Based Method, is based on process-based relationships developed for porous media flow. It uses a fractal model to account for changes in permeability with sediment deposition. Removal efficiencies are also predicted using process-based parameters. Two sets of laboratory experiments previously collected under the supervision of the lead investigator are used to evaluate the parameters and the accuracy of the two methods.

The WATER model has been expanded to allow flow and sediment from different areas within a watershed to be routed through channels and/or stream networks and to be combined to determine the overall response of the watershed. Code has been written to route flows through channels using the relatively simple Muskingum method and using the solution of one-dimensional equations for motion and mass balance (so-called St. Venant equations). The transport of eroded sediment through channels is also an important process. Sediment load between upstream and downstream points can either increase because of channel scour or decrease because of sediment deposition. Since the influent load for construction sites is usually large, sediment deposition is of greater interest. In the WATER model, code has been added to route sediment movement through channels using a relatively simple delivery ratio approach and using a sediment transport relationship.

References

- Barfield, B. J., and J. C. Hayes. 1980. "Modeling sediment filtration by vegetative filters." ASCE Watershed Management Symposium. Boise, Idaho: ASCE.
- Brooks, R.H. and A.T. Corey. 1964. *Hydraulic properties of porous media*. Hydrology Paper #3, CSU, Fort Collins, CO.
- Camp, T.R. 1945. "Sedimentation and the design of settling tanks." *Am. Soc. Civil Engrs.*, Vol. 71, Paper No. 2285: 895-959.
- Chaudhry, M. H. 1993. *Open-Channel Flow*. Prentice-Hall Inc, Englewood Cliffs, NJ.
- Chow, V.T., D. R. Maidment, and L.W. Mays. 1988. *Applied Hydrology*. McGraw Hill, New York, NY.
- Dhamotharan, S., J.S. Gulliver and H.G. Stefan. 1981. "Unsteady one-dimensional settling of suspended sediment." *Water Resources Research*, Vol 17: 1125-1132.
- Haan, C.T., B.J. Barfield, and J.C. Hayes. 1994. *Design Hydrology and Sedimentology for Small Watersheds*. Academic Press, San Diego, California. pp. 49-51.
- Hayes, J. C. 1979. *Evaluation of design procedures for vegetal filtration of sediment from flowing water*. Unpubl. Ph.D. Lexington, Ky.: University of Kentucky.
- Hayes, J.C., B.J. Barfield, and R.I. Barnhisel. 1979. "Filtration of sediment by simulated vegetation II: Unsteady flow with nonhomogeneous sediment." *Transactions of the ASAE*, Vol. 22(5): 1063-1067.
- Hirschi, M. C. 1982. *Efficiency of small scale sediment controls*. Ag. Engr. File Report, University of Kentucky, Lexington, KY.
- Mandelbrot, B. 1977. *The Fractal Geometry of Nature*. W.H. Freeman and Company, New York, NY.
- McWhorter, D.B. and D.K. Sunada. 1977. *Ground-Water Hydrology and Hydraulics*. Water Resources Publications, Littleton, CO.
- Mualem, Y. 1976. "A new model for predicting the hydraulic conductivity of unsaturated porous media." *Water Resources Research*, Vol. 12(3): 513-522.
- Oolman, E.A. and B.N. Wilson. 2003. "Sediment control practices for surface tile inlets." *Applied Engineering in Agriculture*, Vol. 19(1): 161-169.
- Oveson, K.L. 2001. *Evaluation and Design of Rock Inlets as an Alternative Form of Surface Drainage*. M.S. Thesis, University of Minnesota, Graduate School, Minneapolis, MN.

- Press, W.H., B.P. Flannery, S.A. Teukolsky, and W.T. Vetterling. 1992. *Numerical Recipes in C: Art of Scientific Computing*. Cambridge Press, New York, NY.
- Tien, C. 1989. *Granular Filtration of Aerosols and Hydrosols*. Butterworth Series in Chemical Engineering, Butterworth Publishers, Stoneham, MA.
- Tollner, E. W., B. J. Barfield, C. T. Haan, and T. Y. Kao. 1976. "Suspended sediment filtration capacity of simulated vegetation." *Transactions of the ASAE* 19(4): 678-682.
- Tollner, E. W., B. J. Barfield, C. Vachirakornwatana, and C.T. Haan. 1977. "Sediment deposition patterns in simulated grass filters." *Transactions of the ASAE* 20(5): 940-944.
- Tyler, S.W. and S.W. Wheatcraft. 1990. "Fractal processes in soil water retention." *Water Resources Research*, Vol. 26 (5): 1047-1054.
- Williams, J.R. 1975. "Sediment routing for agricultural watersheds." *Water Resources Bulletin*, Vol. 11(5): 965-974.
- Wilson, B.N. 1993. "Development of a fundamentally based detachment model." *Transactions of the ASAE*, Vol. 36(4): 1105-1114.
- Wilson, B. N. and B. J. Barfield. 1984. *Modeling the performance of sediment detention ponds: Volume 2, The BASIN model using diffusion theory*. Technical Report, Institute for Mining and Minerals Research, University of Kentucky, Lexington, KY.
- Wilson, B. N. and B. J. Barfield. 1985. "Modeling sediment detention ponds using reactor theory and advection-diffusion concepts." *Water Resources Research*, Vol. 21(4):523-532.
- Wilson, B.N. and J.C. Hayes. 2004. "Modeling erosion and transport of sediment from urbanizing landscapes." *Proceedings of the 6th International Conference on Hydrosience and Engineering (ICHE-2004)*, Brisbane, Australia.
- Wilson, B.N., B. J. Barfield, I. D. Moore, and R. C. Warner. 1984. "A hydrology and sedimentology watershed model. Part II: Sedimentology component." *Transactions of the ASAE*, Vol. 27(5):1378-1384.
- Wilson, B. N. and J. R. Ruffini. 1988. "Comparison of physically-based Muskingum methods." *Transactions of the ASAE*, Vol. 31(1):91-97.
- Wilson, B.N., H.V. Nguyen, U.B. Singh, S. Morgan, P. Van Buren, D. Mickelson, E. Jahnke, and B. Hansen. 1999. *Evaluation of alternative designs for surface tile inlets using prototype studies*. Final Report, Minnesota Department of Agriculture, St. Paul, MN, Contract number 417121.
- Wilson, B.N., A.Y. Sheshukov. and R. Pulley. 2006. *Erosion Risk Assessment Tool for*

Construction Sites. Minnesota Department of Transportation, Research Report No. MN/RC-2006-27, St. Paul, MN.

Yang, C.T. 1972. "Unit stream power and sediment transport." *J. of Hydraulics Division*, Vol. 98(HY10): 1805-1826.

Yang, C.T. 1973. "Incipient motion and sediment transport." *J. of Hydraulics Division*, Vol. 99(HY10): 1805-1826.